7. SITE 909[1]

Shipboard Scientific Party[2]

HOLE 909A

Date occupied: 15 August 1993

Date departed: 16 August 1993

Time on hole: 17 hr

Position: 78°35.065′N, 3°4.378′E

Bottom felt (drill pipe measurement from rig floor, m): 2530

Distance between rig floor and sea level (m): 10.96

Water depth (drill pipe measurement from sea level, m): 2519

Total depth (from rig floor, m): 2622.5

Penetration (m): 92.5

Number of cores (including cores with no recovery): 11

Total length of cored section (m): 92.5

Total core recovered (m): 94.78

Core recovery (%): 102.5

Oldest sediment cored:
Depth (mbsf): 92.5
Nature: silty clay
Earliest age: Quaternary

HOLE 909B

Date occupied: 16 August 1993

Date departed: 16 August 1993

Time on hole: 16 hr, 45 min

Position: 78°35.074′N, 3°4.380′E

Bottom felt (drill pipe measurement from rig floor, m): 2530.1

Distance between rig floor and sea level (m): 10.99

Water depth (drill pipe measurement from sea level, m): 2519.1

Total depth (from rig floor, m): 2665.2

Penetration (m): 135.1

Number of cores (including cores with no recovery): 16

Total length of cored section (m): 135.1

Total core recovered (m): 140.42

Core recovery (%): 103.9

Oldest sediment cored:
Depth (mbsf): 135.1
Nature: silty clay
Earliest age: Quaternary

HOLE 909C

Date occupied: 31 August 1993

Date departed: 11 September 1993

Time on hole: 11 days, 4 hr, 20 min

Position: 78°35.096′N, 3°4.222′E

Bottom felt (drill pipe measurement from rig floor, m): 2529

Distance between rig floor and sea level (m): 11.02

Water depth (drill pipe measurement from sea level, m): 2518

Total depth (from rig floor, m): 3590.8

Penetration (m): 1061.8

Number of cores (including cores with no recovery): 103

Total length of cored section (m): 976.8

Total core recovered (m): 604.77

Core recovery (%): 61.9

Oldest sediment cored:
Depth (mbsf): 1061.8
Nature: silty clay
Earliest age: late Oligocene
Latest age: early Miocene

Principal results: Site 909 (proposed Site FRAM-1A) had been planned as the deep-water location in Fram Strait on a small abyssal terrace located immediately to the North of Hovgaard Ridge. This terrace comprises the sill between the Arctic Ocean and the Norwegian-Greenland Sea, and is protected against the influx of turbidites by channels or depressions to the West (Hovgaard Ridge and channel between it and the Greenland continental margin), East (northern extension of the active Knipovich Ridge), and North (Molloy Deep). Shallow gravity cores from the terrace had demonstrated the existence of a hemipelagic fossiliferous sediment section with an undisturbed, easily dateable upper Quaternary stratigraphy. As the central part of the Fram Strait was ice-free, we selected the westernmost of the locations proposed for the FRAM-1 site.

Holes 909A (to 92.5 mbsf) and 909B (to 135.1 mbsf) were drilled earlier while waiting for the escort icebreaker *Fennica* in mid-August. Hole 909C (to 1061.8 mbsf) was drilled in early September when the advancing ice had temporarily driven us off all remaining sites on the Yermak Plateau. Recovery and sediment properties at this site were excellent, but at depth where well-defined bedding is observed, Hole 909C deviated by up to 25° from the vertical. The deep hole had to be abandoned for safety considerations because of the stepwise increase of hydrocarbon concentrations at the bottom of the hole.

The drilled sediment section consists of gray to dark gray clays to silty clays to muds with varying amounts of sand and/or dropstones. Numerous subtle color changes follow bedding planes. Bioturbation is pervasive except in the lowermost part of the drilled sequence with laminated intervals that are interrupted by several slumps. No volcanic ashes were observed.

The entire sedimentary sequence can be subdivided into three lithologic units, based on their texture, composition, and sedimentary structures:

[1]Myhre, A.M., Thiede, J., Firth, J.V., et al., 1995. *Proc. ODP, Init. Repts.*, 151: College Station, TX (Ocean Drilling Program).

[2]Shipboard Scientific Party is as given in the list of participants preceding the Table of Contents.

Unit I: (0–248.8 mbsf, Pliocene to Quaternary)

This unit consists of gray to dark gray interbedded clays, silty clays, and clayey muds with varying amounts of dropstones having diameters of >1.0 cm. They are mostly rounded to subrounded clastic sedimentary—in particular black siltstones—and crystalline rocks, rarely limestones. Coal fragments are common in many horizons. Dropstones do not occur beneath 240 mbsf. The upper 50 m contains minor occurrences of calcareous nannofossils. Monosulfides and color banding occur throughout.

Unit II: (248.8–518.3 mbsf, Miocene to Pliocene)

Dark silty clays and clayey silts with pyrite make up this unit. Some of the clays are carbonate-rich. Bioturbation is light to moderate throughout. Concretions and diffuse pods of Fe-sulfide occur sparsely. Nodular pyrite concretions and disseminated pyrite grains are common. Below 499 mbsf the silty clays are increasingly fissile and show some parting along planes, which may be related to foliation but are more likely related to original bedding. Bioturbation is minimal throughout intervals displaying layering, which varies from medium color bands to fine laminations. Mottled surfaces and millimeter- to centimeter-scale burrows attest to moderate to extreme bioturbation in poorly layered sediments.

Unit III: (518.3–1061.8 mbsf, Oligocene to Miocene)

Based on sedimentary structures, this unit can be subdivided into two subunits. The upper subunit (518.3–923.4 mbsf) consists of dark-gray silty clays, clayey silts, and muds, sometimes carbonate bearing; it is also characterized by meter-scale alternations of bioturbated layers and laminations. The lower subunit (923.4–1061.8 mbsf) comprises dark-gray silty clays, clayey silts, clayey and silty muds, which are characterized by several intervals of commonly folded and otherwise deformed bedding. Disseminated pyrite and glauconite are common. Benthic foraminifers and worm tubes occur.

Fossil assemblages are composed mostly of palynomorphs and agglutinated benthic foraminifers. Dinoflagellates suggest a nearly complete Miocene section. Other fossil groups are virtually absent, with the exception of rare calcareous nannofossils in the upper 50 m and from 700 mbsf to base. Calcareous nannofossils in Core 151-909C-102R give a basal age of latest Oligocene to early Miocene, in agreement with dinoflagellate ages. The benthic foraminifers, however, suggest an older age (early Oligocene), indicating unusual diachrony of this group, possibly caused by the migration of benthic habitats. Siliceous microfossils are virtually absent, but dissolved silica in interstitial waters in the upper part of the section are high enough to suggest their original presence. However, in the lower part of the section, dissolved silica is so low that the original sediments may have been opal-free.

The paleomagnetic record is good in the Pliocene and Quaternary where the Brunhes, Matuyama, Gauss, and perhaps the Gilbert chrons can be identified including their major subchrons, and sedimentation rates of 50–80 m/m.y. are suggested for the upper 300–400 mbsf. Below this level, many clear magnetozone boundaries can be identified, but their correlation to the geomagnetic polarity time scale remains problematic at present.

Site 909 was the first site drilled during Leg 151 that displayed disruption due to gas. Organic carbon values are relatively high throughout, with maximum values of 1.5%–2.6% in the lowermost 60 m of the site. At about 450 mbsf, in addition to abundant methane, higher hydrocarbons also started to occur in minor amounts. Drilling was terminated because of the drastic two-step increase in propane, butanes, pentanes, and hexanes at about 1020 and 1050 mbsf, as well as the occurrence of strong light-yellow fluorescence in the lowermost two cores.

Despite the high gas concentrations, a long and good quality data set of physical properties was obtained. Compaction effects are not complete even at the base of Hole 909C. The physical property profiles appear stepped in places, as bulk-density values increase dramatically over short depth intervals, sometimes coinciding with lithostratigraphic boundaries. Physical property measurements are supported by a successful logging program. The average velocity in Hole 909C was 2.02 km/s. The total depth of Hole 909C is equivalent to 1.023 s two-way traveltime. The acoustic basement reflector is probably about 140 m below the terminal depth.

BACKGROUND AND OBJECTIVES

Background

Site 909 (planned as FRAM-1A; see Fig. 17 of "Introduction" chapter, this volume) is located in the center of Fram Strait approximately in the area of the sill depth between the Norwegian-Greenland Sea and the Arctic Ocean (see Fig. 6 of "Introduction" chapter, this volume). This sill has been known for less than 50 years; Nansen (1904) published the first bathymetric map (see Frontispiece) of the area including a clearly defined relatively shallow sill (actually called the Nansen Sill) between the deep-sea basins to the North and South, which he also recognized. Only when Soviet, American, and Norwegian researchers surveyed the bathymetry of the area in the late 1950s did it become clear that a contiguous channel approximately 2500 m deep, connected the Arctic Ocean and the Norwegian-Greenland Sea (Johnson and Eckhoff, 1966). Details such as the Molloy Deep, Hovgaard Ridge, and its surroundings were mapped considerably later (Perry, 1986; Thiede et al., 1990b; Eldholm and Myhre, 1977). Because of the great importance of Fram Strait as a climatically sensitive ocean passage and because of the unresolved position of the boundary between the North American and Eurasian plates, the area will be studied in considerable detail in the future.

After some early oceanographic work (Helland-Hansen and Nansen, 1909), it is only now, through the international efforts of the Marginal Ice Zone Experiments (MIZEX) program and the possibilities of synoptic measurements of surface water mass properties and distributions of sea ice, that the fine-scale details of the recent oceanography of Fram Strait have become better known (Johannessen, J.A., et al., 1987; Shuchman et al., 1987; Gascard et al., 1988). The pattern and variability of the relatively warm surface water masses of the West Spitsbergen Current in the East and the pack-ice-covered East Greenland Current in the West are usually easily identifiable (see Fig. 14 of "Introduction" chapter, this volume). The regional persistence (probably morphology-guided by some deep-sea features such as the Molloy Deep) of some of the major gyres (Johannessen, O.M., et al., 1987), the high degree of recirculation of the Atlantic Ocean waters, and the intensive mesoscale turbulence at the water mass boundaries as seen on satellite imagery, however, has come as a surprise (Manley et al., 1992; Quadfasel et al., 1987). Much less is known about the patterns of water exchange between the Arctic Ocean and Norwegian-Greenland Sea in water depths below 500 m. This is further complicated by the occurrence of brines, identifiable by their high sediment transport, cascading from the Barents Sea shelf area and deflected along the continental slope toward the North into the deep Fram Strait. Systematic surveys with moored, deep-sea current meters along transects across Fram Strait are going to clarify patterns of water mass transport through Fram Strait in the near future (Meincke, unpubl. data).

Considerable uncertainty surrounds how the major water mass boundaries (Spielhagen, 1991) and the ice margin (Hebbeln and Wefer, 1991) have changed over geologic time scales. There seems to be no question that the West Spitsbergen Current has only existed during rare peak interglacials (Hebbeln, 1992), whereas an ice cover with a variable influx of icebergs was the dominant element during glacial periods. Considerable amounts of ice-rafted coarse materials were deposited during the latest glaciations, mostly from the Barents side and Greenland, but high abundances of coal in oxygen isotope stage 6 sediments (Spielhagen, 1991) resemble no modern analog with, at times, completely different source regions. Nothing was known hitherto about Fram Strait depositional environments in early Quaternary and Tertiary times.

The tectonic evolution of the Fram Strait in the northern Greenland Sea during Neogene times had a profound influence on the water mass exchange between the Arctic Ocean and the Norwegian-Greenland Sea (see Fig. 6 of "Introduction" chapter, this volume). As the

only deep-water connection between the Arctic Ocean and the world's ocean, it is of major importance to understand the timing of the plate tectonic events that led to a complete opening of the Fram Strait. Although the present-day plate boundary between the Knipovich Ridge and Gakkel Ridge is established to some extent, nothing is known about how it developed since the plate motion changed from transform to extensional movements between Svalbard and Greenland. Most probably a series of plate boundary adjustments took place, reflected in the present-day oblique position of the Knipovich Ridge in the northeastern part of the Greenland Sea, and the lack of any magnetic seafloor spreading anomalies in most of the Greenland Sea (see Fig. 11 of "Introduction" chapter, this volume).

Another important question to consider is the timing of the thermal subsidence and submersion of the Yermak Plateau and Morris Jesup Rise. A hot-spot origin for the two plateaus, which was active until the early Oligocene, has been suggested. An Icelandic type of subaerial spreading along the southern Gakkel Ridge could explain the two features, and a change to normal seafloor spreading ended the Icelandic type of spreading, and the plateaus subsided below sea level.

An initiation of the deep-water connection may have taken place as early as early Oligocene (Anomaly 13), according to Crane et al. (1982; also see reviews by Vogt, 1986a, b) while others (Lawver et al., 1990; Eldholm, 1990; and Kristoffersen, 1990) have suggested a younger age for the opening, even up to late Miocene.

To some extent the physiography in the Fram Strait reflects the plate boundary with the seamounts and deep depression associated with the Molloy Rift and Molloy and Spitsbergen fracture zones (see Fig. 6 of "Introduction" chapter, this volume). Deep nodal basins with maximum water depths of 4532 and 5607 m have been mapped (Perry, 1986; Thiede et al., 1990b), with seamounts rising to 1537 and 1468 mbsl. The slope West of Svalbard and the Yermak Plateau continues directly into the rift/transform system with a steep upper part and a gradual change to a more gentle gradient on the lower slope. The relief of the slope off Northeast Greenland, however, is much gentler. South-Southwest of the plate boundary the Greenland-Spitsbergen sill acts as a terrace between the rugged bathymetry toward the North and the shallow Hovgaard Ridge to the South. The average depth of the sill is about 2500 m, and the shallowest part of the Hovgaard Ridge is 1171 m (Eldholm and Myhre, 1977).

Multichannel seismic lines from the Greenland-Spitsbergen sill terrace show a complicated pattern of rough basement topography, giving rise to many diffractions that mask part of the sedimentary sequence and also make it difficult to define basement. Site 909 is situated in a small sub-basin where only the uppermost part of the sedimentary sequence appears continuous over two structures, which are partly masked by hyperbolas but could be basement peaks located just off the seismic line.

The multichannel seismic line BU-20-81 (Fig. 1) shows an upper thick sequence of continuous reflectors having high amplitudes and high frequencies alternating with sequences of continuous low-amplitude reflectors. Below this, the next sequence consists of a series of low-amplitude, low-frequency continuous reflectors. This sequence thins eastward and onlaps onto a lower sequence that is characterized by short, discontinuous reflector segments. Just below the site at shot point 465, a sequence of strong hyperbola-like reflectors appears at 1.1 s two-way traveltime (TWT) and masks any deeper horizons. This sequence might be associated with basement, but part of the reflectors may be sideswipe and diffraction hyperbolas making the exact position of true basement difficult to define.

Scientific Objectives

Site 909 is located in the Fram Strait at the Greenland-Spitsbergen sill terrace immediately North of Hovgaard Ridge, a gentle elevated area protected against sediment influx from the Svalbard and Greenland margins. Location of Site 909 is selected to document the timing of the opening of a deep passageway through the Fram Strait and the history of deep and shallow water exchange between the Arctic Ocean and the world ocean. The site will also provide records of the onset and evolution of Arctic glacial history and the climatic variability of the Arctic region.

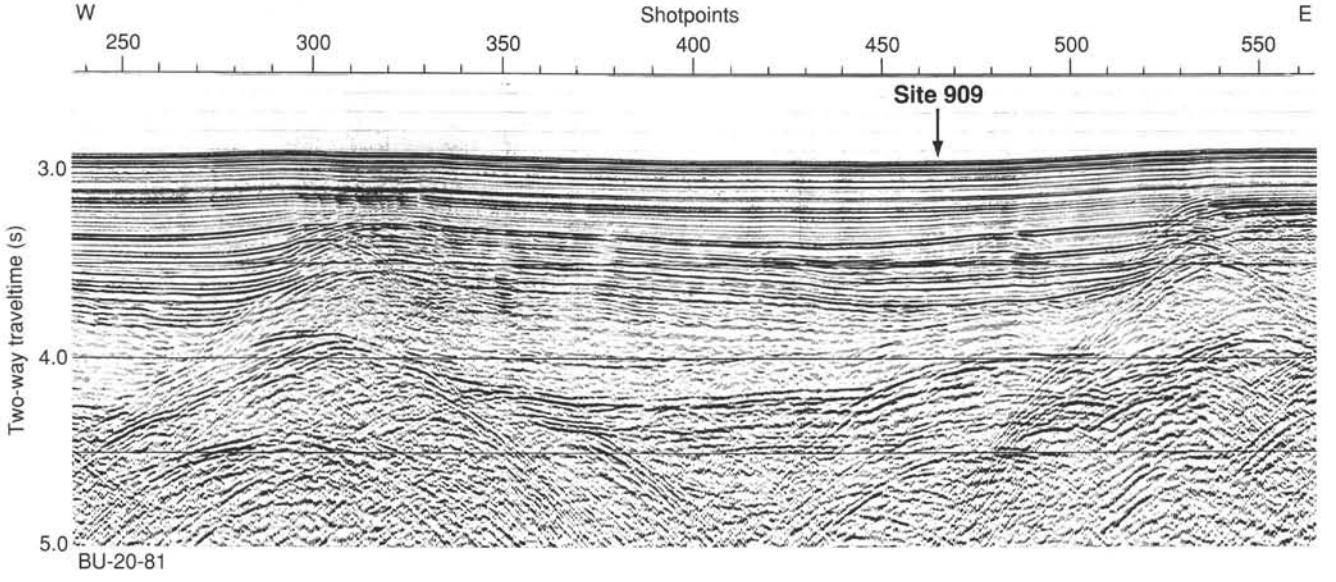

Figure 1. Seismic line BU-20-81, Site 909, located at sp. 465.

OPERATIONS

Transit to Site 909 (FRAM-1A)

The icebreaker *Fennica* advised that it would arrive on schedule at FRAM-1B at 0300 hr, 16 August; therefore, it was decided to initiate coring at FRAM-1A (Site 909) until the ice conditions could be determined in the Yermak Plateau area. The 18-nmi transit required 2.0 hr for an average speed of 9.0 kt. The seismic survey at Site 909 started at 1506 hr, 15 August, and covered 13 nmi in 2.5 hr at 5.2 kt. A Datasonics 354B beacon (S/N 785, 15.0 kHz, 208 dB) was dropped at 1625 hr, the seismic gear was retrieved, and the ship returned to location. A second (original backup) Datasonics 354B beacon (S/N 763, 16.0 kHz, 208 dB) was dropped at 1835 hr.

Hole 909A

An advanced hydraulic piston corer/extended core barrel (APC/XCB) bit was run for the first and second holes. The precision depth recorder (PDR) indicated a water depth of 2534.4 mbrf, and Hole 909A was spudded at 0021 hr, 16 August, at 78°35.065′N, 3°4.378′E. Core 151-909A-1H established the water depth as 2519 mbsl. Cores 151-909A-1H through -11H were taken from 0.0 to 92.5 mbsf (Table 1), with 92.5 m cored and 94.78 m recovered (102.5% recovery). APC-coring was terminated after Core 11H because it was the fourth core with a partial stroke in very stiff clays. Cores were not oriented. Adara heat flow measurements were taken on Cores 4H, 7H, and 10H. The bit cleared the seafloor at 0934 hr, 16 August, ending Hole 909A.

Arrival of Icebreaker *Fennica*

The icebreaker *Fennica* arrived at Site 909 at 0600 hr, 16 August. Two personnel were transferred to the *Fennica* to gauge the fuel tanks as per the contract. Two Scott Polar Research Institute ice scientists and three German Norddeutscher Rundfunk (NDR) TV crewmembers were transferred to the *Resolution* for initial introductions and planning meetings. Personnel were returned to their respective ships, and at 1110 hr, 16 August, the *Fennica* departed the *Resolution* and headed Northwest to locate the pack ice nearest the *Resolution* and determine its condition.

Fennica's First Scouting Trip

The *Fennica* located the ice edge in dense fog at 79°24′N, 02°55′E, and found a tightly packed mix of slush up to rotten, first-year ice, 1 to 1.5 m thick and in 20-m × 20-m blocks. There was a 100-m-wide band of scattered 10-cm × 10-cm brash ice, but no loose ice anywhere. The *Fennica* proceeded up to YERM-4, arriving at 0500 hr, 17 August, and found the area ice-free in a 34-nmi radius at 0900 hr, 17 August. Plans were made to finish Hole 909B (then in progress) and to go immediately to Site YERM-4. The *Fennica* returned to the *Resolution*, arriving at 1500 hr, 17 August. The two Scott Polar scientists and three German NDR TV crew members were transferred to the *Resolution*. Videotapes, course plots, and ice maps were reviewed to better understand ice conditions.

Hole 909B

The ship was moved 20 m North, and Hole 909B was spudded at 1019 hr, 16 August, to provide high-resolution sampling. Core 151-909A-1H established the water depth as 2519.1 mbsl. Cores 151-909A-1H through -16H were taken from 0.0 to 135.1 mbsf (Table 1), with 135.1 m cored and 140.4 m recovered (103.9% recovery). APC-coring was terminated after Core 16H. Cores were not oriented, and heat-flow measurements were not taken. The bit cleared the rotary table at 0213 hr, 17 August, ending Hole 909B. Both beacons were recovered.

Fennica's Second Scouting Trip

YERM-4 was clear of any ice, so the *Fennica* was directed to proceed North to YERM-1 to determine ice conditions and map the edge of the ice pack to the Northeast of the *Resolution* and YERM–3 to determine if YERM–3 was free of ice. *Fennica* departed the *Resolution* at 1735 hr, 18 August.

Return to Site 909

Later during the cruise, we decided to return to complete the deep rotary-core-barrel (RCB) hole at Site 909, because ice floes covered the Yermak Plateau, Site 912, and the other undrilled YERM sites. The 105-nmi transit to Site 909 required 11.0 hr for an average speed of 9.5 kt. No seismic survey was conducted. A single Datasonics 354B beacon was dropped at 1201 hr, 31 August, on the GPS position 78°35.093′N, 3°04.283′E (South and West of the original two holes).

Hole 909C

An RCB bottom-hole assembly (BHA) was run. The water depth was 2529 mbrf. Hole 909C was spudded at 1638 hr, 31 August, and the hole was drilled from 0 to 85 mbsf. Cores 151-909C-1R through -103R were taken from 85 to 1061.8 mbsf, with 976.8 m cored and 604.77 m recovered (61.9% recovery). Heat-flow measurements taken in Hole 909A indicated a temperature gradient of 88°C/km. Deviation survey at 500 mbsf had a 10° angle, and over 17° at 800 mbsf. Logs indicated that below 600 mbsf the hole had an almost straight azimuth of 48° (i.e., Northeast), at an angle that increased steadily from 14° at 600 mbsf to 25.6° at 1010 mbsf.

Headspace and vacutainer gas concentrations were measured, and the Natural Gas Analyzer (NGA) gas chromatograph was also used, owing to the occurrence of significant amounts of higher molecular weight gases. Gas readings remained mostly within the normal range of C_1/C_2 ratio vs. temperature plot. Headspace gas ratios as low as 19:1 were recorded from Core 151-909C-97R (1010 mbsf). The vacutainer C_1/C_2 ratio decreased from 537 at Core 151-909C-75R to 176 at Core 151-909C-103R. The headspace gas C_1/C_2 ratio remained on the border of normal to unusual, with several rapid drops downhole, and reached a low of 13:1 at Core 151-909C-103R. Coring was terminated following the Pollution Prevention and Safety Panel (PPSP) guidelines when anomalous increases in heavy hydrocarbons were detected.

Hole 909C was terminated at 1061.8 mbsf for the following reasons:

1. Heavier hydrocarbons started to appear, with normal hexane (C_6) in Core 151-909C-101R (1051 mbsf), and heptane (C_7) at 151-909C-93R (973 mbsf).
2. Abrupt, strong increases occurred in heavy hydrocarbons (C_3 to C_7) in Cores 151-909C-97R (1019 mbsf) and 151-909C-101R (1051 mbsf).
3. After core samples were treated with 1,1,1-Tri-chloroethane, Core 151-909C-67R (730.4 mbsf) exhibited yellow fluorescence under ultraviolet light on some sample particles 20 min after being soaked. By Core 151-909C-101R (1052.7 mbsf), a strong light-yellow "cut" fluorescence occurred, sample particles fluoresced yellow all over, and a yellow fluorescent ring was left on the sample dish. A white-bluish fluorescence occurred in Cores 151-909C-102R and -103R.
4. A seismic reflector (thought to be acoustic basement) at 1.23 s TWT bsf, was estimated to occur between 1050 and 1200 mbsf. In the cores, siltstones with increasing coarseness to 10% sand were observed interbedded with silty clay/mud and sandy silt. After Core 151-909C-94R (990.7 mbsf), the rate of penetration (ROP) increased from 8.5 to 6.5 min/m. At Core 151-909C-102R, the ROP decreased again from 7.3 to 22.0 to 33.4

Table 1. Coring summary, Site 909.

Core	Date (1993)	Time (UTC)	Depth (mbsf)	Length cored (m)	Length recovered (m)	Recovery (%)
151-909A-						
1H	16 Aug.	0035	0.0–7.5	7.5	7.35	98.0
2H	16 Aug.	0110	7.5–17.0	9.5	9.91	104.0
3H	16 Aug.	0150	17.0–26.5	9.5	9.92	104.0
4H	16 Aug.	0250	26.5–36.0	9.5	10.33	108.7
5H	16 Aug.	0330	36.0–45.5	9.5	10.01	105.3
6H	16 Aug.	0415	45.5–55.5	10.0	8.84	88.4
7H	16 Aug.	0520	55.5–65.0	9.5	10.31	108.5
8H	16 Aug.	0550	65.0–74.0	9.0	9.10	101.0
9H	16 Aug.	0630	74.0–82.6	8.6	9.04	105.0
10H	16 Aug.	0730	82.6–84.4	1.8	1.80	100.0
11H	16 Aug.	0815	84.4–92.5	8.1	8.17	101.0
Coring totals				92.5	94.78	102.4
151-909B-						
1H	16 Aug.	1030	0.0–4.4	4.4	4.39	99.8
2H	16 Aug.	1105	4.4–13.9	9.5	9.75	102.0
3H	16 Aug.	1145	13.9–23.4	9.5	9.89	104.0
4H	16 Aug.	1230	23.4–32.9	9.5	10.07	106.0
5H	16 Aug.	1305	32.9–42.4	9.5	9.86	104.0
6H	16 Aug.	1340	42.4–51.9	9.5	10.10	106.3
7H	16 Aug.	1420	51.9–61.4	9.5	10.10	106.3
8H	16 Aug.	1455	61.4–70.9	9.5	9.20	96.8
9H	16 Aug.	1545	70.9–77.4	6.5	6.48	99.7
10H	16 Aug.	1610	77.4–86.9	9.5	10.21	107.5
11H	16 Aug.	1655	86.9–96.4	9.5	10.38	109.2
12H	16 Aug.	1740	96.4–101.5	5.1	5.17	101.0
13H	16 Aug.	1840	101.5–111.0	9.5	9.95	105.0
14H	16 Aug.	1915	111.0–119.7	8.7	8.84	101.0
15H	16 Aug.	1955	119.7–127.9	8.2	8.66	105.0
16H	16 Aug.	2035	127.9–135.1	7.2	7.37	102.0
Coring totals				135.1	140.42	103.9
151-909C-						
1R	31 Aug.	1955	85.0–94.6	9.6	1.41	14.7
2R	31 Aug.	2045	94.6–104.3	9.7	0.00	0.0
3R	31 Aug.	2135	104.3–113.9	9.6	3.23	33.6
4R	31 Aug.	2220	113.9–123.6	9.7	3.65	37.6
5R	31 Aug.	2315	123.6–133.2	9.6	0.64	6.7
6R	1 Sept.	0015	133.2–142.9	9.7	5.21	53.7
7R	1 Sept.	0115	142.9–152.6	9.7	6.06	62.5
8R	1 Sept.	0215	152.6–162.3	9.7	7.75	79.9
9R	1 Sept.	0320	162.3–171.9	9.6	6.78	70.6
10R	1 Sept.	0420	171.9–181.6	9.7	9.75	100.0
11R	1 Sept.	0525	181.6–191.2	9.6	8.49	88.4
12R	1 Sept.	0610	191.2–200.8	9.6	6.87	71.5
13R	1 Sept.	0705	200.8–210.5	9.7	9.06	93.4
14R	1 Sept.	0820	210.5–220.1	9.6	8.38	87.3
15R	1 Sept.	0930	220.1–229.6	9.5	5.94	62.5
16R	1 Sept.	1045	229.6–239.2	9.6	6.46	67.3
17R	1 Sept.	1145	239.2–248.8	9.6	8.41	87.6
18R	1 Sept.	1315	248.8–258.5	9.7	0.20	2.1
19R	1 Sept.	1440	258.5–268.1	9.6	0.03	0.3
20R	1 Sept.	1540	268.1–277.8	9.7	0.25	2.6
21R	1 Sept.	1640	277.8–287.5	9.7	0.00	0.0
22R	1 Sept.	1840	287.5–297.1	9.6	8.97	93.4
23R	1 Sept.	1955	297.1–306.8	9.7	5.65	58.2
24R	1 Sept.	2110	306.8–316.4	9.6	7.78	81.0
25R	1 Sept.	2225	316.4–326.0	9.6	5.49	57.2
26R	1 Sept.	2335	326.0–335.7	9.7	8.70	89.7
27R	2 Sept.	0105	335.7–345.3	9.6	6.17	64.3
28R	2 Sept.	0245	345.3–354.9	9.6	5.94	61.9
29R	2 Sept.	0430	354.9–364.6	9.7	8.81	90.8
30R	2 Sept.	0625	364.6–374.1	9.5	0.24	2.5
31R	2 Sept.	0910	374.1–383.6	9.5	8.74	92.0
32R	2 Sept.	1055	383.6–393.1	9.5	7.76	81.7
33R	2 Sept.	1245	393.1–402.8	9.7	9.30	95.9
34R	2 Sept.	1420	402.8–412.4	9.6	8.50	88.5
35R	2 Sept.	1605	412.4–422.1	9.7	9.86	101.0
36R	2 Sept.	1805	422.1–431.7	9.6	9.25	96.3
37R	2 Sept.	2010	431.7–441.3	9.6	9.67	101.0
38R	2 Sept.	2150	441.3–451.0	9.7	4.51	46.5
39R	2 Sept.	2330	451.0–460.6	9.6	2.21	23.0
40R	3 Sept.	0115	460.6–470.3	9.7	7.25	74.7
41R	3 Sept.	0330	470.3–480.0	9.7	9.84	101.0
42R	3 Sept.	0530	480.0–489.5	9.5	8.09	85.1
43R	3 Sept.	0725	489.5–499.0	9.5	9.88	104.0
44R	3 Sept.	0930	499.0–508.6	9.6	8.97	93.4
45R	3 Sept.	1120	508.6–518.3	9.7	8.20	84.5
46R	3 Sept.	1245	518.3–528.0	9.7	6.36	65.5
47R	3 Sept.	1425	528.0–537.7	9.7	8.47	87.3
48R	3 Sept.	1610	537.7–547.3	9.6	9.08	94.6
49R	3 Sept.	1800	547.3–556.9	9.6	9.81	102.0
50R	3 Sept.	1915	556.9–566.6	9.7	5.29	54.5
51R	3 Sept.	2130	566.6–576.2	9.6	6.46	67.3
52R	3 Sept.	2330	576.2–585.8	9.6	5.53	57.6
53R	4 Sept.	0130	585.8–595.5	9.7	7.75	79.9
54R	4 Sept.	0310	595.5–605.1	9.6	3.70	38.5
55R	4 Sept.	0510	605.1–614.8	9.7	9.36	96.5
56R	4 Sept.	0645	614.8–624.4	9.6	0.97	10.1
57R	4 Sept.	0915	624.4–634.1	9.7	7.98	82.2
58R	4 Sept.	1100	634.1–643.7	9.6	2.01	20.9
59R	4 Sept.	1315	643.7–653.4	9.7	8.55	88.1
60R	4 Sept.	1505	653.4–663.0	9.6	8.89	92.6
61R	4 Sept.	1725	663.0–672.7	9.7	7.24	74.6
62R	4 Sept.	1925	672.7–682.3	9.6	9.89	103.0
63R	4 Sept.	2155	682.3–692.0	9.7	5.22	53.8
64R	5 Sept.	0000	692.0–701.6	9.6	7.80	81.2
65R	5 Sept.	0255	701.6–711.1	9.5	9.56	100.0
66R	5 Sept.	0510	711.1–720.8	9.7	2.95	30.4
67R	5 Sept.	0750	720.8–730.4	9.6	9.85	102.0
68R	5 Sept.	0945	730.4–740.0	9.6	5.24	54.6
69R	5 Sept.	1230	740.0–749.6	9.6	9.43	98.2
70R	5 Sept.	1440	749.6–759.3	9.7	8.33	85.9
71R	5 Sept.	2040	759.3–769.0	9.7	9.17	94.5
72R	5 Sept.	2225	769.0–778.7	9.7	9.22	95.0
73R	6 Sept.	0055	778.7–788.3	9.6	8.60	89.6
74R	6 Sept.	0405	788.3–798.0	9.7	7.73	79.7
75R	6 Sept.	0745	798.0–807.6	9.6	9.89	103.0
76R	6 Sept.	0935	807.6–817.3	9.7	9.77	101.0
77R	6 Sept.	1120	817.3–827.0	9.7	6.62	68.2
78R	6 Sept.	1345	827.0–836.6	9.6	4.67	48.6
79R	6 Sept.	1655	836.6–846.2	9.6	0.00	0.0
80R	6 Sept.	2105	846.2–855.9	9.7	9.72	100.0
81R	6 Sept.	2255	855.9–865.5	9.6	6.07	63.2
82R	7 Sept.	0055	865.5–875.1	9.6	2.59	27.0
83R	7 Sept.	0340	875.1–884.8	9.7	5.54	57.1
84R	7 Sept.	0655	884.8–894.4	9.6	6.54	68.1
85R	7 Sept.	0940	894.4–904.1	9.7	2.55	26.3
86R	7 Sept.	1210	904.1–913.8	9.7	3.71	38.2
87R	7 Sept.	1430	913.8–923.4	9.6	2.61	27.2
88R	7 Sept.	1625	923.4–933.1	9.7	3.21	33.1
89R	7 Sept.	1910	933.1–942.8	9.7	3.06	31.5
90R	7 Sept.	2245	942.8–952.4	9.6	3.37	35.1
91R	8 Sept.	0055	952.4–962.1	9.7	3.32	34.2
92R	8 Sept.	0345	962.1–971.7	9.6	3.03	31.5
93R	8 Sept.	0615	971.7–981.3	9.6	2.94	30.6
94R	8 Sept.	0910	981.3–990.7	9.4	3.58	38.1
95R	8 Sept.	1150	990.7–1000.4	9.7	1.97	20.3
96R	8 Sept.	1400	1000.4–1010.0	9.6	1.59	16.5
97R	8 Sept.	1615	1010.0–1019.7	9.7	1.27	13.1
98R	8 Sept.	1820	1019.7–1029.2	9.5	2.26	23.8
99R	8 Sept.	2040	1029.2–1038.8	9.6	1.69	17.6
100R	8 Sept.	2250	1038.8–1048.4	9.6	2.32	24.1
101R	9 Sept.	0140	1048.4–1052.7	4.3	2.30	53.5
102R	9 Sept.	0455	1052.7–1058.0	5.3	5.45	103.0
103R	9 Sept.	0830	1058.0–1061.8	3.8	4.34	114.0
Coring totals				976.8	604.77	61.9

min/m, and the siltstone cores became distinctly harder. The combination of events suggested a potential for penetration of successive slightly pressured permeable zones under cap rock seals.

5. Gas was observed bleeding from pores in Core 151-909C-101R, and the core had a much stronger petroleum odor.
6. Kerogen slides indicated a large amount of thermally mature kerogen, and total organic carbon increased from 1.0% to 2.6%.

Resistivity logs indicated that a 7-m-thick sandy unit at 931 mbsf has a 1-m slightly permeable zone, but unprocessed resistivities never exceeded 1.5 Ω/m; therefore, liquid hydrocarbons are not evident in the hole, based on logs.

The hole had been filling rapidly. The open drill string was run to 491 mbsf, where a 150-sack (41 m thick) plug of cement was set from 491 to 440 mbsf. The hole was also loaded with heavy mud. The BHA cleared the rotary table at 1630 hr, 11 September, ending Hole 909C.

Ice Observations

After permission to drill proposed site YERM-1D was rejected, alternate sites were proposed South of that point along Line UB-2-79. The Norwegian Petroleum Directorate (NPD) approved site YERM-1E at sp 1590 on 1 September; therefore, the *Fennica* was directed to proceed immediately to check out the ice conditions there. At 1900 hr, 1 September, the *Fennica* reported that YERM-1 was 3 nmi inside heavy pack ice, YERM-1C was covered by an ice tongue, YERM-1D was clear and 6 nmi from the ice edge. The edge of the ice was 1 nmi South of YERM-1E and moving South at an average speed of 0.4 kt, with North-Northwest winds. The leading edge was 0.1 nmi wide consisting of 30% cover of brash ice with 4-m-thick pack ice behind it. The average edge of the pack ice was 80°5′N between 6 and 8°E.

The *Resolution* was at Hole 909C, so the *Fennica* was recalled to deliver the NDR German TV crew for pickup by helicopter on 5 September. *Fennica* reported an ice field 50 nmi North-Northwest of Site 909 moving Southeast at 1.0 kt under a force-8 gale. The gale had Northwest winds to 41 kt with a strong 1.0-kt Northeast current, and the 8-nmi × 2-nmi ice field passed 17 nmi west of Site 909 on 4 September, moving Southwest at 1.0–1.4 kt. The ice field began to disperse under the heavy winds.

Helicopter Rendezvous

The Bell 406 helicopter from Longyearbyen, Svalbard, arrived at 1118 hr, 5 September, carrying Dr. Phil Rabinowitz and John Beck from ODP, and a dynamic-positioning instructor and computer technician for the *Fennica*. The TV crew took videos of the *Resolution* and *Fennica* from the air, and the helicopter was refueled. The helicopter departed for Longyearbyen at 1326 hr with the three TV crewmen. The four incoming personnel were transferred to the *Fennica*.

Ice Observations

The *Fennica* returned to ice patrol and on 6 September reported the edge of the ice pack was 27 nmi Northwest of Site 909. Site 912 was ice free, but YERM-1E was 31 nmi inside the ice edge. At 80°27′N, 7°37′E, *Fennica* reported 20-m × 10-m × 6-m-thick blocks of ice, so the Scott Polar Research Institute scientists were permitted to work on the ice. The *Fennica* proceeded West into the ice to 80°38′N, 8°34′E on 7 September, where it reported 50-m × 20-m × 6-m blocks of ice; the scientists were again allowed to work on the ice.

Hole 909C was nearing total depth; therefore, the *Fennica* was sent to Site 912 to report on the ice conditions. On 8 September, at 1630 hr, *Fennica* reported that Site 912 had scattered small ice on location, but it was accessible. Heavy ice with 80% cover was 9 nmi Northwest, and blue ice with 10%–20% cover was 10 nmi Northeast. *Fennica* was sent to check Site YERM-5 and gather ice sediment samples. On 9 September, *Fennica* was at 79°5′N, 1°5′E, and the ice scientists were permitted to work on a 0.5-nmi × 1-nmi ice field.

Coring operations were terminated at Site 909 on 9 September; therefore, the *Fennica* was sent to Site 912 and YERM-1E to check on ice conditions. At 1700 hr, *Fennica* reported heavy ice 10 nmi Northwest of Site 912 and small fields 9 nmi Northeast of it. At 0800 hr, 10 September, *Fennica* reported at 80°N, 6°37′E that YERM-1E was in heavy ice. The ice edge was at 80°50′N, 7°13′E, with a big ice tongue leading Southwest. Site EGM-2 was being considered for the next site because of the ice situation, but approval was granted by ODP to keep *Fennica* an additional three days if necessary. We decided to risk a return to the ice-infested waters at Site 912 with the intention of RCB-coring a deep hole. Approval had been granted to core to 1050 m at Site 912.

LITHOSTRATIGRAPHY

Introduction

Three lithologic units make up the 1061.8-m-long sediment column drilled at Site 909 (Table 2). All three units contain sediments composed primarily of fine-grained siliciclastics. They are distinguished by differences in texture and composition (Fig. 2), as well as bedding, color, and minor biogenic constituents. The dominant lithology throughout is silty clay. Clay, clayey silt, clayey mud, and silty mud are also present. Minor lithologies containing a variety of inorganic carbonates form thin layers and nodules. These carbonate clays and carbonate-bearing silty clays are common below 45 mbsf in Holes 909A and 909B, and throughout 909C (Fig. 2). Biogenic sediments are largely absent; no more than trace to very minor components are present within limited intervals.

Lithologic Unit I occupies the entire length of Holes 909A and 909B, and the interval from the first core at 85 mbsf to a depth of 248.8 mbsf in Hole 909C. The unit is characterized by contrasting textures, a range of colors, and the presence of dropstones and Fe-monosulfides.

A 38.7-m interval of negligible recovery separates Unit I and Unit II. The upper boundary of lithologic Unit II is placed at 287.5 mbsf. Below this depth, dropstones are rare to absent, and pyrite is the most common Fe-sulfide. Sediments within Unit II are largely homogeneous.

The boundary between lithologic Unit II and Unit III is placed at 518.3 mbsf, based on the presence of laminations in Unit III. Much

Table 2. Summary of lithostratigraphic units, Site 909.

Unit	Dominant lithology	Interval, mbsf (thickness, m)	Age	Occurrence (hole-core-section)
I	Interbedded clay, silty clay, and clayey mud. Defined by the presence of dropstones Ø≥1.0 cm. Upper 50 m contains minor amounts of calcareous nannofossils. Fe mono-sulfides and color banding throughout.	0–248.8 (248.8)	Quaternary–Pliocene	909A-1H-1 through 16H-CC 909B-1H-1 through 11H-CC 909C-1R-1 through 17R-CC
II	Silty clay and clayey silt. Pyrite is common.	248.8–518.3 (269.5)	Pliocene–Miocene	909C-18R-1 through 45R-CC
IIIA	Silty clay, clayey silt, clayey mud, carbonate-bearing silty clay, and carbonate clay. Characterized by meter-scale intervals of thin bioturbated layers and laminations.	518.3–923.4 (405.1)	Miocene	909C-46R-1 through 87R-CC
IIIB	Silty clay, clayey silt, clayey mud, and silty mud. Characterized by commonly folded and deformed bedding.	923.4–1061.8 (138.4)	Miocene-u. u. Oligocene?	909C-88R-1 through 103R-CC

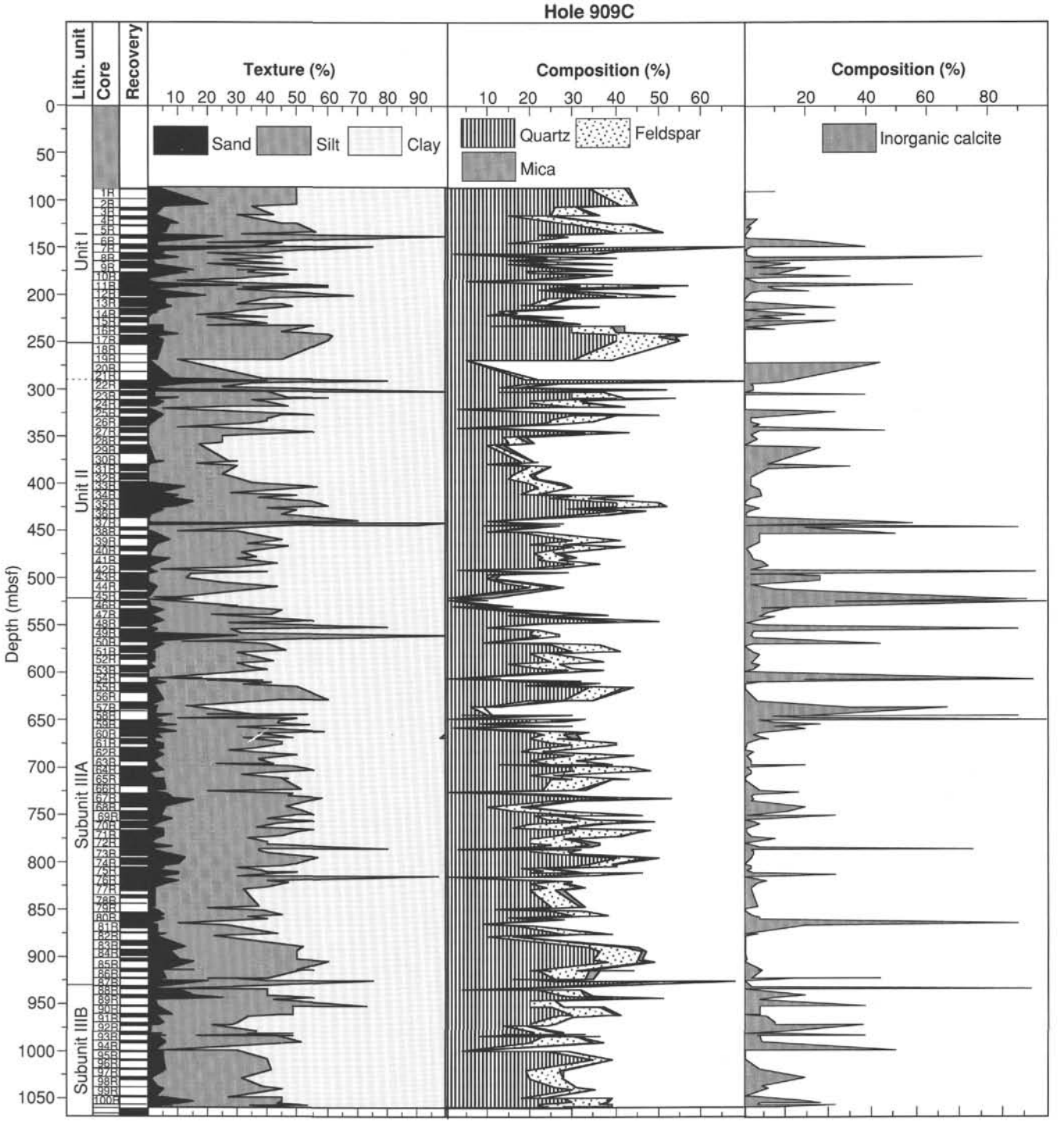

Figure 2. Lithostratigraphic units with smear-slide estimates of sediment texture, major mineralogy and inorganic carbonate content vs. depth for deep Hole 909C.

of the sediment below this horizon contains thin beds. Unit III is subdivided into 2 subunits, with the lower unit containing intervals of contorted bedding and other slump structures.

Drilling disturbance is slight in Unit I and moderate in most of Units II and III, containing biscuit structures and fractures spaced at 3- to 30-cm intervals. Highly fractured intervals and drilling breccias become increasingly common toward the bottom of the hole. At the depth where well-defined bedding is first observed (518.3 mbsf), the bedding has an apparent dip of ~10°. The apparent dip increases with depth to a maximum near 30°. This is an artifact of borehole deviation and does not reflect the true dip of the beds (see "Downhole Measurements" section, this chapter).

Description of Lithologic Units

Unit I

Hole 909A, Sections 151-909A-1H-1, 0 cm, through -11H-6, 150 cm; Hole 909B, Sections 151-909B-1H-1, 0 cm, through -16H-CC, 45 cm; Hole 909C, Sections 151-909C-1R-1, 0 cm, through -17R-CC, 10 cm (0–248.8 mbsf)
Thickness: 248.8 m
Age: Quaternary to Pliocene

Lithologic Unit I consists of major amounts of siliciclastic and minor amounts of biogenic sediment. Silty clays and clayey silts constitute the most common lithologies. They are interbedded with silty muds, clayey muds, and clays. The coarser-grained lithologies are characterized by the presence of quartz/feldspar-dominated sand and silt, as well as dropstones (Table 3, Fig. 3). Most of the dropstones are sub-angular to rounded, clastic, sedimentary fragments, particularly black siltstones. A 5-cm-long solitary coral, apparently of Paleozoic age, was recovered out of place in Section 151-909B-16H-1, 2 cm. The finer-grained lithologies are carbonate clays and carbonate-bearing clays with a wide range of inorganic-carbonate concentrations, from 10% to nearly 100%.

Clear color boundaries and color banding are present throughout Unit I. Colors include olive, olive gray, dark olive gray, grayish brown, gray, dark greenish gray, dark gray, very dark gray, and black. The bands are not always associated with any observed mineralogical or textural contrasts, but sharp contacts are common between sediments of contrasting color and texture.

Calcareous nannofossils are found in limited concentrations (1%–7%) throughout the upper 50 m of the unit. Siliceous microfossils are rare. Diatoms and sponge spicules reach concentrations of 1% each in Section 151-909B-13H-6, 120 cm. Bioturbation is light to moderate, and is evident in the faintly mottled appearance and the occurrence of individual burrows. Many of the burrows are filled with black Fe-sulfides, which are also pervasive as concretions and diffuse patches.

Lithologic Unit II

Hole 909C, Sections 151-909C-18R-1, 0 cm, through -45R-CC, 20 cm, (248.8–518.3 mbsf)
Thickness: 269.5 m
Age: Pliocene to Miocene

Lithologic Unit II is characterized by thick beds of massive silty clays interbedded with thinner layers of carbonate-rich clays and silty clays. The silty clays contain approximately 60% clays. Quartz (~25%) and feldspars (5%–10%) are the other important constituents. Few clayey muds and no silty muds are present in Unit II. The sediments are generally homogeneous and very firm. Color changes are subtle, gradational, and less common than in Unit I. The colors include olive gray, dark gray, and very dark gray. In the upper 38.7 m (Sections 151-909C-18R-1 through -22R-1) recovery was limited to core catchers.

Dropstones were not found below 240.0 mbsf, with the exception of a single 1.8-cm mudstone recovered at the edge of a drilling biscuit in Section 151-909C-24R-5 (316.1 mbsf). Bioturbation is light to moderate throughout. Oblique sections of cylindrical burrows cut by the core-splitter contain loose quartz and feldspar grains. Soft, black, Fe-monosulfide concretions and diffuse pods are present but sparse. Nodular pyrite concretions, up to several centimeters in size, and disseminated pyrite grains are common.

Lithologic Subunit IIIA

Hole 909C, Sections 151-909C-46R-1, 0 cm, through -87R-CC, 20 cm, (518.3–923.4 mbsf)
Thickness: 405.1 m
Age: Miocene

Table 3. Occurrence of dropstones (>1 cm in diameter) at Site 909.

Core, section, interval top (cm)	Depth (mbsf)	Size (cm)	Lithology
151-909A-			
1H-1, 24	0.24	1.6	Angular white quartzite
1H-3, 30	3.30	1.7	Coal
1H-3, 73	3.73	2.5	Subangular flat gneiss
2H-1, 120	8.70	1.0	Black shale
2H-3, 19.5	10.69	1.0	Angular black sandstone
2H-3, 60	11.10	1.0	Slightly rounded black sandstone
2H-3, 88	11.38	1.5	Black shale
2H-4, 24	12.24	1.0	Rounded black sandstone
2H-4, 54		1.0	Sandstone
2H-4, 142	13.42	1.0	Phyllite (white and gray)
2H-5, 100	14.50	1.0	Black shale
2H-6, 13		2.0	Coal
3H-1, 27	17.27	1.5	Siltstone
3H-1, 118	18.18	1.5	Shale?
3H-2, 65	19.15	1.0	Coal
3H-2, 76	19.26	1.5	Coal
3H-2, 133	19.83	1.4	Sandstone
3H-4, 30	21.80	5.0	Siltstone
3H-5, 112	24.12	2.0	Quartzite
4H-1, 96	27.46	1.0	Coal
4H-2, 17	28.17	1.7	Coal
4H-2, 104	29.04	1.2	Gray quartzite
4H-2, 104	29.04	1.1	Gray quartzite
4H-3, 67	30.17	1.1	Coal
4H-3, 129	30.79	1.6	Coal
4H-4, 115	32.15	1.0	Yellow limestone
4H-4, 115	32.15	1.0	Light gray quartzite
4H-5, 110	33.60	1.0	Pink granite
4H-6, 64	34.64	1.0	Black siltstone
4H-6, 127	35.27	1.0	Yellow limestone
4H-6, 128	35.28	1.0	Brown sandstone
4H-7, 22	35.72	1.7	Black metamorphic
4H-7, 29	35.79	1.6	Black metamorphic (split?)
5H-1, 63	36.63	1.0	Siltstone
5H-1, 104	37.04	2.0	Quartzite
5H-5, 98	42.98	3.0	Slightly rounded siltstone
6H-1, 51	46.01	1.0	Coal
6H-1, 95	46.45	5.0	Limestone
6H-1, 139	46.89	1.5	Gray limestone
6H-2, 17		1.7	Coal
6H-2, 36	47.36	1.0	Gray quartzite
6H-7, 97	53.97	3.0	Mesozoic?
7H-4, 116	61.16	1.6	—
7H-7, 134	64.50	1.0	—
7H-CC, 23		1.0	—
8H-2, 21	66.71	1.0	Dolostone
8H-3, 96	68.96	3.0	Basaltic?
8H-5, 25	70.75	1.5	Quartzite
8H-7, 84	73.04	3.5	Basaltic?
9H-2, 86	76.36	1.2	Black siltstone
9H-3, 42	77.42	1.2	Light gray siltstone
9H-3, 108	78.08	1.4	Sandstone
9H-3, 132	78.32	4.5	Schist
11H-2, 71	86.71	1.5	Siltstone
11H-3, 61	88.01	1.0	Dolostone
11H-6, 53	91.93	2.0	Sandstone
11H-6, 60	92.00	1.5	Quartzite
11H-CC, 10	93.30	1.5	Dolostone
151-909B-			
2H-1, 39	4.79	32.0	Sandstone
2H-2, 1	5.91	8.0	Granodiorite
2H-3, 97	8.37	3.0	Shale
2H-6, 116	13.06	1.5	Slate/shale?
3H-5, 140	21.30	1.0	Coal
3H-6, 53	21.93	5.0	Quartz
4H-1, 98	24.38	2.5	—
4H-1, 136	24.76	4.0	Coal
4H-4, 135	29.25	5.0	Siltstone
4H-5, 65	30.05	3.0	Quartzite
4H-6, 14	31.04	1.5	—
5H-1, 70	33.60	2.0	—
5H-2, 92	35.32	2.5	Siltstone
5H-2, 134	35.74	1.0	—
5H-3, 148	37.38	2.5	—
5H-4, 80	38.20	3.5	Siltstone
5H-6, 70	41.10	1.0	Siltstone
5H-7, 51	42.41	2.0	Siltstone
6H-1, 10	42.50	1.5	Coal
6H-2, 53	44.43	5.0	—
6H-3, 26	45.66	2.0	Coal
6H-4, 16	47.06	2.0	Siltstone
7H-1, 46	52.36	1.5	Siltstone
7H-1, 72	52.62	2.0	Siltstone
7H-2, 42	53.82	2.0	Siltstone
7H-2, 101	54.41	3.0	Siltstone
7H-3, 106	55.96	3.0	Siltstone
7H-4, 145	57.85	3.5	Siltstone
7H-7, 61	61.51	1.5	Coal

Table 3 (continued).

Core, section, interval top (cm)	Depth (mbsf)	Size (cm)	Lithology
7H-CC, 17	61.85	1.0	Plutonic, sand
9H-2, 111	73.51	1.0	—
9H-3, 19	74.09	1.5	Siltstone
10H-1, 26	77.66	1.0	Black limestone
10H-1, 129	78.69	1.2	Buff dolostone
10H-2, 34	79.24	1.6	Coal
10H-2, 78	79.68	1.2	Coal
10H-3, 31	80.71	1.6	Coal
10H-5, 27	83.67	1.3	Black
10H-7, 59	86.99	3.0	Coal
10H-CC, 5	87.34	2.0	Shale
11H-3, 65	90.55	3.0	Carbonate cemented siltstone
11H-4, 50	91.90	1.5	—
11H-5, 10	93.00	3.0	Carbonate
11H-5, 116	94.06	1.0	Shale
11H-6, 110	95.50	2.0	Pyritized shale
11H-CC, 36	97.19	2.0	—
12H-CC, 15	101.52	4.5	Sandstone
13H-6, 15	107.85	1.5	Sandstone
14H-1, 47	111.47	1.0	Shale/slate?
14H-2, 83	113.33	1.0	Shale
14H-4, 99	116.49	4.0	Siltstone
15H-1, 44	120.14	2.0	Claystone
15H-1, 137	121.07	1.7	Quartz
15H-5, 26	125.96	2.0	Quartz
16H-1, 8	127.98	5.0	Solitary coral (in place?)
151-909C-			
1R-1, 80	85.8	1.0	Rounded siltstone
4R-1, 41	114.31	2.6	Igneous
4R-2, 54	115.94	2.8	Sandstone
6R-3, 123	134.43	4.0	Dolostone
7R-1, 2	142.92	3.8	Rounded black siltstone
7R-1, 20	143.1	4.1	Subrounded black siltstone
7R-1, 121	144.11	4.3	Cross-laminated black siltstone
7R-2, 147	145.87	1.1	Angular black siltstone
7R-3, 9	145.99	3.1	Carbonate concretion
7R-4, 57	147.97	1.5	Fractured carbonate mudstone
8R-3, 63	156.13	3.5	Flat semi-angular siltstone
8R-4, 74	157.84	6.0	Flat sandstone, dark
8R-5, 107	159.67	5.0	Rounded sandstone
9R-1, 54	162.84	2.5	Mafic, gabbro?
9R-1, 67	162.97	1.3	Subrounded black siltstone
9R-3, 72	166.42	5.8	Iron-rich sandstone
9R-4, 114	167.94	3.4	Coal
9R-4, 124	168.04	3.6	Rounded sandstone
9R-5, 9	168.39	3.3	Gray siltstone (quartzite)
9R-5, 14	168.44	5.2	Gray sandstone (quartzite)
10R-2, 121	174.66	2.2	Sandstone
10R-5, 96	178.86	1.5	Siltstone
10R-6, 34	179.74	1.2	Siltstone
10R-7, 31	181.05	3.5	Metamorphic
11R-2, 83	183.93	1.1	Metamorphic
11R-5, 74	188.34	2.5	Siltstone
12R-1, 36	191.56	2.5	Sandstone
12R-1, 45	191.65	1.5	Sandstone
12R-5, 28	197.48	1.0	Siltstone
13R-1, 90	201.7	6.0	Altered volcanic
13R-3, 11	203.91	2.5	Shale
13R-3, 32	204.12	1.0	Sandstone
15R-1, 141	221.41	1.8	Coated mudstone
15R-2, 17	221.77	1.0	Sandstone
15R-2, 134	222.94	1.5	Siltstone
16R-3, 73	233.33	1.5	Coal
24R-5, 146	314.26	1.8	Black siltstone (in place?)

Note: — = lithology not defined.

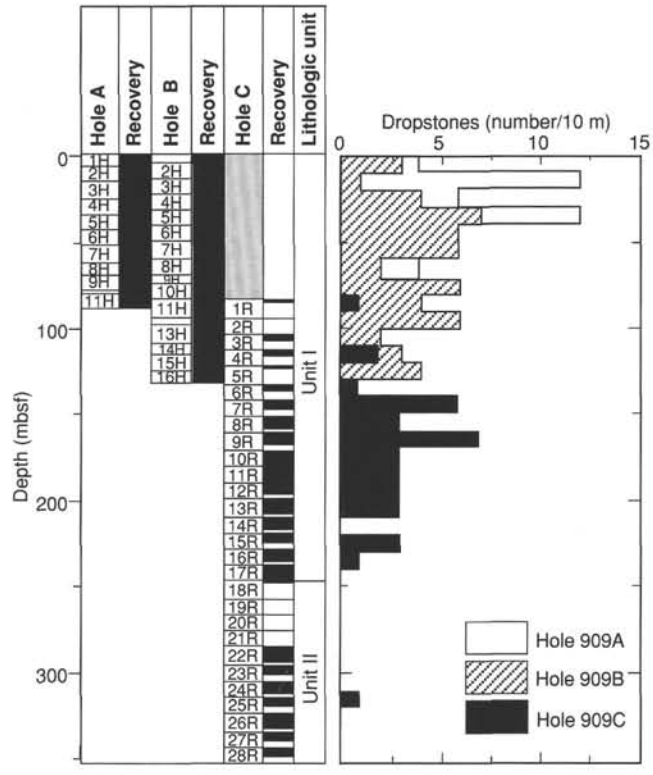

Figure 3. Occurrences of dropstones (>1 cm in diameter) per 10 m of core vs. depth for Holes 909A, 909B, and 909C.

Subunit IIIA is dominated by very dark gray silty clay and, with the exception of Core 151-909C-80R where a clay bed is present, contains coarser sediment at the base than at the top. The base of the subunit is placed at the top of the slump structures.

Clayey silt is present in minor amounts throughout. Beginning in Core 68R (730 mbsf) and continuing to the base of the subunit, clayey mud is also present as both a major and minor lithology. The clayey mud in Core 68R forms a thick, very dark gray layer, and minor thin layers of very dark greenish gray. Thin layers of very dark greenish gray silty clay and clayey mud are also present in Core 70R (749.6–759.3 mbsf). In Core 72R (769.0–778.7 mbsf) the silty clay is dark greenish gray and very dark grayish brown, as well as very dark gray. The coarsest sediment in this unit, very dark gray silty mud, is present in laminae in Sections 151-909C-84R-3 through -84R-CC. The minor lithologies are dominated by sediments with carbonate contents above 10%, primarily in laminae. Several meter-thick intervals of carbonate and carbonate-bearing sediments, as well as concretions, also are present. Some of the carbonate includes dolomite and siderite.

The coarse fraction is dominated by quartz but also includes 2%–14% feldspar, although generally less than 10%, and a few percent of mica, carbonates, glauconite, accessory minerals, and opaques, primarily sulfides as rhombs, framboids, and irregular clasts. Clay minerals include smectite, illite, kaolinite, and chlorite. Agglutinated recrystallized calcareous benthic foraminifers are observed in the coarse fraction (>63 μm) and on the surface of the split core.

The most striking feature of this subunit is the extensive lamination and bioturbation. Laminae are composed of millimeter-scale, compositional, grain-size and/or color changes (Fig. 4). The different types of laminae may be present within a short interval of the core, (e.g., 20 cm), although they are more likely to be separated by intervals of moderate to heavy bioturbation. The laminations are in part identified by the fissility of the sediments and the irregular sawtooth edge on the cores, somewhat like the weathering of sedimentary rocks. Variation in drilling disturbance as a result of sediment heterogeneity is not uncommon. In this case, however, in contrast to weathering, coarser grains are slightly more likely to be in the narrower parts of the core and at the inflection points.

In some cases, the lighter, browner laminae (brown, dark grayish brown, grayish brown, olive gray, light brownish gray) have carbonate concentrations that exceed those of adjacent darker laminae by more than 10%. The carbonate-rich laminae are commonly clay rather than silty clay, although in Core 73R (778.7–783.3 mbsf) dark grayish brown carbonate silt laminae and burrows are present. Intervals of carbonate clay greater than 10 cm thick are laminated. Clay composed solely of noncarbonate grains was observed only in this subunit in Core 80R.

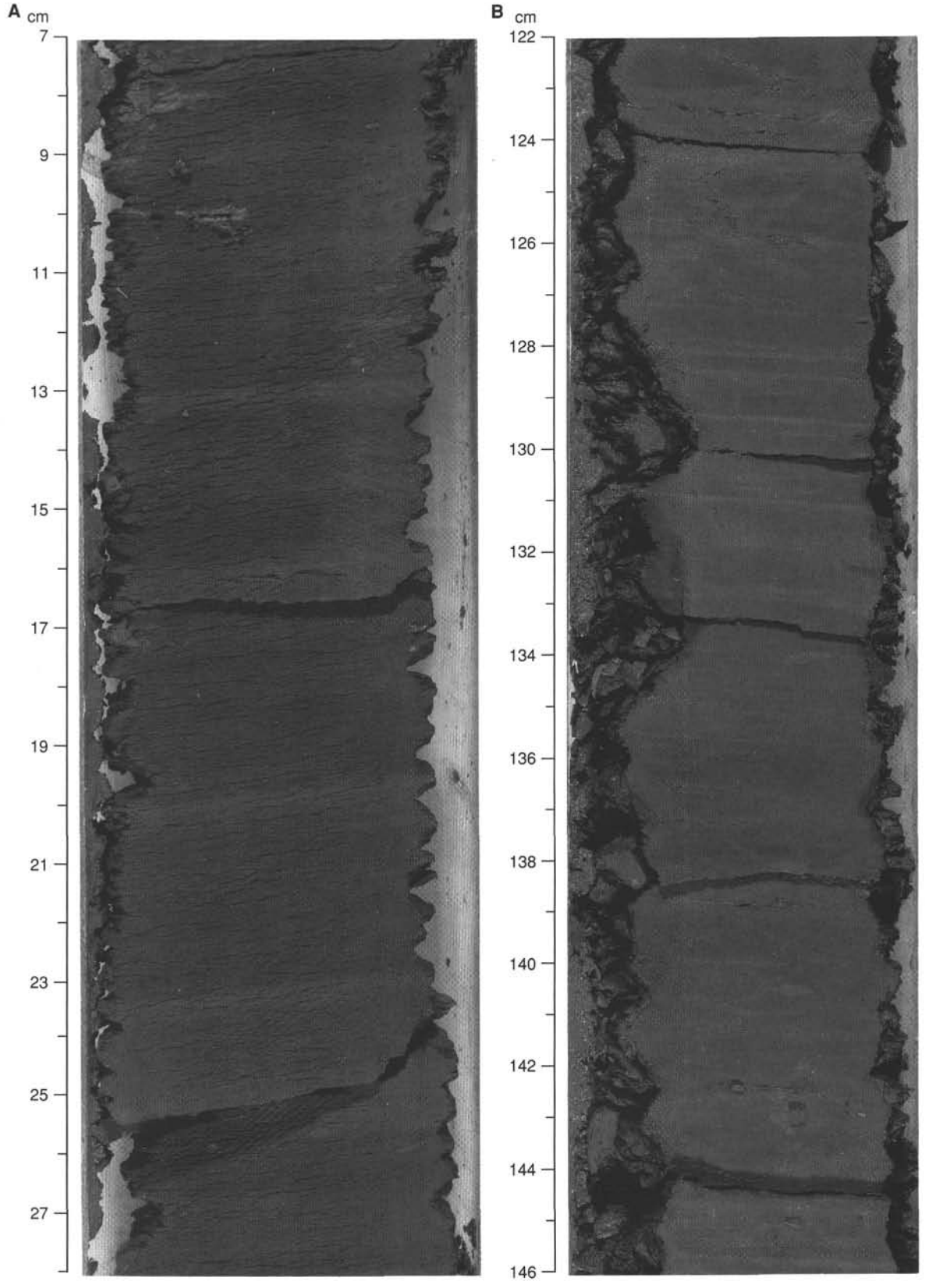

Figure 4. **A.** Interval 151-909C-48R-2, 7–28 cm, laminations defined by minor color and grain size changes and fissility. **B.** Interval 151-909C-50R-2, 122–146 cm. Laminations defined primarily by color changes.

Laminae also are composed of coarse silt, commonly only a grain or two thick. These laminae may be continuous or discontinuous, and are composed primarily of quartz.

Color changes are common. Very dark gray laminae are interlayered with brown, dark grayish brown, grayish brown, olive gray, and light brownish gray laminae. These thin color bands have both gradational and sharp upper and lower contacts. In these laminae, although the changes appear to be primarily in color, the association of lighter colored laminae with somewhat less eroded parts of the core suggests more drilling-resistant, indurated sediment.

Bioturbation is present throughout almost the entire section. Even in intervals with the best-developed laminae there are rare burrows. In some areas, the homogeneity of color and composition of this subunit precludes any distinction between extreme bioturbation and homogeneous sedimentation. Many originally laminated intervals appear extensively bioturbated, but burrows that parallel the bedding appear to enhance rather than obscure the laminations. Changes in the intensity of bioturbation are gradational (Fig. 5), with the most extensive bioturbation affecting 5- to 20-cm-thick intervals.

Distinct trace fossil burrows can be identified and include *Chondrites, Zoophycos, Planolites, Teichichnus*, and one composite burrow. Smaller distinct burrows (1–5 mm) are commonly filled with white quartz silt and sand. Carbonate (clay, silt, and mud) is the dominant burrow-filling component of the larger (>0.5 cm) burrows. Pyrite fills burrows of all sizes. Some pyritized burrows have coarser, yellower grains in the center, and finer, softer, more silvery grains along the rim.

Lithologic Subunit IIIB

Hole 909C, Sections 151-909C-88R-1, 0 cm, through -103R-CC, 20 cm, (923.4–1061.8 mbsf)
Thickness: 138.4 m
Age: Miocene to upper upper Oligocene)

Below 923.4 mbsf, meter-scale intervals of bioturbated, thin, subparallel beds are punctuated by meter-scale intervals containing slump structures (Figs. 6 and 7). The slumps exhibit millimeter- to tens of centimeter-scale folds, rip-up clasts, pinched and tilted layers, and sharp basal contacts. Some disturbed layers have sharp upper contacts. Contorted layers are also present within some of the clasts. Bioturbation is absent from the thickest slumps, and is moderate to extensive elsewhere.

Sediments within Subunit IIIB have a wide range of textures from clay to silty mud. The thin, less-disturbed bedding is similar in color and texture to those seen in the overlying unit. Colors include grayish brown, dark olive gray, dark greenish gray, dark gray, and very dark gray.

Sand-sized particles can be seen along the split core, and disseminated pyrite and glauconite grains are common. Agglutinated and rare calcareous benthic foraminifers are present. The calcareous foraminifers appear decalcified, whereas many of the agglutinated forms are fragmented.

Interpretation

Subunit IIIB

The thin planar bioturbated beds of Subunit IIIB are similar in texture, color, and composition to those of the overlying Subunit IIIA. They likely represent most of the time interval associated with the deposition of Subunit IIIB. The slumps and flows were probably episodic events resulting in rapid sediment accumulation. Deformed yet continuous bedding, similar lithologies, and heterogeneous matrixes indicate transport of unlithified sediments, with some cohesion, over short distances. These events may be related to collapsing channel walls, although there is little other evidence for the local presence of

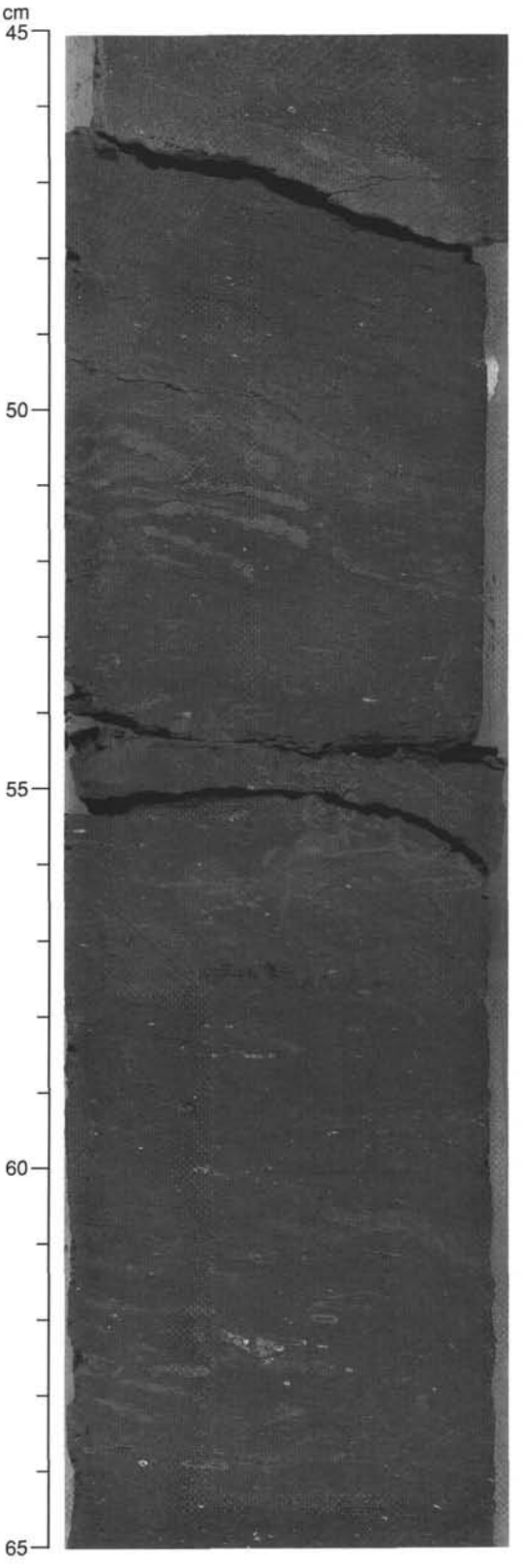

Figure 5. Interval 151-909C-68R-4, 45–65 cm. Bioturbation, poorly developed laminations, and shell fragments (especially prominent between 58 and 64 cm).

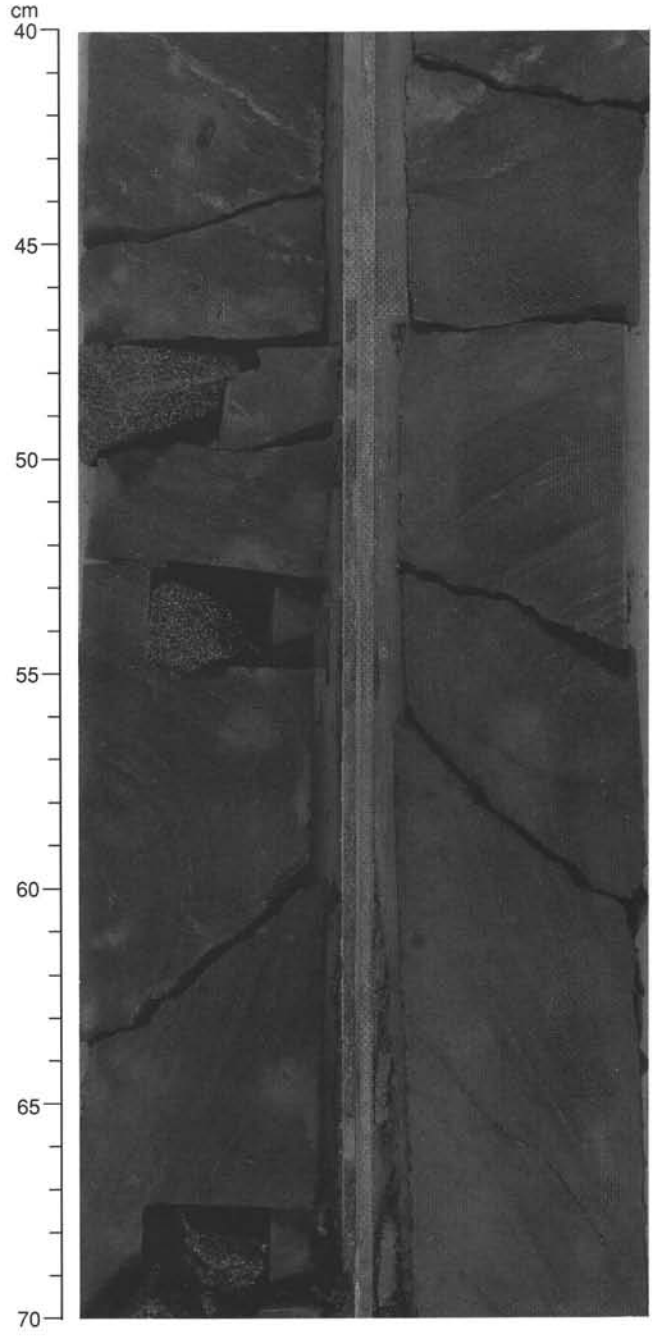

Figure 6. Interval 151-909C-102R-3, 40–70 cm. Folded bedding shown in archive and working half. Styrofoam plugs indicate location of samples taken from the working half. The upper beds appear inclined due to the borehole deviation from the vertical.

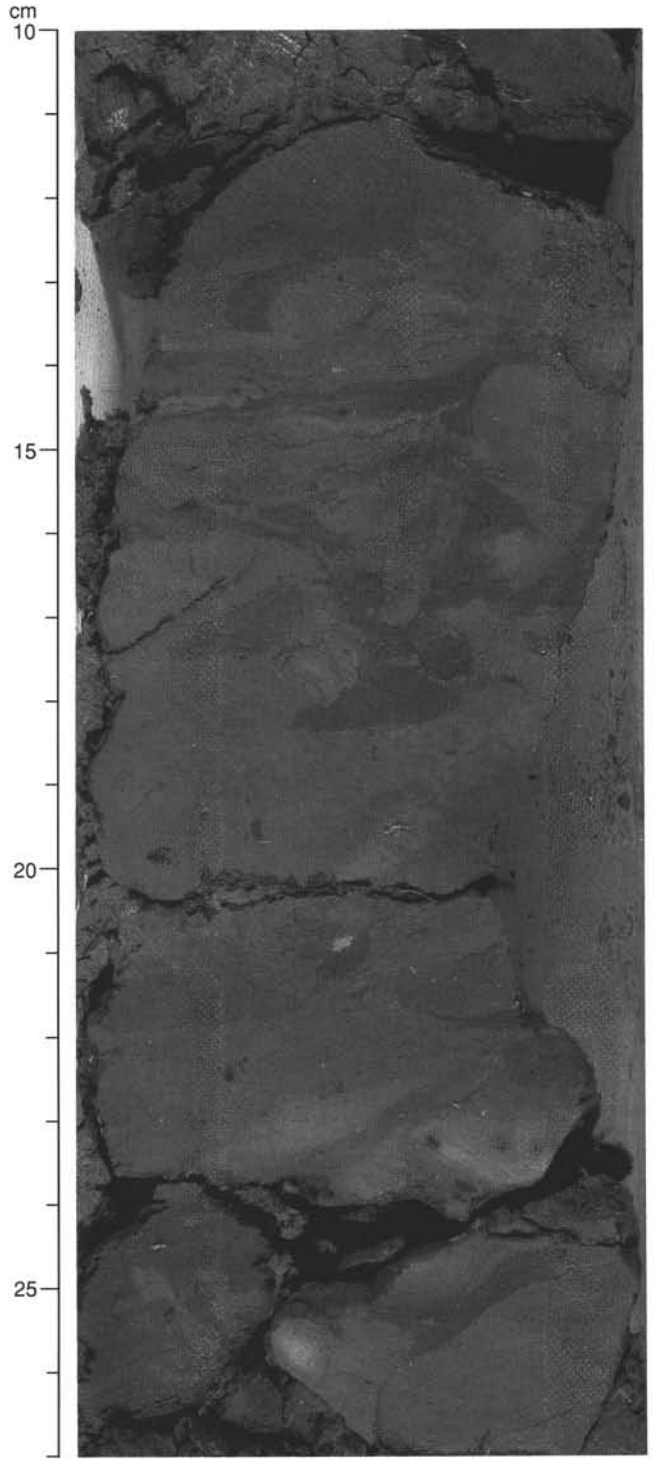

Figure 7. Interval 151-909C-94R-3, 10–27 cm. Slumped sediment with heterogeneous clasts and matrix.

channels. The slumps are more likely to be associated with relatively high sedimentation rates and small local textural differences. Such slumps may occur on slopes as gentle as 0.5° (Stow, 1986). Small earthquakes owing to local tectonic activity, would be sufficient to trigger downslope motion. Compaction and cementation have contributed to the subsequent lithification.

Subunit IIIA

The thin lineations that characterize Subunit IIIA reflect a record of variable, possibly rhythmic, depositional processes extending perhaps 15 million years. During this time the sediment composition, and to a slightly lesser extent texture, remained remarkably constant. This reflects some combination of: a single sediment source; relatively constant integration of multiple sources; or changes between source regions with sediments of similar composition. One possible explanation for the constancy of sediment type and the laminations is deposition in a relatively restricted basin, perhaps in shallow communication with the open ocean. Variable benthic activity has resulted

in a range of structures from well-defined laminations to extremely mottled and burrowed color bands. Changes in burrowing style and intensity reflect changing water column conditions such as surface productivity and bottom water oxygen content.

The lack of fossils is puzzling. Moderate to heavy burrowing and interruption of thin bedding attest to a vigorous benthos. Organic carbon concentrations are substantial, and a good fraction of the carbon rain was marine (see "Organic Geochemistry" section, this chapter). Therefore, the sediment contains some evidence of soft tissue burial, yet it is devoid of the siliceous and calcareous remains that typically dominate the marine sedimentary record. The sea surface evidently was warm and light enough to support some productivity, and the marine organic carbon in the sediment implies the availability of nutrients at the surface. Either conditions specifically inveighed against calcareous production, or productivity may have been relatively modest. Any limited production of biogenic calcite may have been dissolved by corrosive bottom waters or within the sediment column because of elevated CO_2 concentrations associated with the oxidation of organic matter. The widespread presence of pyrite and monosulfides is evidence that dissolved oxygen was depleted in the sediment pore waters. Agglutinated foraminifers provide additional support for the influence of calcite dissolution (Gooday, 1990). Minimal dissolved silica concentrations, however, indicate a different biosilica productivity regime throughout Unit III (see "Inorganic Geochemistry" section, this chapter). It is possible that silica was more limiting than phosphate and nitrate and thus strongly suppressed surface productivity of siliceous organisms in particular. In the case of a restricted basin, inflow of nutrient-depleted surface waters might have such an effect. Surface productivity generally may have been limited, with terrigenous material supplying the bulk of the organic carbon eaten by benthic organisms.

Tectonics may account for the sedimentary changes observed within Unit III. The split of Hovgaard Ridge from the Svalbard Platform beginning in the Oligocene (Myhre and Eldholm, 1988) would have contributed to episodic re-sedimentation at this site through earthquakes generated by strike-slip motion along the plate boundary, although the precise relative positions of ridge and basin are unclear. De-activation of the shear zone/transform during the Miocene (Crane et al., 1988) might account for the cessation of re-sedimentation seen in Subunit IIIA. The generally fining-upward character of Subunit IIIA from clayey muds to silty clays may in turn reflect the transition to seafloor spreading between Site 909 and Svalbard. An increasingly distal position relative to Svalbard, the likeliest source of sediment, might account for the textural evolution and compositional homogeneity. Alternatives to this interpretation are viable. They include the time-dependent erosion of different lithologies on Svalbard, and the varying influence of disparate source regions, including Greenland.

Lithologic Unit II

The sediments of Unit II record deposition in a less pronounced glacial to nonglacial climate. Fine-grained sediments predominate, indicating a hemipelagic setting. The absence of dropstones and coarse muds limits ice-rafting as an important transport mechanism. Massive beds of dark-colored silty clays containing few fossils reflect the delivery of terrigenous material from suspension. Somewhat lower potassium concentrations in Unit II than in Unit I (see "Inorganic Geochemistry" section, this chapter) are indicative of a change in source region or the relative importance of chemical and mechanical weathering. Both possibilities are likely related to diminished glacial grinding and ice transport. The high accumulation rate and substantial silt fraction probably indicate a nearby source of terrigenous material.

Microfossil evidence of surface productivity is not found in Unit II. As in all sediments from Site 909, organic carbon concentrations are high. At least some bioturbation is evident in the form of discrete burrows throughout the unit, indicating oxygenated bottom water. Dissolved silica concentrations imply some dissolution of biogenic opal within the pore water. A likely explanation for the limited biosilica involves moderate surface productivity, with dilution by siliciclastics and post-depositional dissolution. The absence of calcareous microfossils in Unit II is probably due to conditions similar to those during the deposition of Unit III. The deposition of Unit II apparently preceded the glacial onset and any associated environmental degradation, and marine organic carbon indicates available, if not abundant, nutrient supply. Any calcareous production in the surface waters was more than matched by dissolution caused by corrosive bottom and interstitial water. The oxidation of buried organic matter probably released sufficient dissolved CO_2 to leave pore waters highly undersaturated with respect to $CaCO_3$.

Lithologic Unit I

Lithologic Unit I is interpreted to contain the marine record of glacially derived terrigenous sediments delivered by ice-rafting during the Pliocene and Quaternary. Layers containing poorly sorted sediment including sand and individual stones as large as 6.0 cm indicate at least a seasonal presence of detritus-bearing ice. Icebergs and sea ice are both feasible delivery mechanisms, and the relative importance of the two remains controversial (e.g., Clark and Hanson, 1983; Wollenburg, 1993). Dropstones serve as the least ambiguous indicator of ice-rafted debris (IRD). Based on the initial appearance of dropstones, the onset of glacial conditions is recorded at Site 909 at approximately 3.5 Ma (see "Paleomagnetics" and "Biostratigraphy" sections, this chapter). This age, although preliminary, is nevertheless nearly 1 million years older than the substantial increase in IRD documented in the Norwegian Sea (Henrich et al., 1989b). Contrasts in texture and color throughout Unit I, and particularly in the upper portion, reflect extreme climatic variability during the late Quaternary.

Calcareous nannofossils in Unit I may reflect warm interglacial periods, possibly related to the presence of North Atlantic surface water. Alternatively, the overall scarcity of calcareous microfossils and their absence below 50 mbsf may reflect dissolution and recrystallization of deposited calcite. These processes also may account for the presence of the inorganic carbonate that occurs within all units (Fig. 2). Coarser recrystallized carbonate, (silt-sized) dolomite, and siderite were recovered in layers and concretions at depth, strengthening the case for a diagenetic origin.

BIOSTRATIGRAPHY

Introduction

Site 909 was drilled with the objectives of constraining the timing of the opening of Fram Strait and the history of deep- and shallow-water mass exchange between the Arctic Ocean and the North Atlantic Ocean. Calcareous microfossils and dinoflagellate cysts, recovered from three holes at Site 909, indicate a Quaternary through Miocene (and possibly upper upper Oligocene) sequence (Fig. 8). Siliceous microfossils are either absent or consist of rare, reworked specimens. Calcareous nannofossils and planktonic foraminifers provide good biostratigraphic control in the upper 300 m of the Quaternary–Pliocene section. These fossil groups are absent in the deeper sections of the site, with the exception of a lower Miocene/upper upper Oligocene nannofossil assemblage at the bottom of Hole 909C. Continuous occurrences of rare to few dinoflagellate cysts below Core 151-909C-23R provide a Miocene age for this interval. Diverse and abundant assemblages of agglutinated benthic foraminifers are found below Sample 151-909C-52R-CC. According to calcareous nannofossil data from the base of the hole, this interval correlates to

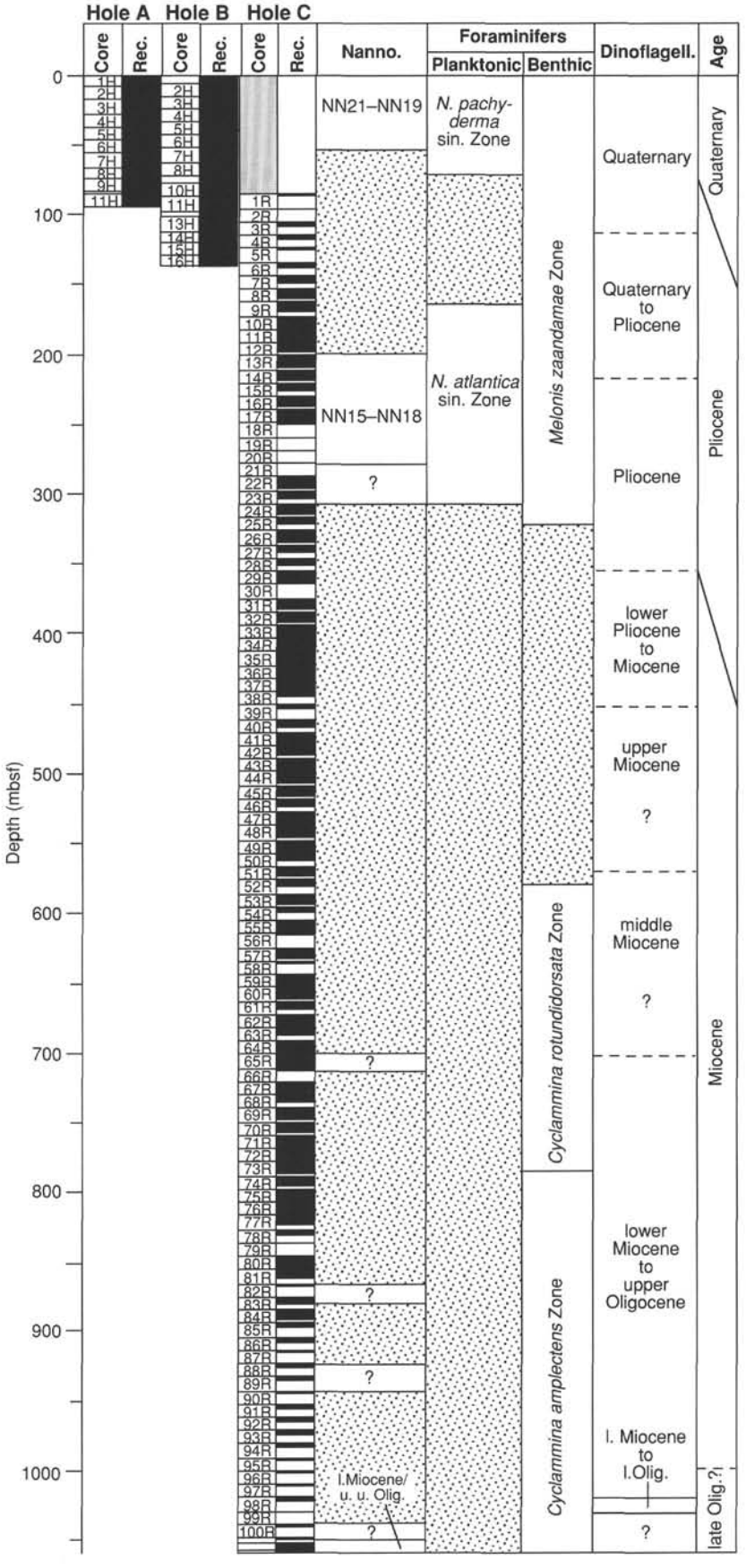

Figure 8. Biostratigraphic zonation and correlation of the different microfossil groups present at Site 909.

Table 4. Distribution of calcareous nannofossils in Cores 101R and 102R, Hole 909C.

Age	Sample	Abundance	Preservation	Small coccolith gen. sp. indet.	*Braarudosphaera bigelowi*	*Coccolithus pelagicus*	*Coccolithus miopelagicus*	*Dictyococcites bisectus*	*Dictyococcites* sp. (small)	*Cyclicargolithus abisectus*	*Helicosphaera carteri*
early Miocene	101R-2, 26 cm	C	P	C		R	R		R	R	R
	101R-CC	R	P	R	R	R					
or	102R-1, 35 cm	C	P	C		R	R		R	R	R
	102R-2, 77 cm	R	P	R							
	102R-3, 35 cm	C	P	C		R	R	R	R	R	R
latest Oligocene	102R-CC	C	P	C	R	R	R	R	R	R	R

the lowermost Miocene/uppermost Oligocene. Therefore, this agglutinated foraminiferal fauna is younger than similar assemblages recorded from the Oligocene and Eocene sediments of the North Sea, Labrador Sea, and the Vøring Plateau.

Diatoms

Diatoms are virtually absent in samples from Site 909. Smear slides were examined from all core-catcher samples, as well as from selected intervals in cores from Holes 909A and 909C. Very rare and poorly preserved diatom debris was recognized in Sample 151-909B-13H-CC, prompting additional preparation (see "Explanatory Notes" chapter, this volume). Slides of Sample 151-909B-13H-CC include heavily silicified, long-ranging diatoms, such as *Paralia sulcata* and *Stephanopyxis turris*, and rare unidentified species that are probably Eocene or older, indicating reworking in the section.

Silicoflagellates

No silicoflagellates were observed in diatom slides from Site 909.

Radiolarians

Core-catcher samples from Site 909 are barren of age-diagnostic radiolarians with the exception of a single specimen of *Stylotractus universus* in Sample 151-909B-9H-CC. *S. universus* is a cosmopolitan species, ranging from the middle Miocene (or older) to 0.42 Ma (Morley and Shackleton, 1978). Rare, infilled, and recrystallized specimens of *Actinomma*, *Stylodictya*, *Prunopyle*, and spongodiscids occur sporadically from Core 151-909C-6R through Core 151-909C-62R.

Calcareous Nannofossils

All core-catcher samples and some additional samples from Hole 909C were examined for calcareous nannofossils. Preservation is good and abundance is moderately high in Core 151-909A-1H; nannofossils are rare or absent below Sample 151-909A-1H-CC. Reworked specimens from the Cretaceous and Paleogene occur in the upper sequences of Holes 909A and 909B.

Emiliania huxleyi, which indicates the presence of the upper Quaternary NN21 Zone, occurs in Samples 151-909A-1H-1, 100 cm, through -1H-4, 120 cm. Samples from 151-909A-1H-5, 13 cm, through -2H-6, 20 cm, are barren. *Pseudoemiliania lacunosa*, which defines the top of the NN19/NN20 zonal boundary, is present with *Gephyrocapsa* spp. from Samples 151-909A-2H-CC through -6H-2, 14 cm. These samples therefore are correlated to the Quaternary NN19 Zone. Samples from 151-909A-6H-CC through -11H-CC contain rare calcareous nannofossils, or are barren.

In Hole 909B, *Gephyrocapsa* spp. occurs in Sample 151-909B-1H-CC; all other samples from Hole 909B are barren of nannofossils.

Nannofossils are not present in Samples 151-909C-1R-CC through -12R-CC. Samples 151-909C-13R-CC through -20R-CC are characterized by an abundance of *Crenalithus doronicoides*, co-occurring with *P. lacunosa* and *Helicosphaera sellii*. These assemblages indicate the middle to upper Pliocene NN15 to NN18 Zones. In the interval from Sample 151-909C-21R-CC through -100R-CC, nannofossils are absent, with the exception of a few samples that contain a few poorly preserved specimens.

Samples 151-909C-101R-2, 26 cm, -102R-1, 35 cm, -102R-3, 35 cm, and -102R-CC, contain common, moderate to poorly preserved nannofossils (Table 4). Species include *Coccolithus miopelagicus*, *Cyclicargolithus abisectus*, and *Helicosphaera carteri*, which are correlated to the lower Miocene. However, specimens of *Dictyococcites bisectus*, which ranges from the middle Eocene to the Oligocene, occur in Samples 151-909C-102R-3, 35 cm, and -102R-CC. If these specimens of *D. bisectus* are not reworked, the age of these samples may extend into the uppermost Oligocene. If the sediments are upper Oligocene, rather than lower Miocene, this would be the oldest recorded occurrence of *H. carteri*.

Planktonic Foraminifers

Core-catcher samples from Holes 909A, B, and C were processed and examined for foraminifers. Planktonic foraminifers were observed in the upper 300 m of the sequence. The preservation of planktonic foraminifers in this interval is good, although the diversity is generally low. Planktonic foraminifer abundance varies considerably, especially in the Quaternary successions.

The Quaternary *Neogloboquadrina pachyderma* sin. Zone is documented in Hole 909A from the top of the sequence down to Sample 151-909A-8H-CC, and in Hole 909B from Samples 151-909B-1H-CC through -3H-CC. Fifty-two additional samples were taken from the Quaternary sequence of Hole 909A, between Sample 151-909A-1H-1, 16 cm (0.16 mbsf), and Sample 151-909A-6H-1, 132 cm (46.82 mbsf), in an effort to better document the alternations of low and high planktonic foraminifer abundance. The number of specimens (in 10 cm^3 of sediment) ranges from zero to nearly 100,000 specimens in alternate samples, as shown in Figure 9. Such alternations seem to be typical of the changes between glacial and more interglacial conditions.

A barren interval separates the Quaternary *N. pachyderma* sin. Zone from the Pliocene *N. atlantica* sin. Zone. A similar barren zone is observed at Sites 907, 910, 911 and 912. This barren interval is documented in Sample 151-909A-9H-CC and in Samples 151-909B-4H through -16H-CC, as well as in Samples 151-909C-1R-CC through -8R-CC. The Pliocene *N. atlantica* sin. Zone is present from Samples 151-909C-9R-1, 86–88 cm, through -23R-CC. Planktonic

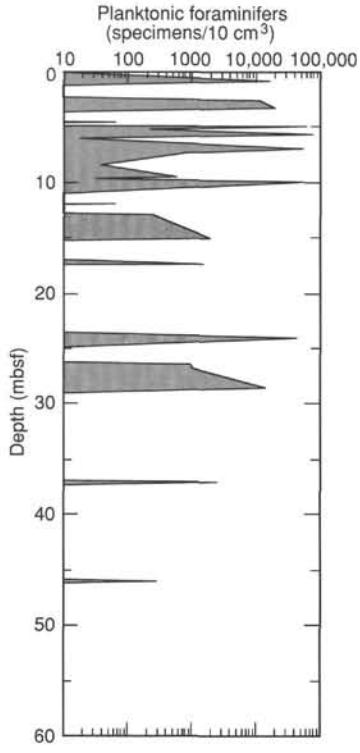

Figure 9. Alternations of low and high *Neogloboquadrina pachyderma* sin. abundances in Quaternary sediments from Hole 909A.

foraminifer species include *N. atlantica* sin. and *N. asanoi*. The latter species is more common in the Pacific region than in the Atlantic. All samples below 151-909C-23R-CC are barren of planktonic foraminifers.

Benthic Foraminifers

Benthic foraminifers were examined from the core-catcher samples of Holes 909A and 909C. The benthic foraminifers can be divided into two zones, separated by a barren interval. The upper zone found throughout Hole 909A and above Sample 151-909C-25R-CC consists of Quaternary and Pliocene species including *Melonis zaandamae*, *Cassidulina teretis*, *Elphidium* spp. and *Epistominella* spp. Rare agglutinated foraminifers occur at the base of this assemblage, from Samples 151-909C-7R-CC through -25R-CC. These agglutinated forms (1–2 specimens per sample) are assumed to be reworked because they are so rare and are similar to the agglutinated specimens found in the lower part of this hole. A barren interval occurs from Sample 151-909C-25R-CC through -52R-CC.

The lower part of Hole 909C is dominated by a diverse and abundant assemblage of agglutinated benthic foraminifers, which is found in almost all samples below Sample 151-909C-52R-CC. Single specimens of the calcareous foraminifer *Millionella* sp. also were found in Samples 151-909C-75R-CC, -81R-CC, and -100R-CC. Several agglutinated species, such as the tube forms *Hyperammina* spp. and *Reophax nodulosa*, are found consistently in the entire lower section. However, there is a clear stratigraphic zonation of the last occurrences of other species including, from bottom to top, *Litotuba litoformis* and *Ammolagena clavata* in Sample 151-909C-92R-CC, *Budashavella multicamerata* in Sample 151-909C-84R-CC, *Rhabdammina* sp. in Sample 151-909C-74R-CC, and large multichambered *Cyclammina amplectens* in Sample 151-909C-73R-CC. In addition, species such as *Cyclammina rotundodorsata* and *Trochammina deformis* are more abundant in the upper section from Samples 151-909C-52R-CC through -82R-CC, but are found throughout the section. Additional work is necessary before a refined biostratigraphy can be presented.

The diversity, preservation, and abundance of the agglutinated assemblages increase throughout the section, reaching maximum values in the middle of the zone. Approximately 20–30 species, represented by several thousands of specimens per sample, occur in this interval. Many of them are very small fragile forms that have not been recognized before.

Another interesting aspect of the agglutinated assemblages is a recognizable color change with depth in Hole 909C. In the upper part of the section, Samples 151-909C-52R-CC through -66R-CC, the agglutinated foraminiferal tests are white. In Samples 151-909-66R-CC through -96R-CC, the tests are light brown, and in the lowermost core-catcher samples, 151-909C-96R-CC through -103R-CC, the tests are grayish brown. The reason for this color change is unknown, but could be either the result of increasing age or a chemical reaction to the increasing presence of heavy hydrocarbons, including propane and butane, in the lowermost part of Hole 909C (see "Organic Geochemistry" section, this chapter).

The lowermost sample of this hole, 151-909C-103R-CC, contains an interesting monospecific assemblage of an attached, very fine-grained agglutinated benthic foraminifer, *Kechenotiske expansus*. This species has been reported previously as a free-living form from the Carboniferous to lower Cretaceous. Its presence in the Miocene of the Fram Strait is the youngest occurrence as well as the first report of its attached habitat. This occurrence, of more than 500 individuals, is assumed to be in situ because of the delicate nature of the shells and the presence of an organic lining. The organic inner lining also was observed on radiolarian strewn slides.

Discussion of Benthic Foraminifers

The first and last occurrences of the identified agglutinated foraminifer species in Hole 909C follow a pattern similar to that observed on the Vøring Plateau (Kaminski et al., 1990). There is, however, a very important age difference between these two sites. At Site 643 of ODP Leg 104, the agglutinated foraminifers were Oligocene and Eocene in age, whereas correlation with dinocysts and calcareous nannofossils in Hole 909C yields an age of early Miocene to late Oligocene. Thus, the age of the agglutinated assemblage in Hole 909C appears to be diachronous with other reported occurrences of these species. If the age of this assemblage is accurately constrained by the calcareous nannofossil age of early Miocene in Sample 151-909C-102R-CC, then this assemblage is unique in its occurrence.

Although the agglutinated assemblage found in the lower part of Hole 909C is similar to many "flysch-type assemblages," all previous reports place them in older sediments including the Eocene deposits of the North Sea and the Labrador Sea (Miller et al., 1982), and Eocene to Oligocene deposits of the Vøring Plateau (Kaminski et al., 1990) and the Leg 38 sites (Talwani, Udintsev, et al., 1976).

This assemblage also bears some similarities to the Pliocene–Miocene assemblage at Site 645 (Kaminski et al., 1989) and a Pliocene assemblage at Site 344 (Talwani et al., 1976). In both instances, however, the agglutinated foraminifers occurred with ice-rafted sediments. At 909C the first undisputed dropstone occurs in Core 151-909C-16R (see "Lithostratigraphy" section, this chapter), well above the last occurrence of this assemblage at Core 52R-CC. Similar faunas also have been reported from the Miocene of the Mackenzie Basin (McNeil, 1989), but co-occur with calcareous foraminifers.

Two main differences are found between these reported Miocene agglutinated assemblages and the fauna in Hole 909C: (1) the diversity and abundance that are observed in this Miocene assemblage; and (2) the absence of *Martinottiella communis*, which is always found in the Miocene sediments of the North Atlantic Ocean, includ-

ing Sites 907, 643, 645, 646, and 647. The reason for the absence of this species in the Miocene sediments at this site is unclear. This species possibly could occur in unsampled intervals between the core-catcher samples. However, this is unlikely because in the 50 samples that contained the agglutinated assemblage not one specimen of *M. communis* was observed. Most likely, this species never existed at this location.

Another reason for the absence of *M. communis* might be the very low level of silica in the pore waters of Site 909C. *M. communis* is a siliceous agglutinated foraminifer, and is always found in Miocene siliceous biogenic oozes, although it is present in the clastic deposits of Site 645 (Kaminski et al., 1989), and the Mackenzie Basin (McNeil, 1989). The absence of this species at Site 909 may be because of the total absence of biogenic silica. Nevertheless, other siliceous genera including *Rzehakina* and *Silicosigmoilina* do occur rarely throughout the lower section of Hole 909C.

One final problem in interpreting the age of the agglutinated assemblage at Site 909 is the relationship of a similar agglutinated assemblage observed at Site 908 (Hovgaard Ridge). In the lower five core-catcher samples (from Sample 151-908A–32R-CC through -37R-CC) a similar agglutinated assemblage co-occurs within the Oligocene benthic foraminifer *Turrilina alsatica* Zone. This assemblage is sparse, with only four robust species and no more than 10 specimens per sample. In comparison to the individuals in Hole 909C, the specimens at Site 908 are in poor condition and suggest transportation by reworking. However, this is stratigraphically inconsistent, and suggests that the Miocene agglutinated foraminifers at Hole 909C could be reworked into Oligocene sediments in Hole 908A. One possibility is that the Oligocene agglutinated foraminifers found at Site 908 are long ranging and extend into the Miocene sediments at Site 909. Another possibility is that the sediments at Site 909 are Oligocene. More work is necessary to understand the stratigraphic relationship between these two sites.

Palynology

Forty-three core-catcher samples from Hole 909C were processed for palynological analysis. Effort was concentrated on the lower part of the hole, below Core 151-909C-24R, because calcareous microfossils do not occur below that level. All samples contain abundant amorphous organic matter (AOM), plant debris, and terrestrial pollen and spores. Kerogen at the bottom of the hole, in Samples 151-909C-102R-CC and -103R-CC, appears dark orange to light brown and indicates a mature stage of organic maturation.

Dinoflagellate cysts are typically rare to few in slides, owing to the flood of terrestrial organic matter in the sediments. Many cysts are broken or obscured by other particles; hence, many identifications of taxa are preliminary. The most common element of the dinoflagellate cyst assemblages in Hole 909C is protoperidiniacean taxa, represented by *Selenopemphix* spp., *Lejeunecysta* spp.,? *Phelodinium* spp., and ?*Trinovantedinium* sp. (Table 5). The second most common element of the assemblages is species of *Spiniferites*.

A possible occurrence of *Multispinula minuta* in Sample 151-909C-3R-CC indicates a Quaternary age. A specimen of *Filisphaera filifera* in Sample 151-909C-24R-CC suggests an age of Pliocene to early Quaternary (Bujak and Matsuoka, 1986), although the range of *F. filifera* is known to occur into the Miocene (see discussion in Head et al., 1989c).

Beginning from Sample 151-909C-28R-CC, the occurrences of *Cristadinium* sp. cf. *C. cristatoserratum*, *Cristadinium* sp. 1 (of Head et al., 1989b), *Selenopemphix brevispinosa* and *Selenopemphix dionaeacysta* suggest an age of Miocene to early Pliocene down to Sample 151-909C-38R-CC, based on comparison with their ranges in the Labrador Sea and Baffin Bay (Head et al., 1989a, b). Sample 151-909C-40R-CC has the highest definite occurrence of *Palaeocystodinium* sp. This genus has its highest occurrence in the upper Miocene (see discussion in Head et al., 1989c). A single questionable occurrence of *Unipontidinium aquaeductum* in Sample 151-909C-46R-CC suggests a middle Miocene age for this sample (Powell, 1992).

Sample 151-909C-66R-CC has the highest occurrence of *Distatodinium* sp. This genus ranges into the lowest middle Miocene (Powell, 1992), which indicates that below this sample the sediments are at most lowest middle Miocene. A couple of different taxa give evidence for a lower age boundary for the lower hole. *Tuberculodinium vancampoae* occurs in Sample 151-909C-84R-CC, which indicates an age for this sample of no older than latest Oligocene (Powell, 1992). A specimen similar to *Impagidinium* sp. 1 of Manum et al. (1989) in Sample 151-909C-96R-CC suggests an age no older than late Oligocene for this sample (Manum et al., 1989). Sample 151-909C-98R-CC contains *Reticulatosphaera actinocoronata* and a specimen similar to *Melitasphaeridium choanophorum*, both of which indicate an age for this sample of no older than early Oligocene (Powell, 1992). This sample also contains a specimen of *Deflandrea phosphoritica*, which according to Powell (1992) has its highest occurrence in lower upper Oligocene, but according to Williams and Bujak (1985) ranges up to the top of the Oligocene. Powell (1992) also records *D. phosphoritica* in the lowest Miocene in Italy, but this occurrence may be a result of reworking. No definite specimens of *Chiropteridium* spp. were observed, which is usually considered to be an indicator of Oligocene-age sediments (Powell, 1992). A couple of questionable specimens of this genus were observed in the lower part of nearby Hole 908A. If *D. phosphoritica* is not reworked (a specimen similar to *D. phosphoritica* is found in Sample 151-909C-28R-CC; Table 5), then Sample 151-909C-98R-CC would be of Oligocene age. Samples below Core 151-909C-98R do not contain taxa that are age indicative, thus the age of the very bottom of the hole cannot be well constrained by dinoflagellate cysts.

Reworking is evident through much of the section, with the following Cretaceous taxa observed: *Chatangiella* sp., *Florentinia* spp., *Fromea* sp. cf. *F. fragilis*, *Isabelidinium* sp. cf. *I. cooksoniae*, *Odontochitina* sp., and *Oligosphaeridium* spp. In addition, specimens of *Cribroperidinium* sp., *Cerodinium* sp., *Wetzeliella* and cf. *Apectodinium*, which are indicative of older Paleogene, are presumed reworked in this hole.

Biostratigraphic Synthesis

Sediments recovered at Site 909 contain calcareous nannofossils, planktonic and benthic foraminifers, and dinoflagellate cysts. The sediments are virtually devoid of siliceous microfossils, with the exception of rare, recrystallized and clay-infilled radiolarians. The top 83 m of the section is assigned to the Quaternary based on the recognition of nannofossil Zones NN21 to NN19 and the planktonic foraminifer *Neogloboquadrina pachyderma* sin. Zone (Fig. 8). A barren interval separates these Quaternary nannofossil and planktonic foraminifer zones from the Pliocene nannofossil Zones NN15–NN18 (in Cores 151-909C-13R through -20R) and the planktonic foraminifer *N. atlantica* sin. Zone (in Cores 151-909C-9R through -23R). The boundary between the Quaternary and the Pliocene occurs somewhere within this barren zone. Continuous occurrences of rare to few dinoflagellate cysts in the lower part of the hole, below Core 151-909C-23R, provide a Pliocene to early Oligocene age for this interval. The boundary between the Pliocene and the Miocene is tentatively placed between Samples 151-909C-28R-CC and -38R-CC based on dinoflagellates.

The nannofossils *Dictyococcites bisectus, Cyclicargolithus abisectus*, and *Helicosphaera carteri* at the bottom of Hole 909C (Cores 151-909C-101R and -102R) indicate an early Miocene (possibly latest Oligocene) age for the bottom of the sequence. Agglutinated benthic foraminifer zones containing *Cyclammina rotundidorsata* and *C. amplectens*, which are present below Sample 151-909C-52R-

Table 5. Range chart of selected dinoflagellate cyst taxa in Hole 909C.

Age	Core, section	Depth (mbsf)	AOM/plant fragments	Pollen/spores	*Capillacysta gloriana*	*Cribroperidinium* sp. cf. *C. tenuitabulatum*	*Cristadinium diminutivum*	*Cristadinium* sp.	*Cristadinium* sp. 1 (Head et al., 1989b)	*Cristadinium* sp. cf. *C. cristatoserratum*	*Deflandrea phosphoritica*	*Distatodinium* sp.	*Filisphaera filifera*	*Impagidinium* sp. cf. I. sp. 1 (Manum et al., 1989)	*Lejeunecysta* sp.	*Melitasphaeridium choanophorum*	*Multispinula minuta*	*Nematosphaeropsis* sp. cf. *N. lemniscata*	*Operculodinium* sp.	*Palaeocystodinium* sp.	*Phelodinium* sp.	*Reticulatosphaera actinocoronata*	*Selenopemphix brevispinosa*	*Selenopemphix dionaecysta*	*Selenopemphix nephroides*	*Selenopemphix* sp.	*Spiniferites* sp.	*Svalbardella* sp.	*Trinovantedinium* sp.	*Tuberculodinium vancampoae*	*Unipontidinium aquaeductum*
Quaternary	3R-CC	113.90	A	A												CF.														
Pliocene	15R-CC	229.60	A	A																					X					
	18R-CC	258.50	A	A											X															
	22R-CC	297.10	A	A															X						X					
	24R-CC	316.40	A	A									X						X						X					
Miocene to early Pliocene	26R-CC	335.70	A	A												?			X						X					
	28R-CC	354.90	A	A					X	X	CF.				X					?				X	X					
	30R-CC	374.10	A	A															X		X									
	32R-CC	393.10	A	A																			X	X						
	34R-CC	412.40	A	A											X								X	X		X	X			
	36R-CC	431.70	A	A						X					X				X				CF.	X	CF.		X			
	38R-CC	451.00	A	A												CF.														
? late Miocene	40R-CC	470.30	A	A																X	X			X		X	X			
	42R-CC	489.50	A	A				CF.	X						X				X	X			X	X	X	X				
	44R-CC	508.60	A	A				X							X								X	X	X	X				
? middle Miocene	46R-CC	528.00	A	A																X	X				X		X			?
	48R-CC	547.30	A	A				CF.		X								X		X				X	X		X		X	
	50R-CC	566.60	A	A																X			X				X			
	54R-CC	605.10	A	A											X										X	X				
	56R-CC	624.40	A	A		X									X										X					
	62R-CC	682.30	A	A	X														X						X					
	64R-CC	701.60	A	A											X				X						X					
	65R-CC	711.10	A	A											X				X	X	X					X		X		
late Oligocene to early Miocene	66R-CC	720.80	A	A								X			X				X		X				X	X	X	X		
	68R-CC	740.00	A	A															X		X					X	X		X	
	70R-CC	759.30	A	A																						X	X			
	72R-CC	778.70	A	A															X											
	74R-CC	798.00	A	A															X		X			CF.		X				
	76R-CC	817.30	A	A											X											X	X			
	78R-CC	836.60	A	A																					X				X	
	80R-CC	855.90	A	A								X									X				X	X				
	82R-CC	875.10	A	A																	X					X	X			
	84R-CC	894.40	A	A								X			X					X	X				X	X	X		X	X
	86R-CC	913.80	A	A								X							X		X				X	X	X			
	88R-CC	933.10	A	A															X	X					X	X	X		X	
	90R-CC	952.40	A	A								X															X			
	92R-CC	971.70	A	A											X					X							X			
	94R-CC	990.70	A	A															X	X							X		X	
	96R-CC	1010.00	A	A										X					X	X	X	X			X	X	X		X	
e. Oligo–e. Mio.	98R-CC	1029.20	A	A							X					CF.			X	X		X			X	X	X		CF.	
?	100R-CC	1048.40	A	A																						X	X			
?	102R-CC	1058.00	VA	A		?																								
?	103R-CC	1061.80	VA	A															X							X	X			

Note: X = present; ? = questionable species identification or questionable age; CF. = specimen similar to taxa; AOM = amorphous organic matter.

CC, are assigned to lower Miocene/upper upper Oligocene, based on correlation with the calcareous nannofossils from the base of the hole. Similar agglutinated foraminifer assemblages recorded from the North Sea, Labrador Sea, and the Vøring Plateau have diachronous Eocene to Oligocene ages. If the correlation at this site is correct, this is the youngest recorded observation of these benthic foraminifer assemblages.

PALEOMAGNETICS

Shipboard paleomagnetic studies performed at Site 909 followed the general methods described in the "Explanatory Notes" chapter (this volume). Paleomagnetic studies provided significant temporal constraints for only the uppermost part (0 to 40 mbsf) of the sedimentary column with the identification of the Brunhes Chronozone and the Jaramillo subchronozone. Limited recovery as well as the uncertain occurrence of hiatuses in the sedimentary column prevented definitive temporal constraints at this site. The reliability of the magnetostratigraphic interpretations proposed for this site decreases downsection, with several equally tenable and widely divergent hypotheses below 200 mbsf.

General Magnetic Character of the Site 909 Sediments

Sediments recovered at Site 909 exhibit median values of magnetic susceptibility of about 44×10^{-5} SI units and intensity of NRM after 30-mT demagnetization treatment (NRM_{30mT}) of about 3.6×10^{-3}

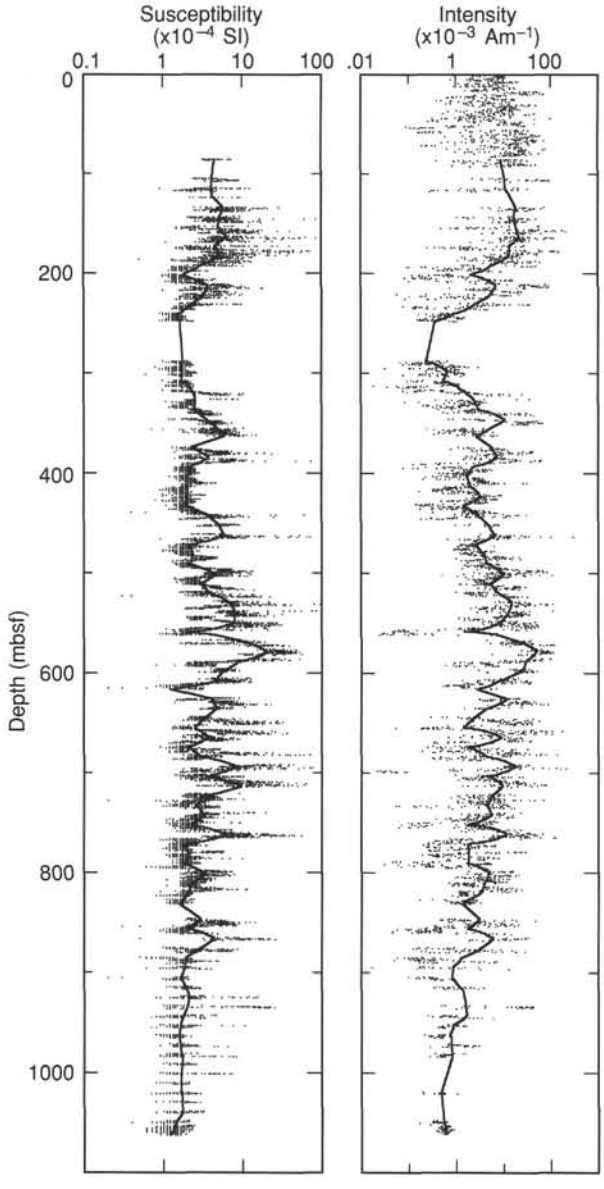

Figure 10. The variation of magnetic susceptibility (left) and NRM intensity (right) after 30-mT demagnetization treatment in Hole 909A.

Am^{-1}. The downhole variations in susceptibility and NRM_{30mT} include occasional spikes in both parameters possibly related to iron sulfide concretions; however, a well-defined indication of a shallow diagenetic front, similar to that observed at Site 912, was not evident in these records (Fig. 10). The NRM_{30mT} and susceptibility profiles exhibit well-defined oscillations with amplitudes ranging from 2 to 10 times the mean, as well as broad scale changes in magnetic character downhole. These preliminary observations suggest a probable complex behavior of the magnetic mineralogy resulting from the combined effects of depositional changes and diagenetic sulfate reduction processes. Iron oxide dissolution and secondary magnetizations acquired by early diagenetic iron sulfides may play a large role in the natural remanent magnetization measured in Site 909 cores, similar to that observed at other Leg 151 sites.

Oscillations in magnetic susceptibility and remanent intensity are well-developed in the record between 600 and 800 mbsf (Fig. 10). However, a similar oscillatory variation, with peak to peak wavelengths of about 30–40 m, is observable throughout most of the record. In addition to this relatively short period variation, there are longer period trends in the variation of magnetic properties that roughly parallel the lithostratigraphic units defined in the "Lithostratigraphy" section (this chapter). Unit I in Hole 909C (80 to 248.8 mbsf) is characterized by very low values of magnetic susceptibility, NRM, and NRM_{30mT} at the base of the unit and a steep rise to a maximum between 150 and 200 mbsf, above which the magnetic properties gently decrease toward the water sediment interface. Unit II (248.8 to 518.3 mbsf) is characterized by well-developed oscillations impressed upon a general decrease up the hole in susceptibility and remanent intensity toward minimum values at a depth just below the broad interval of very poor recovery that marks the boundary between Units I and II. Subunit IIIA (518.3 to 923.4 mbsf) shows a general increase up the hole in susceptibility and remanent intensity with a maximum just below its boundary with Unit II. Subunit IIIA also shows well-developed oscillations in magnetic properties. The magnetic properties of Subunit IIIB (923.4 to 1061.8 mbsf) show a rather low and flat character, although the very poor recovery and drilling disturbances in the recovered core limit the interpretability of the magnetic properties in this interval. Magnetic properties show a fairly high correlation with the lithological units at this site, although the oscillatory variations in magnetic properties evident in this section do not correlate with any obvious changes in lithology.

The respective distributions of magnetic susceptibility, intensity of NRM, and NRM_{30mT} values are presented in Figure 11. All three properties have strongly asymmetric distributions heavily skewed toward low values. The log distribution of susceptibility is also strongly asymmetric, whereas the distribution of NRM more closely approaches log normal, and the distribution of NRM_{30mT} is nearly log normal. These trends are consistent with the interpretation that the susceptibility and NRM distributions are a combination of two processes, one detrital and the other diagenetic, whereas the NRM_{30mT} intensity is primarily related to only one process, likely detrital or early diagenetic.

AF Demagnetization Behavior

The AF demagnetization of a representative discrete sample (Fig. 12) demonstrates the presence of very high coercivity magnetic materials with median destructive fields in excess of 40 mT. The complicated demagnetogram obtained from Sample 151-909C-48R-2, 131–133 cm, along with the high median destructive fields observed in these sediments, suggests that a concerted shore-based study of these sediments is warranted to confirm that a reliable and unbiased estimate of the polarity of the geomagnetic field is obtained.

A comparison of the NRM intensity before and after the AF treatment yields some indication of the effectiveness of the pass-through 30-mT demagnetization treatment. The median intensity of the NRM decreases from 5.6 to 3.6×10^{-3} Am^{-1} (a 36% loss of NRM intensity) during the 30-mT AF treatment; however, in the same data set the mean intensity decreases from 18 to 10×10^{-3} Am^{-1} (a loss of 42% of the initial NRM), which reflects the preferential demagnetization of the high-intensity magnetic carriers probably associated with diagenetic concretions. Further indications that the 30-mT demagnetization is effectively isolating a characteristic magnetization that is early acquired are the decrease in the relative proportion of low and intermediate inclinations, and the remarkably symmetric distribution of steep positive and negative inclinations (Fig. 13). The similarity in the location of the positive and negative peaks indicates that a present-day overprint does not consistently contaminate the determination of a characteristic magnetization. The expected inclination of a characteristic magnetization is significantly modified by the borehole deviation in Hole 909C. The deviation of Hole 909C increases from 14° at 600 mbsf to 25.6° at 1010 mbsf at a constant 048° geographic azimuth (see "Downhole Measurements" section, this chapter). This large deviation would shallow the expected magnetic

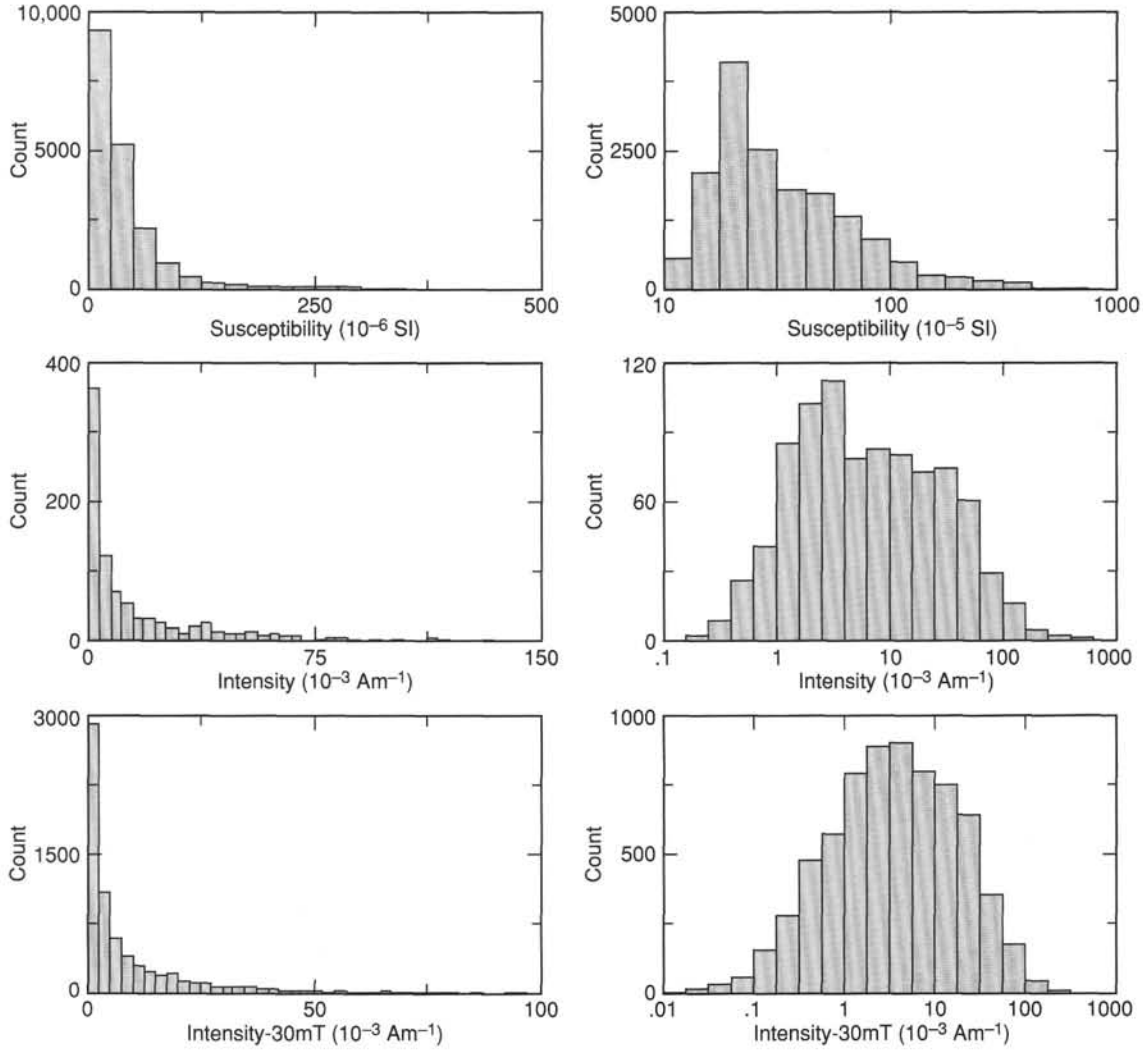

Figure 11. Histograms of magnetic susceptibility values, NRM intensity, and NRM intensity after 30-mT AF demagnetization at Hole 909C. Histograms on the left have arithmetic ordinates, whereas those on the right have logarithmic ordinates.

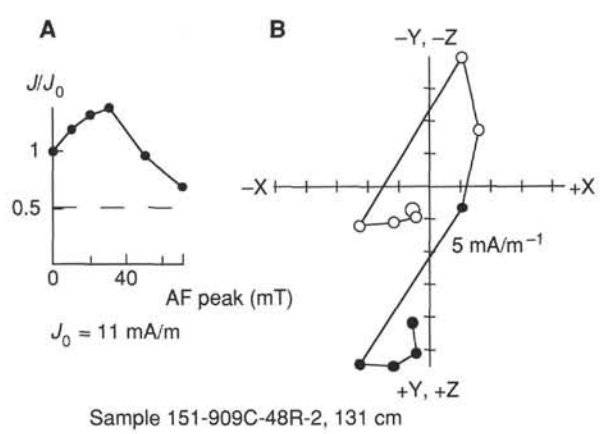

Figure 12. **A.** Normalized NRM intensity for Sample 151-909C-48R-2, 131 cm, during AF demagnetization. **B.** AF demagnetization diagram for the same sample. Black circles = projection onto the horizontal plane; white circles = projection onto the vertical plane parallel to the split face of the core. Demagnetization up to 30 mT accomplished in the 2G pass-through system with the treatment schedule extended to include 50- and 70-mT steps in the GSD-1 demagnetizer.

inclination from ±84° (based on the axial dipole inclination at 79.6°N) to ±79° at 600 mbsf and ±68° at 1010 mbsf. This inclination shallowing is significant but not detectable in the inclination record (Fig. 14) from shipboard measurements and does not enter into the interpretation of the polarity stratigraphy. The Hole 909C borehole geometry does present a unique opportunity to orient core material from the entire deep portion (deeper than ~600 mbsf) of the hole, and, when possible, the orientation of discrete shipboard paleomagnetic samples was recorded relative to apparent tilt.

Magnetic Polarity Stratigraphy

Pass-through measurements of NRM after a 30-mT demagnetization were performed on Hole 909A archive core halves from just below the seafloor down to 92.5 mbsf, on Hole 909B archive halves from just below the seafloor to a depth of 135.1 mbsf, and on Hole 909C archive halves to a depth of 1061.8 mbsf. The magnetic polarity stratigraphy was interpreted from the inclination of the NRM after the 30-mT treatment. Comparison of the inclination vs. depth for Holes 909A and 909B indicates a fair degree of correlation between the two records and supports the notion that the magnetostratigraphies from the two holes are faithful records of the geomagnetic field. However, important discrepancies between the two data sets point out the use-

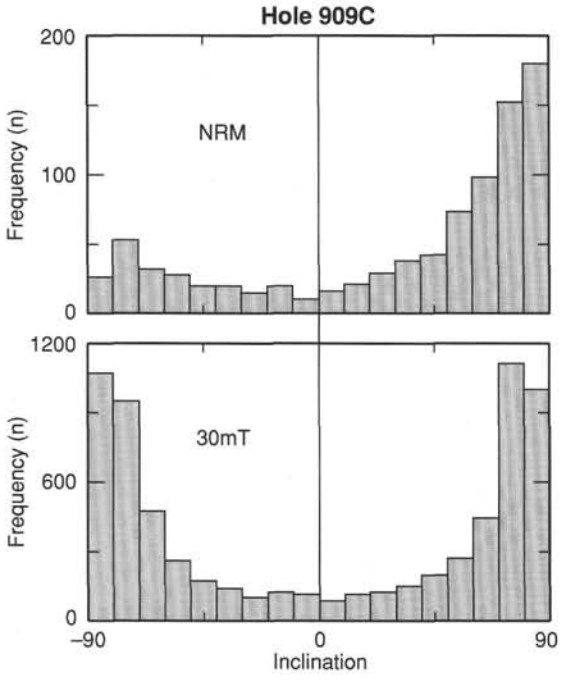

Figure 13. Distribution of inclination values before and after 30-mT demagnetization treatment in Hole 909C. The total number of NRM inclinations is less than the number of 30-mT inclinations because NRM measurements were not run on every core section.

fulness of double cored intervals (Fig. 15). The most important discrepancy is the inclination recorded from 65 mbsf to about 72 mbsf that is characterized by dominantly negative inclinations in Hole 909A, contrasting with the intermediate positive inclinations in the Hole 909B record. Visual inspection of Cores 151-909A-8H, 151-909B-8H, and 151-909B-9H indicated that, in this interval, the Hole 909A cores were recovered with slightly less deformation than the 909B cores, and we accept the 909A record of this interval as more reliable. At this site, as well as at others in this leg, double cored intervals have proved themselves extremely valuable in resolving difficulties in the interpretation of the magnetostratigraphic record.

In Figure 14 we propose an interpretation of the inclination record from Holes 909A and 909C in terms of normal and reversed polarity zones. The frequency of intermediate direction measurements makes it difficult to draw magnetozone boundaries on the basis of individual data points. We have added a smoothed (running mean) curve through the data points that captures many of the salient features of the inclination record and have picked most of the magnetozone boundaries at the stratigraphic level where the smoothed inclination crosses 0°. We have added some very short polarity intervals (e.g., the normal interval interpreted at ~310 mbsf) to the interpreted magnetozone record where the polarity seems established by a consistent string of steep inclinations but the smoothed curve does a poor job at capturing these thin intervals. Missed recovery creates large gaps in the section resulting in many significant ambiguities in the magnetostratigraphy. Poor recovery and largely indeterminate inclinations prevent any meaningful interpretation of the polarity below 830 mbsf.

Correlation with Geomagnetic Polarity Time Scale and Biostratigraphy

Biostratigraphic interpretations suggest that the age of sediment recovered at Site 909 extends from the lowermost Miocene/uppermost Oligocene to the present. The bottom-hole age is based largely

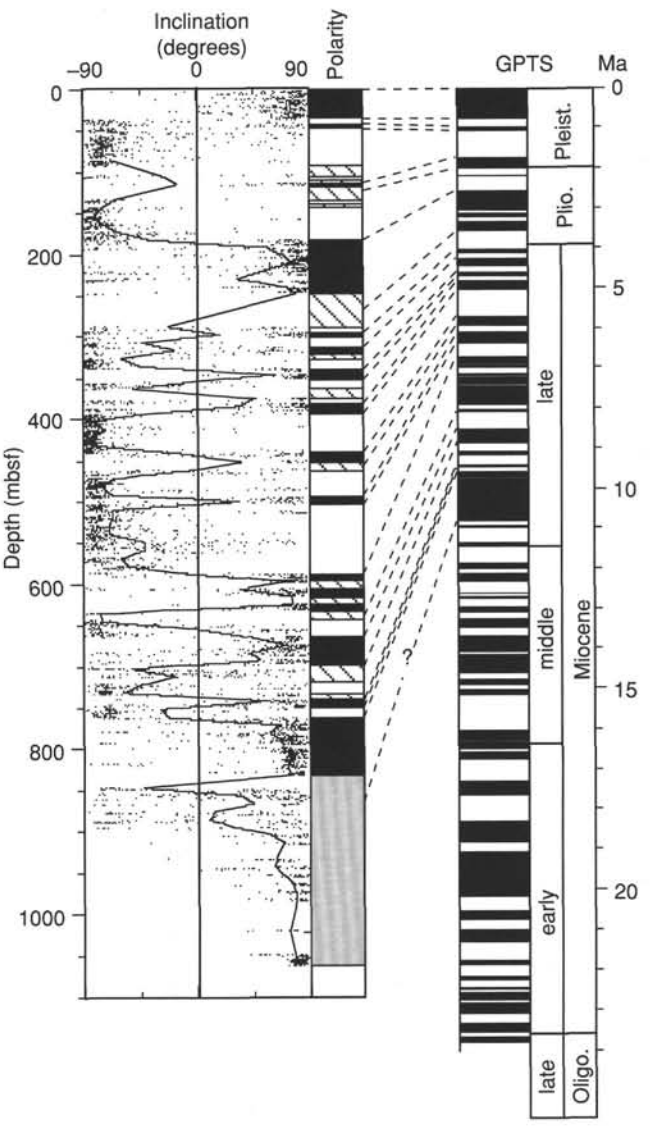

Figure 14. The paleomagnetic record from Holes 909A and 909C. The left column shows the variation of the inclination of NRM_{30mT} with depth. Adjacent to this graph is the interpreted polarity of the sedimentary section: black indicates normal polarity, white indicates reversed polarity, and the cross-hatching indicates missing recovery. On the right is Cande and Kent (1992) geomagnetic polarity time scale (GPTS). Dashed lines indicate one possible correlation to the GPTS (Model 1). This model suggests a significant hiatus somewhere below 760 mbsf.

on calcareous nannofossils (see "Biostratigraphy" section, this chapter). Upon comparison of the magnetostratigraphy from Site 909 with the earliest Miocene to present geomagnetic polarity time scale (GPTS) of Cande and Kent (1992), we note an obvious discrepancy in the number of chronozones interpreted in the Site 909 record and the number of chrons in the GPTS during the earliest Miocene to present (Fig. 14). Especially anomalous is the thick dominantly reversed interval between 400 and 590 mbsf. If we accept that the Site 909 sediments are faithful recorders of the geomagnetic field, then the Site 909 sediments must represent sedimentation during a considerably shorter interval than the ~24 m.y. that the Miocene to present represents in modern time scales. Alternately, the Site 909 magnetostratigraphy has suffered episodic remagnetizations, which reset the magnetization of parts of the sedimentary section. The best test of

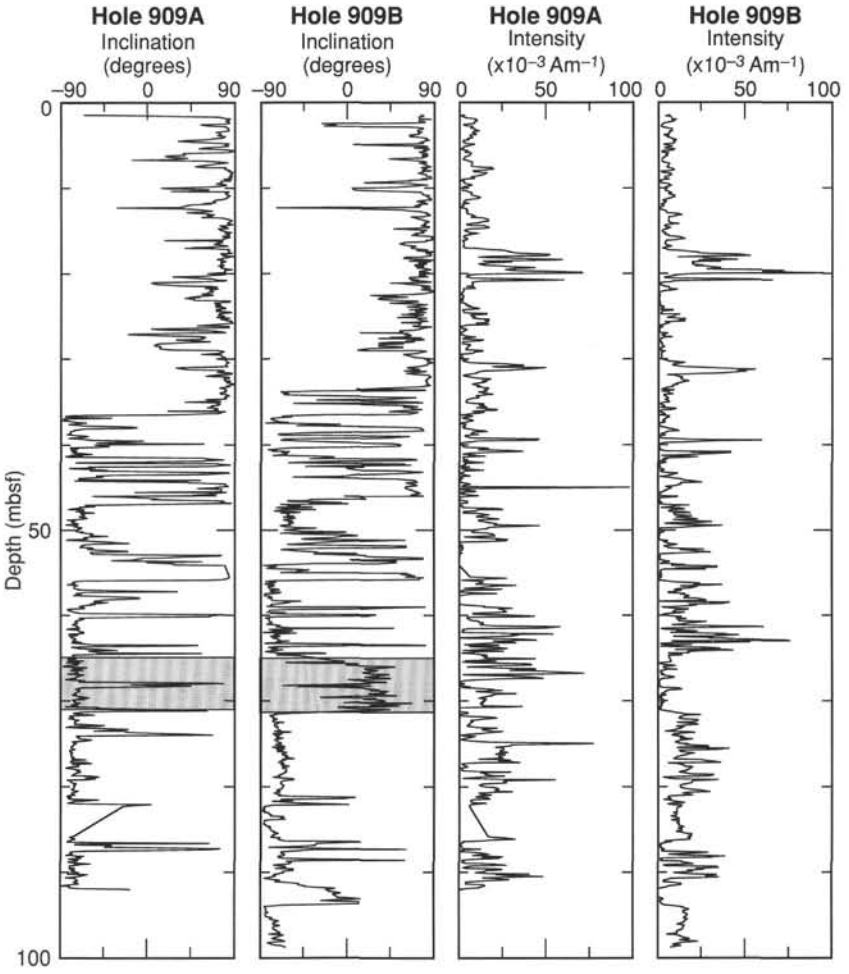

Figure 15. Comparison of the intensity after 30-mT demagnetization treatment and inclination records of the upper 100 mbsf of Holes 909A and 909B. The poor correlation between Hole 909A and Hole 909B inclinations from 65 to 72 mbsf is most likely because of drilling disturbance.

Table 6. Magnetozone boundaries and apparent sedimentation rates in Holes 909A and 909C.

Model 1 depth (mbsf)	Sedimentation rate (m/m.y.)	Model 2 depth (mbsf)	Sedimentation rate (m/m.y.)	Age (Ma)	Chron
0		0		0	
	47		47		C1n
36.6		36.6		0.780	
	38		38		
44.3		44.3		0.984	
	43		43		C1r.1n
47.1		47.1		1.049	
	90		87		
186.4		181.75		2.600	
					C2An.1n
				3.054	
	64		68		
				3.325	
					C2An.3n
247		247		3.553	
	100		87		
294.9		288.55		4.033	
			24		C3n.1n
		291		4.134	
			31		
		295		4.265	
			37		C3n.2n
		301.15		4.432	
	96		70		
		313.75		4.611	
			54		C3n.3n
		318.25		4.694	
			175		
		338.85		4.812	
			52		C3n.4n
391.7		351.05		5.046	
	74		26		
440.7		368		5.705	
					C3An1n

Model 1 depth (mbsf)	Sedimentation rate (m/m.y.)	Model 2 depth (mbsf)	Sedimentation rate (m/m.y.)	Age (Ma)	Chron
		?		5.946	
	94				
		?	144	6.078	C3An2n
503.6		?		6.376	
		590		7.245	
					C4n.1n
		?		7.376	
			66		
		?		7.464	
	74				C4n.2n
		633		7.892	
		?		8.047	
			38		C4r.1n
		?		8.079	
663.7		657		8.529	
			114		C4An
	93	695		8.861	
			92		
762.7		762.4		9.592	
					C5n.1n
		?		9.735	
			61		
		?		9.777	
					C5n.2n
		838.5		10.834	

Note: Sedimentation rates are calculated by linear interpolation between two successive ages.

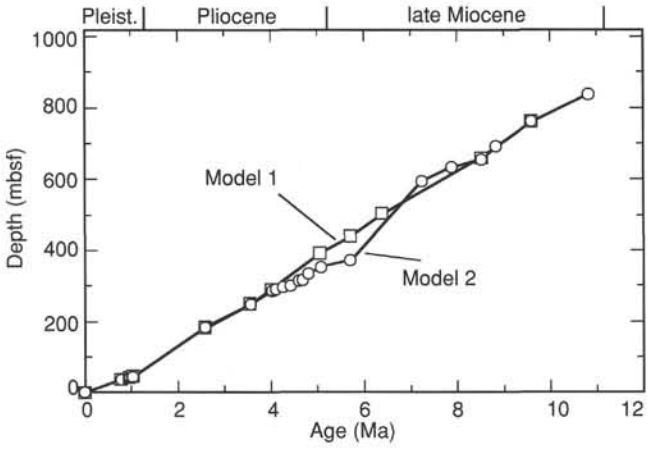

Figure 16. Age-depth model based on the magnetostratigraphy of sediments at Hole 909A and 909C.

these two hypotheses would be some independent indications of sedimentation rate, perhaps from additional biostratigraphic control or the recognition of astronomical cyclicity in the sedimentary section.

In the absence of any additional independent age control, it is possible to make many correlations of the observed magnetostratigraphy to the GPTS; one such possibility is indicated by the dashed lines in Figure 14. This correlation (Model 1 of Fig. 16 and Table 6) is in fact neither unique nor definitive, and the reader should remain skeptical. As a testable working hypothesis, it shows a fairly good correspondence with the GPTS on the interval between approximately 0 and 400 mbsf, but below that level the correlation is largely ad hoc and requires independent verification. An alternative correlation to the GPTS (Model 2 of Fig. 16 and Table 6) implies different ages and highly variable sedimentation rates. Without independent age control, it is difficult to distinguish between the two models.

Sedimentation Rates

Using Model 1, sedimentation rates at Site 909 were nearly 100 m/m.y. during pre-Jaramillo times and were reduced to less than 50 m/m.y. since the Jaramillo (see Table 6). In the Model 2 scenario, sedimentation rates varied considerably, from less than 50 m/m.y. in the post-Jaramillo, to greater than 150 m/m.y. during parts of the Miocene. Both models would demand a significant hiatus in the lower part of the hole (deeper than 750 mbsf). The extreme dependence of sedimentation rates on the age models only serves to point out the importance of independent temporal constraints to the interpretation of the sedimentary history of this site. Until we have independent verification of the magnetostratigraphy, the temporal control at this site will have significant uncertainties.

Conclusions

Preliminary correlations of the Site 909 paleomagnetic record to the GPTS yield little definitive age control on Site 909 sedimentation except in the uppermost sediments (0–37 mbsf), which apparently were deposited during the Brunhes Chron. Below 37 mbsf we observe a fairly well-defined pattern of normal and reversed polarity zones, which can be correlated to the GPTS with decreasing reliability downcore. With only a few additional independent age constraints, it should be possible to settle on a more unique age model, but with the present data set it is impossible to eliminate the ambiguity in correlation. Two age models have been presented as working hypotheses, and await testing by independent methods.

INORGANIC GEOCHEMISTRY

Interstitial Water

The compositions of interstitial waters sampled from Holes 909A and 909C are shown in Table 7 and Figure 17. Sodium varies little beyond the common dilution by desorbed water from clay minerals. Potassium, on the other hand, shows a substantial decrease from normal values at the surface to very low levels, deep in the hole. This distribution is presumably the result of potassium uptake by clays during diagenesis.

Calcium and magnesium show different trends. After an initial sharp decrease from the boundary layer value to around 3 mmol/L, calcium increases with depth down to about 400 mbsf, then is more or less constant in the remainder of the profile. Magnesium falls rapidly with depth in the upper 100–150 mbsf, then decreases slowly down to about 10 mmol/L at the bottom of Hole 909C.

Chloride is relatively constant at this site, showing a slight decrease below 450 mbsf. The chloride content is below the seawater level as a result of the dilution discussed above for sodium. Sulfate shows the expected profile: close to seawater at the surface, dropping to zero immediately below and remaining zero to the bottom of the hole.

Ammonia and silica show similar distributions. Ammonia rises to levels above 10,000 µmol/L below 400 mbsf, then decreases to 5000–6000 µmol/L near the bottom of the hole. Silica shows an unusual distribution with silica concentrations rising rapidly with depth to the 500–600 µmol/L range down to about 500 mbsf. These values are well below saturation with amorphous silica and are probably in equilibrium with a diagenetic silica phase, probably opal CT. Below 500 mbsf, however, silica concentrations decrease to the 100 µmol/L range, indicative of equilibrium with quartz.

Alkalinity and pH show no outstanding trends in Holes 909A and 909C. Alkalinity rises rapidly below the surface, then varies in a wide range around 10 meq/L. Insufficient interstitial water was recovered below 650 mbsf for alkalinity and pH measurements.

Sediment Geochemistry

The major element compositions measured on sediment samples from Site 909 are shown in Table 8 and Figure 18. Silica and titania show virtually no variation. Silica is very high for sediments the equivalent of shales, averaging 60 wt% or more. Alumina and total iron (shown as Fe_2O_3) are relatively constant. No indications of variations in the alumina carrier phase are seen in these data.

CaO is constant from top to bottom at around 1.7 wt%. Two CaO spikes are shown in Figure 18, representing carbonate-rich samples. MgO shows a steady decline from concentrations above 3.0 wt% near the seafloor to below 2.5 wt% at the bottom of the hole.

Sodium shows a gently declining trend with depth, falling from around 2.0 wt% near the seafloor to around 1.5 wt% at the bottom of the hole. Potassium proves to have an anomalous distribution at this site. Figure 19 shows the histogram of potassium concentrations from Holes 909A and 909C. This distribution is clearly bimodal. The potassium concentration in sediments down to approximately 200 mbsf is substantially higher (around 3.3 wt%) than in sediments from greater depths (around 2.8 wt%).

Discussion

The most interesting geochemical phenomenon at this site is shown in the K_2O profile. The shift in K_2O content at about 200 mbsf indicates a profound change in sediment source. The close correspondence of this change in sediment source to the inception of dropstone occurrence in these sediments indicates that these changes signal the inception of glacial climates in the region. Further study should show this change in more detail and, perhaps, with better time resolution.

Table 7. Composition of interstitial waters in Holes 909A and 909C.

Core, section	Depth (mbsf)	Na (mmol/L)	K (mmol/L)	Mg (mmol/L)	Ca (mmol/L)	Cl (mmol/L)	SO_4 (mmol/L)	NH_4 (µmol/L)	SiO_2 (µmol/L)	pH	Alkalinity (meq/L)
151-909A-											
1H-4	5.95	475	12.46	50.70	9.84	546.00	22.72	292	4	7.33	5.725
4H-5	33.95	487	9.15	40.83	3.60	541.00	0.00	1153	4	7.74	14.085
7H-6	64.00	474	8.54	38.39	3.99	542.00	0.00	2347	153	7.87	12.232
11H-5	91.35	472	7.61	35.08	5.07	542.00	0.10	2994	179	7.93	10.162
151-909C-											
3R-1	105.73	449	7.74	33.64	5.53	540.00	0.70	5295	494	7.72	9.288
6R-2	136.13	450	7.17	33.34	6.51	535.00	0.60	5548	449	7.74	9.252
9R-3	166.73	442	6.50	34.50	8.42	525.00	0.00	5872	465	7.63	8.636
12R-3	195.63	441	6.98	30.82	9.82	536.00	0.00	7119	437	7.76	9.203
15R-3	224.53	438	6.48	31.04	10.84	537.00	0.00	6655	347	7.83	9.580
22R-5	294.90	437	5.90	31.92	13.20	534.00	0.50	8970	548	7.77	13.056
25R-3	320.80	432	5.89	32.28	14.45	538.00	0.30	8094	351	7.70	10.942
28R-3	349.70	438	5.72	33.39	14.91	531.00	0.20	9466	403	7.82	9.832
31R-3	378.50	432	5.05	31.55	14.11	532.00	1.00	8727	582	7.09	8.949
34R-3	407.20	449	6.02	32.65	14.80	534.00	0.40	11357	705	7.82	9.926
37R-5	439.10	411	5.18	29.30	12.33	535.00	0.00	9635	404	7.73	7.315
40R-4	466.50	440	5.26	30.87	12.63	536.00	0.00	11311	342	7.70	5.564
43R-5	496.90	428	4.54	29.27	11.55	519.00	1.50	8056	306	7.71	5.290
46R-3	522.70	405	3.96	29.16	11.59	500.00	2.80	8289	104	n.d.	n.d.
49R-5	553.95	397	3.00	25.19	10.05	488.00	1.00	6831	152	n.d.	n.d.
52R-3	580.55	439	3.49	25.55	11.31	510.00	1.70	7864	159	7.79	8.514
54R-1	596.85	361	2.20	21.37	9.45	422.00	0.40	4572	76	n.d.	n.d.
57R-4	628.90	429	2.58	23.04	10.95	497.00	1.90	7046	76	8.30	8.971
60R-5	660.85	409	2.12	21.05	11.19	485.00	0.50	6038	66	n.d.	n.d.
63R-1	683.65	408	1.88	19.54	11.15	469.00	0.70	5421	38	n.d.	n.d.
67R-5	728.20	435	1.73	20.21	13.07	493.00	0.90	5018	104	n.d.	n.d.
70R-4	755.50	424	1.33	18.25	12.67	491.00	0.80	5644	80	n.d.	n.d.
73R-5	786.10	430	1.61	17.43	12.82	483.00	0.80	4689	99	n.d.	n.d.
76R-5	815.00	423	1.26	16.07	12.80	473.00	n.d.	4457	78	n.d.	n.d.
80R-5	853.60	415	1.37	13.82	12.43	n.d.	n.d.	n.d.	n.d.	n.d.	n.d.
83R-3	879.50	438	1.24	14.02	13.17	n.d.	n.d.	n.d.	n.d.	n.d.	n.d.
86R-1	905.50	446	1.46	14.02	14.23	n.d.	n.d.	n.d.	n.d.	n.d.	n.d.
93R-2	973.20	429	1.83	12.98	13.58	n.d.	n.d.	n.d.	n.d.	n.d.	n.d.

Note: n.d. = not determined.

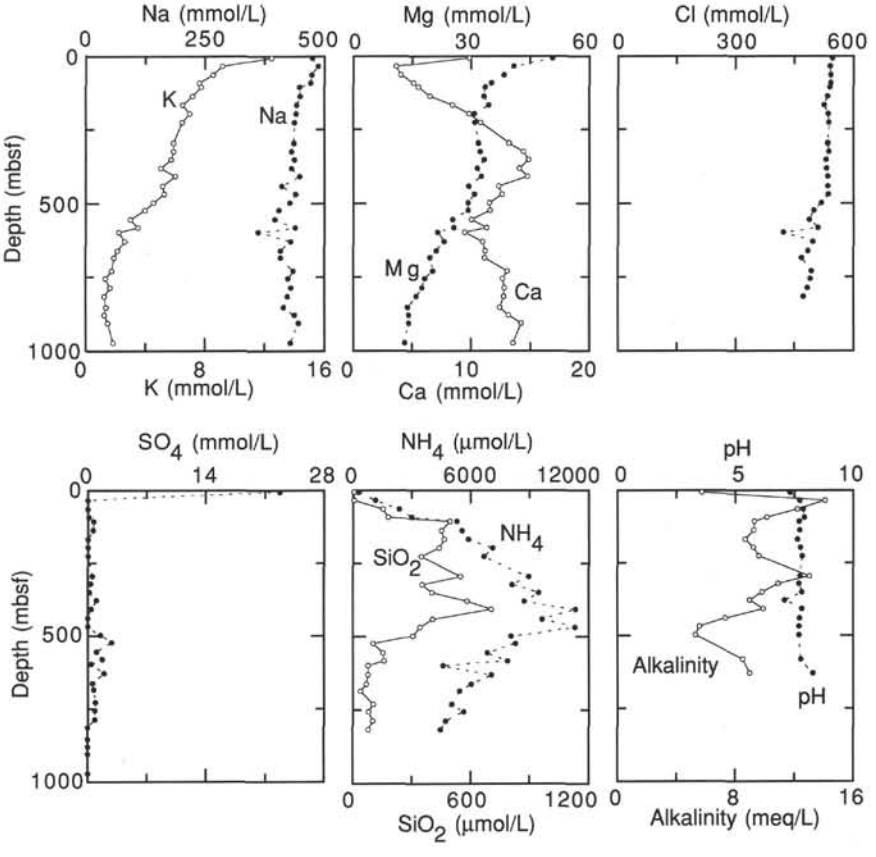

Figure 17. Interstitial water compositions at Site 909.

Table 8. Major element composition of sediments in Holes 909A and 909C.

Core, section	Depth (mbsf)	SiO_2 (wt%)	TiO_2 (wt%)	Al_2O_3 (wt%)	Fe_2O_3 (wt%)	MnO (wt%)	MgO (wt%)	CaO (wt%)	Na_2O (wt%)	K_2O (wt%)	P_2O_5 (wt%)	Total (wt%)
151-909A-												
1H-3	3.64	55.16	0.93	15.56	7.65	0.16	3.46	3.22	1.93	3.33	0.24	91.63
2H-3	11.13	58.49	0.94	15.42	6.98	0.19	3.27	2.04	1.98	3.34	0.21	92.86
3H-3	20.63	56.67	1.04	17.62	8.34	0.14	3.36	1.84	2.00	3.13	0.16	94.29
4H-3	30.14	59.59	1.00	16.87	7.48	0.05	3.16	1.83	1.91	3.57	0.20	95.65
5H-5	43.05	64.54	0.80	13.46	5.38	0.14	2.49	1.93	2.50	2.78	0.17	94.19
6H-3	48.51	60.19	0.94	16.89	6.63	0.05	3.02	1.78	2.07	3.57	0.16	95.30
7H-3	58.95	59.62	0.94	15.82	7.68	0.04	3.11	1.82	2.11	3.50	0.17	94.79
8H-3	68.44	61.36	0.94	16.59	6.32	0.08	3.04	1.81	2.09	3.31	0.17	95.69
9H-3	77.44	60.22	0.92	15.37	6.22	0.12	2.71	1.91	2.12	2.71	0.18	92.48
11H-3	87.88	60.98	0.95	16.02	6.31	0.08	3.06	1.87	1.97	3.42	0.15	94.81
151-909C-												
3R-1	105.00	61.10	0.96	16.49	6.82	0.04	2.90	1.82	2.03	3.31	0.17	95.64
4R-2	116.09	60.07	0.93	15.93	7.12	0.05	3.15	1.95	2.05	3.34	0.17	94.76
5R-1	123.95	60.86	0.93	16.11	6.94	0.05	3.00	1.91	2.11	3.30	0.15	95.36
6R-3	136.92	59.71	0.93	16.52	7.80	0.04	2.83	1.78	1.81	3.36	0.15	94.94
7R-3	146.60	61.17	0.94	16.73	7.02	0.05	3.03	1.88	2.12	3.42	0.16	96.50
8R-3	156.30	61.33	0.95	16.37	7.40	0.04	2.89	1.81	2.02	3.24	0.15	96.23
9R-2	164.49	60.79	1.00	17.41	6.83	0.04	2.73	1.77	1.84	3.43	0.15	95.99
10R-3	175.60	60.41	0.96	16.44	7.67	0.18	3.19	1.95	2.01	3.63	0.16	96.59
11R-3	185.42	59.60	1.00	17.30	7.56	0.05	3.33	1.96	2.09	3.38	0.14	96.41
12R-3	194.90	58.39	1.04	18.17	7.75	0.06	3.46	2.02	2.30	3.29	0.15	96.62
13R-3	204.50	61.19	0.97	16.32	6.22	0.04	2.92	1.85	2.09	2.99	0.13	94.70
14R-3	214.19	59.71	0.99	17.15	7.25	0.04	2.97	1.94	2.02	3.12	0.13	95.33
15R-3	223.79	57.87	0.98	16.46	8.01	0.05	2.90	1.86	1.87	2.96	0.16	93.12
16R-3	233.29	62.04	0.99	16.38	5.93	0.04	2.82	1.87	2.08	2.96	0.12	95.23
17R-3	242.90	62.25	1.05	17.23	6.43	0.03	2.91	1.75	2.12	2.81	0.07	96.65
18R-3	248.86	60.65	1.02	17.95	6.98	0.04	2.95	1.81	2.09	3.16	0.11	96.76
20R-3	268.16	62.43	1.00	16.78	6.05	0.03	2.79	1.77	2.18	2.92	0.13	96.09
22R-3	291.23	62.40	0.93	14.99	6.70	0.04	2.75	1.73	1.97	2.72	0.12	94.35
23R-3	300.78	59.87	1.02	17.38	7.04	0.04	3.22	1.88	2.12	3.26	0.15	96.00
24R-3	310.50	59.63	1.00	17.49	7.18	0.05	3.21	1.83	2.05	3.22	0.15	95.81
25R-3	320.10	58.84	1.03	18.46	7.74	0.07	2.97	1.83	1.97	2.99	0.14	96.05
26R-3	329.71	62.27	0.95	16.00	7.28	0.04	2.71	1.71	1.91	2.79	0.13	95.78
27R-3	339.40	60.86	1.00	17.01	7.43	0.04	2.91	1.81	2.03	2.96	0.16	96.22
28R-3	349.00	60.81	0.99	16.67	7.31	0.04	2.80	1.77	1.94	2.85	0.15	95.32
29R-3	358.59	60.92	1.03	17.77	7.35	0.06	2.78	1.75	1.95	2.98	0.14	96.73
30R-3	364.72	63.55	0.94	15.67	6.49	0.04	2.57	1.69	1.98	2.69	0.12	95.72
31R-3	377.79	56.82	0.99	19.13	8.24	0.05	2.95	1.81	1.94	2.91	0.12	94.96
32R-3	387.30	62.94	1.05	17.33	6.85	0.03	2.58	1.67	1.87	2.77	0.08	97.17
33R-3	396.80	62.93	0.98	16.23	6.93	0.04	2.66	1.69	1.91	2.77	0.12	96.25
34R-3	406.51	63.97	0.94	15.26	6.55	0.03	2.61	1.68	1.89	2.72	0.15	95.79
35R-3	416.09	63.73	0.98	15.83	6.64	0.03	2.65	1.67	1.91	2.78	0.11	96.33
36R-3	425.80	63.13	1.00	16.24	7.09	0.04	2.72	1.68	1.92	2.90	0.10	96.81
37R-3	435.39	62.92	1.00	16.15	6.72	0.03	2.69	1.70	1.91	2.95	0.12	96.17
38R-3	445.00	58.06	0.93	16.98	9.15	0.12	2.73	1.74	1.86	2.64	0.15	94.37
40R-3	464.29	63.05	1.00	16.57	7.33	0.04	2.61	1.74	1.99	2.89	0.11	97.34
41R-3	473.90	64.87	0.93	15.13	6.84	0.04	2.51	1.66	1.91	2.79	0.14	96.81
42R-3	483.68	63.42	0.99	16.09	7.08	0.04	2.75	1.73	1.99	3.12	0.12	97.33
43R-3	493.20	64.12	0.96	15.66	7.28	0.04	2.63	1.73	1.87	2.92	0.15	97.35
44R-3	502.70	66.66	0.95	14.98	7.00	0.03	2.49	1.62	1.86	2.80	0.09	98.48
45R-3	512.30	61.85	0.98	16.52	7.81	0.05	2.69	1.77	1.89	2.86	0.16	96.58
46R-3	522.00	60.54	0.97	17.75	7.68	0.06	2.73	1.67	1.97	2.71	0.12	96.19
47R-3	531.82	43.49	0.57	10.62	13.81	0.21	2.90	2.45	1.15	2.04	0.40	77.64
48R-3	541.39	60.60	1.02	16.94	7.72	0.05	2.64	1.74	1.89	2.92	0.13	95.64
49R-3	550.28	63.15	0.96	15.72	7.12	0.04	2.50	1.68	1.90	2.73	0.17	95.97
50R-3	560.60	60.17	0.94	17.39	7.95	0.06	2.63	1.63	1.83	2.55	0.11	95.27
51R-3	570.30	64.29	0.98	15.82	6.39	0.03	2.35	1.62	1.85	2.71	0.11	96.14
52R-3	579.89	60.72	0.96	16.04	8.36	0.05	2.56	1.77	1.81	2.76	0.22	95.24
53R-3	589.50	63.05	0.97	15.69	7.42	0.04	2.48	1.67	1.85	2.75	0.12	96.03
54R-3	599.01	62.74	0.98	16.42	6.59	0.03	2.50	1.64	1.92	2.76	0.13	95.71
55R-3	608.78	62.37	1.04	18.38	6.78	0.04	2.44	1.66	1.81	2.99	0.07	97.59
56R-1	615.23	61.16	0.90	15.57	8.33	0.04	2.56	1.67	1.77	2.82	0.19	95.00
57R-3	628.08	61.73	0.96	16.28	7.38	0.04	2.59	1.69	1.88	2.66	0.16	95.37
58R-1	634.96	57.43	1.04	19.09	8.66	0.10	2.60	1.77	1.77	2.70	0.14	95.30
59R-3	647.41	61.87	0.99	16.82	7.34	0.04	2.46	1.70	1.71	2.80	0.15	95.87
60R-3	657.10	61.82	1.07	18.37	6.91	0.04	2.45	1.69	1.58	3.20	0.13	97.24
61R-3	668.68	62.83	1.05	17.97	6.75	0.03	2.27	1.63	1.75	2.81	0.07	97.16
62R-3	676.40	64.38	0.98	16.11	6.97	0.03	2.40	1.65	1.87	2.72	0.13	97.24
63R-3	686.01	64.40	1.01	16.64	6.76	0.03	2.36	1.62	1.85	2.79	0.08	97.55
64R-3	695.70	61.59	1.05	17.96	7.36	0.04	2.26	1.70	1.66	2.82	0.07	96.51
65R-3	705.30	61.99	0.99	17.08	7.26	0.03	2.47	1.67	1.79	2.74	0.14	96.17
66R-2	713.00	60.28	1.07	18.30	6.93	0.03	2.35	1.68	1.56	2.91	0.13	95.22
67R-3	724.53	58.21	0.93	16.44	8.98	0.04	2.41	1.68	1.61	2.74	0.16	93.20
68R-3	734.10	61.13	1.04	17.46	7.16	0.03	2.49	1.71	1.66	2.99	0.16	95.83
69R-3	743.70	61.72	1.01	17.29	7.12	0.03	2.50	1.68	1.75	2.79	0.15	96.03
70R-3	753.32	62.10	1.01	17.15	7.05	0.03	2.63	1.64	1.78	2.84	0.09	96.32
71R-3	763.02	62.12	1.06	17.71	6.79	0.04	2.30	1.70	1.58	3.01	0.13	96.42
72R-3	772.70	61.67	0.98	16.41	7.22	0.04	2.63	1.66	1.79	2.70	0.11	95.20
73R-3	782.37	62.68	0.97	16.31	6.35	0.03	2.53	1.61	1.81	2.71	0.09	95.09
74R-3	791.52	62.62	0.97	16.13	7.72	0.04	2.48	1.70	1.72	2.86	0.14	96.36
75R-3	801.68	61.92	1.01	17.30	6.77	0.03	2.42	1.65	1.68	2.84	0.09	95.71
76R-3	811.35	61.00	0.90	15.65	8.37	0.04	2.42	1.61	1.71	2.51	0.11	94.33
77R-3	820.99	63.01	0.97	15.84	7.17	0.03	2.49	1.66	1.84	2.54	0.11	95.66
78R-3	830.70	64.07	0.90	14.83	6.79	0.03	2.44	1.61	1.87	2.44	0.12	95.11
80R-3	849.90	63.19	1.04	17.13	6.95	0.03	2.29	1.67	1.69	2.70	0.09	96.79
81R-3	859.59	62.69	0.97	16.32	6.63	0.03	2.34	1.64	1.71	2.58	0.13	95.02
82R-3	867.70	61.40	1.00	16.77	6.90	0.03	2.29	1.66	1.60	2.61	0.10	94.37

Table 8 (continued).

Core, section	Depth (mbsf)	SiO_2 (wt%)	TiO_2 (wt%)	Al_2O_3 (wt%)	Fe_2O_3 (wt%)	MnO (wt%)	MgO (wt%)	CaO (wt%)	Na_2O (wt%)	K_2O (wt%)	P_2O_5 (wt%)	Total (wt%)
83R-2	876.87	61.54	1.05	17.25	7.12	0.03	2.33	1.69	1.64	2.64	0.09	95.38
84R-3	888.51	63.12	1.05	17.55	6.20	0.02	2.37	1.63	1.73	2.67	0.07	96.41
85R-2	896.66	63.22	1.10	18.65	5.92	0.02	2.27	1.63	1.61	2.86	0.04	97.33
86R-3	907.62	61.88	1.05	17.71	6.49	0.03	2.43	1.64	1.67	2.70	0.08	95.68
87R-2	916.00	60.42	1.04	17.47	7.64	0.03	2.43	1.70	1.57	2.73	0.10	95.12
88R-2	925.58	61.80	1.10	18.42	6.11	0.02	2.40	1.69	1.62	2.81	0.11	96.06
89R-2	935.37	61.52	0.94	15.06	6.76	0.03	2.28	1.65	1.57	2.54	0.08	92.43
90R-2	945.02	67.46	0.69	10.48	4.93	0.02	1.83	1.47	1.82	2.38	0.16	91.26
91R-2	954.60	61.58	1.04	17.60	6.51	0.03	2.36	1.67	1.58	2.81	0.09	95.25
92R-2	964.30	62.28	0.96	16.97	6.40	0.03	2.25	1.57	1.52	2.65	0.07	94.70
93R-2	973.93	62.80	1.10	18.02	6.39	0.02	2.28	1.67	1.61	2.79	0.08	96.75
94R-3	984.48	33.27	0.35	7.10	9.20	0.22	3.49	2.31	0.74	1.32	0.52	58.52
95R-1	991.46	61.19	1.02	17.17	7.49	0.04	2.34	1.76	1.57	2.65	0.17	95.38
96R-1	1000.98	63.77	1.10	17.70	5.28	0.02	2.18	1.64	1.62	2.70	0.06	96.07
97R-1	1010.74	59.63	1.03	16.46	7.85	0.04	2.35	1.79	1.50	2.52	0.19	93.36
98R-1	1020.44	61.10	1.08	17.34	6.84	0.03	2.28	1.74	1.52	2.64	0.13	94.69
99R-1	1029.90	57.89	0.96	15.76	9.06	0.05	2.31	1.83	1.39	2.39	0.21	91.86
100R-1	1039.50	60.40	1.05	16.45	7.38	0.05	2.31	1.90	1.46	2.54	0.21	93.72
101R-2	1050.59	63.03	1.04	16.14	6.19	0.03	2.21	1.73	1.59	2.55	0.10	94.61
102R-3	1056.41	63.96	1.05	15.68	5.78	0.03	2.12	1.73	1.59	2.50	0.11	94.56
103R-3	1061.70	62.42	1.06	17.23	6.22	0.03	2.29	1.71	1.59	2.55	0.11	95.22

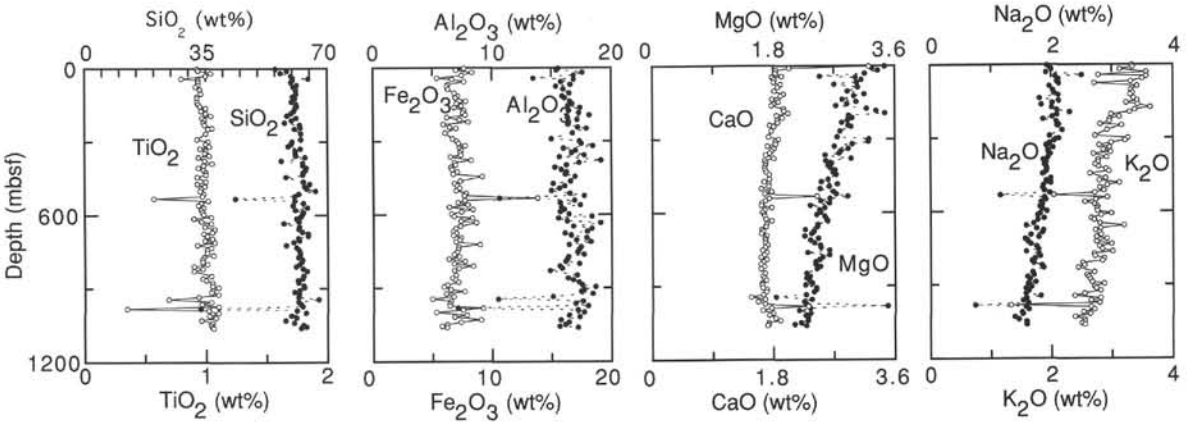

Figure 18. Sediment compositions at Site 909.

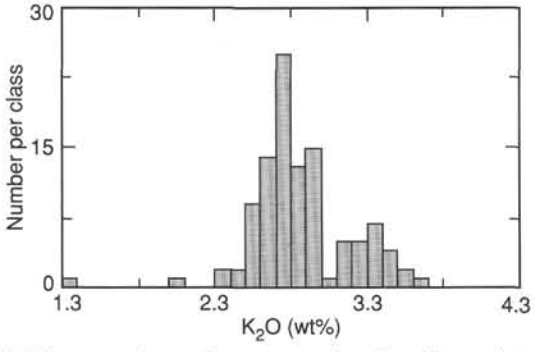

Figure19. Histogram of potassium concentrations in sediments from Holes 909A and 909C.

ORGANIC GEOCHEMISTRY

The shipboard organic geochemistry program at Site 909 included analyses of volatile hydrocarbons; determinations of inorganic carbon, total nitrogen, total carbon, and total sulfur; and pyrolysis measurements (for methods see "Explanatory Notes" chapter, this volume).

Volatile Hydrocarbons

Compositions and concentrations of hydrocarbon gases were measured using two different gas chromatographs. As part of the shipboard safety and pollution monitoring program, concentrations of methane (C_1), ethane (C_2), and propane (C_3) gases were routinely monitored every core using standard ODP headspace and vacutainer sampling techniques. These routine measurements were performed using the Hach-Carle gas chromatograph. Due to the occurrence of significant amounts of higher molecular weight gases (C_{2+}) in the lower part of the sedimentary sequence of Hole 909C, monitoring of hydrocarbon gases through heptane (C_7) was performed using the Natural Gas Analyzer (NGA).

Except for in the uppermost approximately 25 mbsf, concentrations of headspace methane are high throughout the sedimentary section, varying between about 10,000 and 75,000 ppm (Fig. 20, Table 9). No distinct long-term change is obvious; however, distinct minima in methane concentrations around 10,000–20,000 ppm occur at 70–80 mbsf, 220–270 mbsf, 370–390 mbsf, 430–450 mbsf, and 710–750 mbsf. Most of these minima are paralleled by minima in ethane and propane as well, and they also are reflected in the vacutainer data (Fig. 20). The minimum in gas content centered at 220–270 mbsf occurs just around the calculated depth of the base of gas hydrates. According to the pressure-temperature stability field of gas hydrates (cf., Kvenvolden and Barnard, 1983), a geothermal temperature gradient of about 88°C/km (see "Downhole Measurements" section, this chapter), a water depth of 2590 m, and a bottom-water temperature of

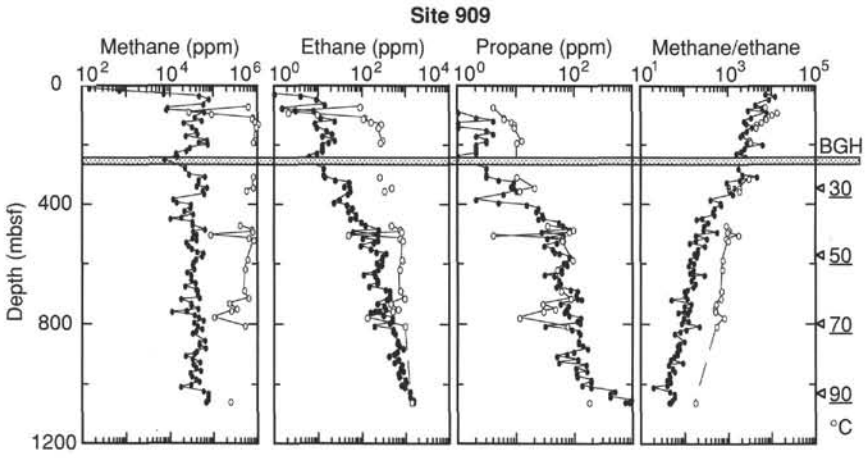

Figure 20. Records of headspace and vacutainer methane (C_1), ethane (C_2), and propane (C_3) concentrations and C_1/C_2 ratios in sediments from Holes 909A, 909B, and 909C. Data were determined by means of the Hach-Carle gas chromatograph. "BGH" marks the calculated depth of theoretical occurrence of the base of gas hydrates (i.e., 240 mbsf). Underlined numbers on the right side of the C_1/C_2 diagram indicate sediment temperature (°C). Open circles = vacutainer data; closed circles = headspace data.

Table 9. Results of headspace and vacutainer gas analysis from Holes 909A, 909B, and 909C, using the Hach-Carle gas chromatograph.

Core, section, interval top (cm)	Depth (mbsf)	Sed. temp. (°C)	C_1-HS (ppm)	C_2-HS (ppm)	C_3-HS (ppm)	C_1/C_2-HS	C_1-VAC (ppm)	C_2-VAC (ppm)	C_3-VAC (ppm)	C_1/C_2-VAC
151-909A-										
1H-5, 0	6.03	0.53	144	0						
2H-6, 0	15.03	1.32	698	0						
3H-6, 0	24.53	2.16	7149	1		7149				
4H-6, 0	34.03	2.99	47241	4		11810				
5H-5, 0	42.03	3.7	76383	9		8487				
7H-5, 0	61.03	5.37	58088	14		4149				
8H-6, 0	72.53	6.38	8868	1.5		5912				
9H-5, 0	80.03	7.04	8329	3		2776				
151-909B-										
8H-6, 0	68.93	6.07					608803	87	4	6998
10H-6, 0	84.93	7.47					25900	2		12950
11H-6, 0	94.43	8.31					84691	9		9410
12H-6, 0	103.93	9.15					742752	109	6	6814
13H-6, 0	109.03	9.59					719580	101	6	7125
14H-6, 0	118.53	10.43					845669	152	8	5564
15H-6, 0	127.23	11.2					1134405	259	9	4380
16H-6, 0	135.43	11.92					911650	222	9	4107
151-909C-										
1R-1, 0	85.03	7.48	59372	8	1	7422				
3R-2, 0	105.83	9.31	35950	11	2	3268				
4R-2, 0	115.43	10.16	51520	23	4	2240				
5R-1, 0	123.63	10.88	20140	8	1	2518				
6R-3, 0	135.63	11.94	30773	9	1	3419				
7R-4, 0	147.43	12.97	38659	15	3	2577				
8R-5, 0	158.63	13.96	41437	20	4	2072				
9R-4, 0	166.83	14.68	22931	12	2	1911				
10R-6, 0	179.43	15.79	68266	23	3	2968	840797	284	12	2961
11R-5, 0	187.63	16.51	45072	17	3	2651	776002	251	10	3092
12R-4, 0	195.73	17.22	71873	12	2	5989				
13R-4, 0	205.33	18.07	28328	12	2	2361				
14R-4, 0	215.03	18.92	23360	12	2	1947				
15R-4, 0	224.63	19.77	13655	9	2	1517				
16R-4, 0	234.13	20.60	14587	6	1	2431				
17R-4, 0	243.73	21.45	7352	4	1	1838				
20R-6, 0	275.63	24.26	21849	13	3	1681				
22R-6, 0	295.03	25.96	26940	13	3	2072				
23R-4, 0	301.63	26.54	62705	14	3	4479	773588	245	10	3158
24R-5, 0	312.83	27.53	44160	24	5	1840				
25R-4, 0	320.93	28.24	45207	50	9	904				
26R-6, 0	333.63	29.36	39654	39	8	1017				
27R-4, 0	340.23	29.94	70293	52	9	1352	783490	452	20	1733
28R-4, 0	349.83	30.78	55313	53	10	1044	550633	316	11	1743
29R-5, 0	360.93	31.76	58970	46	6	1282				
31R-4, 0	378.63	33.32	11678	30	2	389				
32R-4, 0	388.13	34.16	14316	22	5	651				
33R-4, 0	397.63	34.99	30312	44	15	689				
34R-4, 0	407.33	35.84	28942	60	24	482				
35R-4, 0	416.93	36.69	21311	48	22	444				
36R-6, 0	429.63	37.81	33724	71	28	475				
37R-6, 0	439.23	38.65	18068	72	29	251				
38R-3, 0	444.33	39.10	10090	54	24	187				
39R-3, 0	454.03	39.95	32711	96	53	341				
40R-3, 0	463.63	40.80	32660	116	63	282	392587	444	34	884
41R-6, 0	477.83	42.05	61792	232	83	266	728421	713	95	1022
42R-6, 0	487.53	42.90	33296	61	27	546	743085	776	80	958
43R-6, 0	497.03	43.74	40619	229	65	177	81767	48	4	1703

Table 9 (continued).

Core, section, interval top (cm)	Depth (mbsf)	Sed. temp. (°C)	C_1-HS (ppm)	C_2-HS (ppm)	C_3-HS (ppm)	C_1/C_2-HS	C_1-VAC (ppm)	C_2-VAC (ppm)	C_3-VAC (ppm)	C_1/C_2-VAC
44R-6, 0	506.53	44.57	31992	101	34	317	623220	708	61	880
45R-6, 0	516.13	45.42	40619	229	65	177	791682	817	62	969
46R-4, 0	522.83	46.01	23445	183	50	128				
47R-5, 0	534.03	46.99	26507	93	30	285				
48R-6, 0	545.23	47.98	31017	155	42	200				
49R-6, 0	554.83	48.82	42290	208	45	203				
50R-3, 0	559.93	49.27	57935	344	55	168				
51R-4, 0	571.13	50.26	53557	286	82	187				
52R-4, 0	580.73	51.10	38269	283	89	135	586581	787	91	745
53R-5, 0	591.83	52.08	33373	210	64	159				
54R-2, 0	597.03	52.54	32352	268	74	121				
55R-6, 0	612.63	53.91	34499	224	60	154	502752	701	50	717
56R-6, 0	622.33	54.76	24242	183	59	132				
57R-3, 145	628.88	55.34	30182	107	30	282				
58R-2, 0	635.63	55.94	30254	196	44	154				
59R-5, 0	649.73	57.18	30039	218	53	138				
60R-6, 0	660.93	58.16	37230	214	57	174				
61R-5, 0	669.03	58.87	21773	141	48	154				
62R-6, 0	680.23	59.86	38284	339	86	113				
63R-2, 0	683.73	60.17	40935	415	111	99	493833	726	58	680
64R-5, 0	698.03	61.43	41694	410	106	102				
65R-6, 0	709.13	62.40	46383	416	111	111	598934	900	84	665
66R-2, 0	712.63	62.71	17705	359	131	49				
67R-6, 0	728.33	64.09	30250	215	57	141	218772	433	28	505
68R-3, 0	733.43	64.54	30328	317	79	96				
69R-4, 0	744.53	65.52	43553	331	72	132	324133	640	46	506
70R-3, 0	752.63	66.23	24197	197	69	123				
70R-4, 0	754.13	66.36	23426	239	74	98	243118	486	29	500
70R-5, 0	755.63	66.50	10940	154	67	71				
71R-6, 0	766.83	67.48	36559	301	80	121				
72R-6, 0	776.53	68.33	45077	473	126	95	98295	126	11	780
73R-6, 0	786.23	69.19	56994	480	110	119				
74R-5, 0	794.33	69.90	34300	415	124	83				
75R-5, 0	804.03	70.75	41788	191	31	219	498565	928	75	537
76R-5, 135	814.98	71.72	54509	494	90	110				
77R-4, 0	821.83	72.32	38861	496	119	78				
78R-2, 0	828.53	72.91	32775	554	123	59				
80R-6, 0	853.73	75.13	62816	654	117	96				
81R-4, 0	860.43	75.72	46815	628	119	75				
82R-2, 0	867.03	76.30	46941	695	138	68				
83R-4, 0	879.63	77.41	64110	848	166	76				
84R-4, 0	889.33	78.26	40132	614	97	65				
85R-2, 0	895.93	78.84	35598	529	75	67				
86R-2, 0	905.63	79.70	22181	396	49	56				
87R-2, 0	915.33	80.55	32460	677	114	48				
88R-2, 0	924.93	81.39	48492	536	54	90				
89R-2, 0	934.63	82.25	33711	810	157	42				
90R-2, 145	945.78	83.23	38290	737	106	52				
91R-2, 145	955.38	84.07	50613	873	164	58				
92R-2, 0	963.63	84.80	28977	663	108	44				
93R-2, 0	973.23	85.64	31538	688	110	46				
94R-2, 0	982.83	86.49	38504	961	190	40				
95R-2, 0	992.23	87.32	47041	984	194	48				
96R-1, 0	1000.43	88.04	30514	775	134	39				
97R-1, 0	1010.03	88.88	17503	923	194	19				
98R-2, 50	1021.71	89.91	57507	1246	494	46				
99R-1, 140	1030.61	90.69	73161	1253	404	58				
100R-2, 55	1040.86	91.60	73889	1250	410	59				
101R-2, 74	1050.65	92.46	73944	1476	944	50				
102R-4, 75	1057.96	93.10	65812	1377	745	48				
103R-2, 145	1060.98	93.37	65908	1487	882	44	234526	1336	176	176

about 0°C, gas hydrates are stable down to about 240 mbsf (Fig. 20). However, no obvious gas hydrates were observed at Hole 909C.

Similar distinct minima in gas content also were recorded at Sites 910 and 911. These distinct variations in gas concentrations may indicate distinct variations in primary gas production and/or lithological parameters such as porosity, grain size, etc. On first view, some of the minima appear to coincide with organic carbon minima, suggesting a decrease in primary gas production. A more detailed comparison of the gas data with other lithological as well as geochemical parameters should help to distinguish among different mechanisms causing the variations in gas content.

In general, ethane consistently increases downhole, from values <10 ppm typical for the upper 100m to about 1500 ppm at the bottom of the hole. Propane concentrations are low in the upper 400 mbsf (<10 ppm), increasing between 400 and 1010 mbsf to values of almost 200 ppm. Between 1010 and 1061 mbsf, a sharp two-step increase in propane was recorded (i.e., to almost 500 ppm at 1010 mbsf and to >900 ppm at 1045 mbsf) (Fig. 20).

The vacutainer concentrations are generally higher than the headspace concentrations; however, they show similar general trends. These differences between headspace and vacutainer data, which decrease downhole as well as from methane through ethane to propane (Fig. 20), might be explained by the different sampling techniques (e.g., a loss of the more mobile methane before sealing the headspace sediment sample in the glass vial?).

Below 440 mbsf, higher molecular weight hydrocarbon occurred in detectable amounts: isobutane, *n*-butane, isopentane, and *n*-pentane started to occur at 440 mbsf (Core 151-909C-37R); isohexane started to occur at 700 mbsf (Core 64R), and *n*-hexane and *n*-heptane started to occur below 970 mbsf (Core 93R) (Table 10, Fig. 21).

Table 10. Results of headspace gas analysis from Hole 909C, using the Natural Gas Analyzer (NGA).

Core	Depth (mbsf)	C_1	C_2	C_3	IC_4	NC_4	IC_5	NC_5	IC_6	NC_6	NC_7	C_1/C	C_1/C_{2+}
151-909C-													
37R	439	11029	59	21	10	3	5	5				187	107
38R	444	8343	53	23	13	3	6	5				157	81
39R	454	8399	49	21	15	3	5	5				171	86
40R	464	10674	76	34	26	5	7	6				140	69
41R	478	26016	138	59	45	7	10	6	2			189	97
42R	488	15064	65	31	28	4	8	5				232	107
43R	497	12995	115	37	28	3	9	5	1			113	66
44R	507	9481	70	18	15	2	7					135	85
45R	516	9188	78	26	19	3	7	5				118	67
46R	523	4745	57	14	8	1	4					83	56
47R	534	9488	73	18	8	2	4					130	90
48R	545	14008	130	35	11	4	5	5				108	74
49R	555	19057	136	29	8	3	4	5				140	103
50R	560	22594	173	33	6	3	4	5				131	101
51R	571	23229	165	57	12	8	7	6				141	91
52R	581	16399	182	73	15	10	9	6				90	56
53R	592	12536	103	31	7	5	6	5				122	80
54R	597	12104	144	49	10	7	7	6				84	54
55R	613	11623	136	42	10	7	6	6				85	56
56R	622	7087	90	28	9	4	6	6				79	50
57R	629	10859	97	23	5	2	5					112	82
58R	636	7302	88	20	4	2	6					83	61
59R	650	9302	114	30	7	4	5					82	58
60R	661	9025	85	24	6	4	5					106	73
61R	669	7858	103	32	9	4	5	5				76	50
62R	680	17062	221	73	21	9	8	7				77	50
63R	684	15691	233	86	27	11	9	7				67	42
64R	698	16355	241	85	29	11	9	7	1			68	43
65R	709	16471	216	79	29	11	9	7	2			76	47
66R	713	6579	176	94	42	15	13	9	2			37	19
67R	728	4329	51	13	6	2	4	4				85	54
68R	733	10338	173	55	21	6	6	5				60	39
69R	745	12480	167	47	19	5	6	6				75	50
70R	753	4018	59	21	12	4	7	6				68	37
70R	754	11290	201	79	40	11	12	8				56	32
70R	756	2041	38	15	11	3	5					54	28
72R	777	14543	249	94	51	13	16	8	2			58	34
73R	786	18502	237	75	39	10	12	7	1			78	49
74R	794	11333	232	89	53	13	18	8	2			49	27
75R	804	12245	129	24	13	3	5					95	70
76R	815	16406	239	59	31	6	9	7				69	47
77R	822	9979	198	63	37	7	13	6				50	31
78R	829	9776	279	84	50	10	17	8	2			35	22
80R	854	254	2									127	127
81R	860	17396	397	98	56	12	18	8	2				
82R	867	15029	394	103	61	12	21	9	2				
83R	880	19933	472	115	64	15	24	10	4			42	28
84R	889	14667	428	86	42	9	15	7	2			34	25
85R	896	13243	333	60	26	5	9	6				40	30
86R	906	20359	539	96	38	8	13	7	1			38	29
87R	915	9620	339	69	28	6	11	6	1			28	21
88R	925	20660	371	47	14	3	6	5				56	46
89R	935	6326	290	64	26	6	11	6				22	16
90R	946	14869	502	81	24	6	9	6				30	24
91R	955	16148	487	99	36	10	13	7	1			33	25
92R	964	11151	423	82	28	8	11	6	1			26	20
93R	973	11929	459	88	29	10	13	6	2		4	26	20
94R	983	9928	547	119	36	12	14	7	2		2	18	13
95R	992	15998	713	151	41	17	17	8	3		3	22	17
96R	1000	12572	619	130	32	13	14	6	1			20	15
97R	1010	3699	380	92	22	9	11	6				10	7
98R	1022	23608	1389	353	78	41	32	11	4			17	12
99R	1031	31993	1335	292	55	33	22	10	2		4	24	18
100R	1041	32927	1334	291	48	32	19	9	2			25	19
101R	1051	28417	1836	633	133	97	60	26	7	2	8	15	10
102R	1058	29712	1914	596	111	83	49	25	6	1	4	16	11
103R	1061	24914	1964	599	100	79	42	22	6	3	11	13	9

Note: Methane (C_1), ethane (C_2), propane (C_3), isobutane (IC_4), *n*-butane (NC_4), isopentane (IC_5), *n*-pentane (NC_5), isohexane (IC_6), *n*-hexane (NC_6), and *n*-heptane (NC_7) concentrations are given in parts per million (ppm).

Hydrocarbon Formation, Source Rock Potential, and Safety Considerations

For safety considerations, the C_1/C_2 ratio is generally used to get quick information about the origin of the hydrocarbons (i.e., to distinguish between biogenic gas and gas migrated from a deeper source of thermogenic hydrocarbons). Very high C_1/C_2 ratios indicate a gas (C_1) formation by microbiological processes. On the other hand, the occurrence of major amounts of C_2 (to C_5) in shallow depths is associated with thermogenic hydrocarbon generation. In general, the C_1/C_2 ratios consistently decrease with burial depth because of the increasing influence of early diagenetic generation of hydrocarbons.

At Site 909, the headspace C_1/C_2 ratios show the "normal" general decrease with depth and temperature, from values of >10,000 in shallow depths to values of about 50 at 1061 mbsf (or 93°C in temperature) (Figs. 20 and 22). Just above the major increase in heavier hydrocarbons at 1010 mbsf, the absolute minimum C_1/C_2 ratio of 19 was reached. The vacutainer data, although based on limited data points, also show a downhole decrease in C_1/C_2 ratios, with an offset, however, toward higher values. The C_1/C_2 ratios derived from NGA

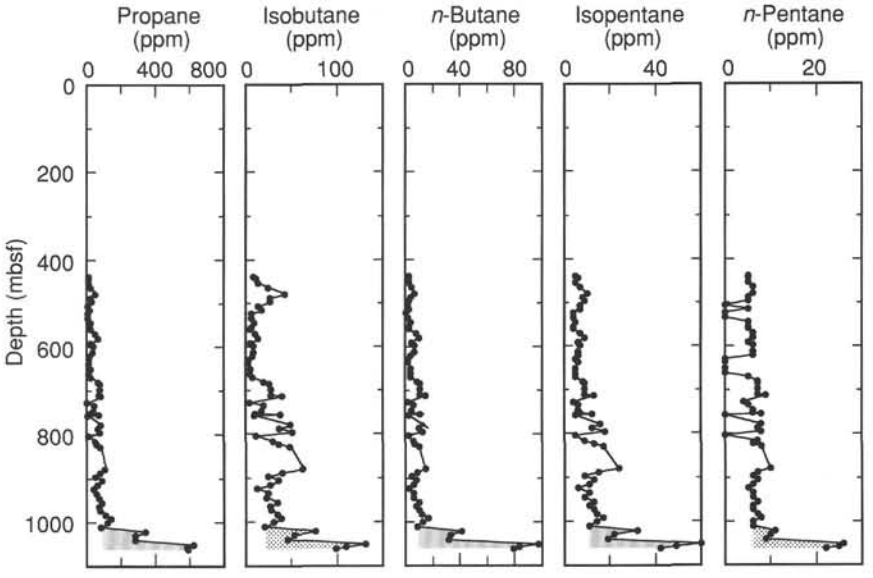

Figure 21. Records of headspace propane, isobutane, *n*-butane, isopentane, and *n*-pentane concentrations in sediments from Hole 909C. Data were determined using the NGA gas chromatograph.

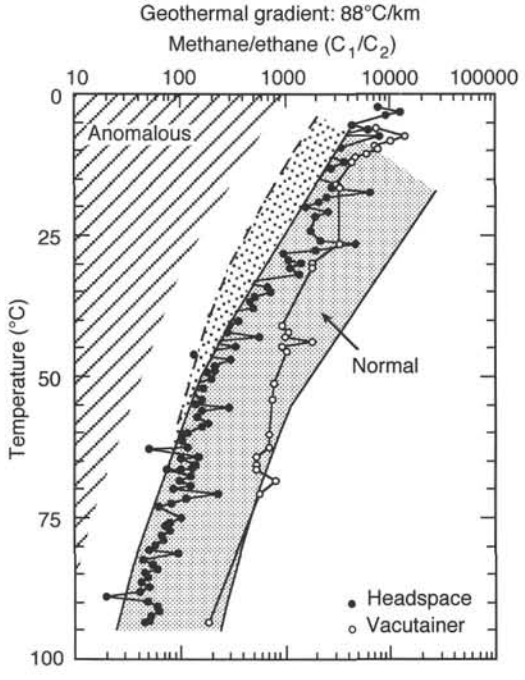

Figure 22. Headspace and vacutainer C_1/C_2 ratios vs. sediment temperature at Site 909. The distinction between "normal" and "anomalous" is based on DSDP/ODP drilling results (after JOIDES PPSP, 1992; supplemented by Leg 151 data). "Anomalous" C_1/C_2 ratios suggesting migrated thermogenic hydrocarbons (for more detailed discussion of C_1/C_2 vs. temperature relationships, see Stein et al., this volume).

analyses of headspace samples, on the other hand, are slightly lower, but show exactly the same trend as the headspace C_1/C_2 ratios derived from the Hach-Carle analyses (Tables 9 and 10).

The high C_1/C_2 ratios in depths <400 mbsf suggest in-situ microbial production of methane from marine organic carbon, which is present in major amounts in the entire sedimentary sequence. At Hole 909A, the methanogenesis has begun at depths shallower than 25 mbsf, as clearly indicated by the sharp increase in methane concentrations and the contemporaneous sharp cessation of sulfate reduction (see "Inorganic Geochemistry" section, this chapter).

The first occurrence of heavier hydrocarbons (such as hexane at about 700 mbsf or 60°C) and their consistent increase with increasing depth (or temperature) indicate the beginning of significant thermogenic hydrocarbon formation increasing further downhole. Under these temperature conditions of >60°C, the occurrence of C_5–C_7 hydrocarbons and their smooth increase with depth are "normal" and have been reported at other DSDP and ODP sites (e.g., Sites 467 and 471, Whelan and Hunt, 1981; Site 603, Schaefer and Leythaeuser, 1987) where drilling was continued without incident. Thus, at Site 909 drilling was continued below 700 mbsf despite the occurrence of heavier hydrocarbons.

At 1010 mbsf, however, a sharp change in the hydrocarbons was recorded that, together with other geological observations, required the termination of drilling at 1061.8 mbsf (see "Operations" section, this chapter):

1. A drastic and abrupt increase in heavier hydrocarbon concentrations (C_3–C_7) occurred in two steps at 1010 mbsf and 1050 mbsf (Fig. 21, Table 10).
2. After treatment with 1, 1, 1-tri-chloroethane as solvent, a strong light-yellow fluorescence of the sediment and a white-blue fluorescence of the fluid occurred in samples from Cores 151-909C-102R and -103R ("cut fluorescence"), indicating the presence of liquid hydrocarbons.
3. The drilling time for the last two cores was distinctly increased because the sediment became significantly harder, and a strong seismic reflector was predicted for this depth. Thus, the possibility of reaching a cap rock could not be excluded, and drilling had to be terminated immediately for considerations of safety and pollution prevention.

Rock-Eval data (Table 11), which were not available at the time of decision to continue or stop drilling, support the presence of distinctly increased amounts of free hydrocarbons (i.e., gas and/or oil) in the lowermost cores, indicated by distinctly increased S_1 values (Fig. 23). This increase appears to be contemporaneous with an increase in total organic carbon (TOC) contents (Fig. 24; see below), suggesting increased in-situ hydrocarbon formation. The S_2 values, a measure for the quantity of hydrocarbons that could be produced in these sediments by cracking the kerogen, are also higher in these lower cores (Fig. 23). The temperatures at which the maximum amount of S_2 hydrocarbon was generated during Rock-Eval pyrolysis ("T_{max}"), reach values of 428°–433°C, suggesting a level of thermal maturity near the bottom of the oil window (Table 11). Unfortunately

Table 11. Results of Rock-Eval pyrolysis of sediments from Hole 909C.

Core, section, interval top (cm)	TOC (%)	T_{max} (°C)	S_1 (mgHC/gRock)	S_2 (mgHC/gRock)	PI $[S_1/(S_1+S_2)]$	HI (mgHC/gTOC)
27R-4, 37	1.71	432	0.22	1.30	0.14	76
38R-1, 24	1.38	431	0.14	1.38	0.09	100
55R-1, 26	1.43	437	0.10	1.27	0.07	88
68R-1, 44	1.09	429	0.11	1.02	0.10	93
80R-5, 43	1.35	433	0.09	1.62	0.03	120
93R-1, 27	1.18	431	0.12	1.25	0.09	105
97R-1, 40	1.51	433	0.13	2.10	0.06	139
99R-1, 59	1.43	433	0.15	2.30	0.06	160
101R-1, 44	1.52	428	0.43	2.20	0.16	144
102R-4, 52	2.59	433	0.39	6.39	0.06	246
103R-1, 32	1.86	428	0.89	2.77	0.24	148

Note: Due to technical problems with the Rock-Eval instruments, the S_3 peak could not be measured, and, thus, the oxygen index (OI) could not be calculated.

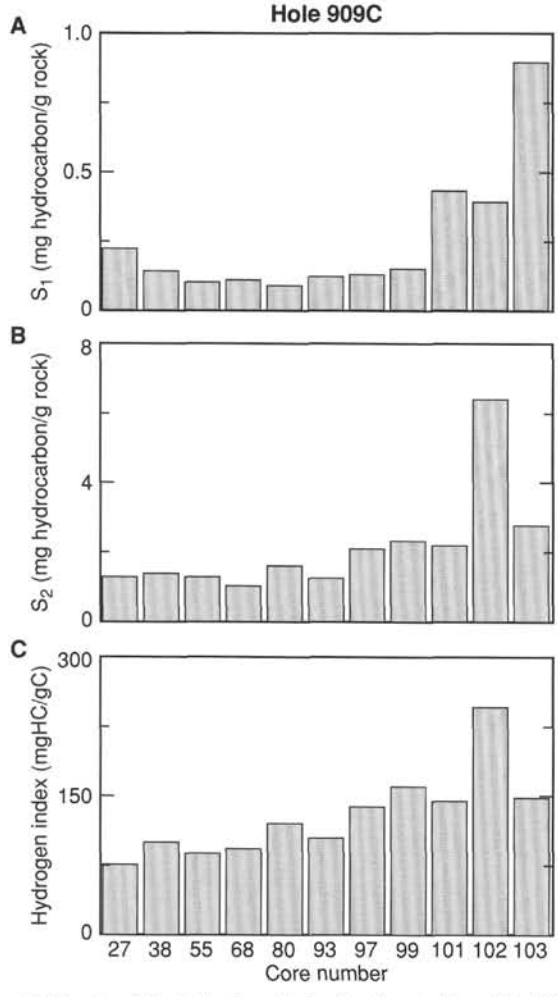

Figure 23. Results of Rock-Eval pyrolysis of sediments from Hole 909C. **A.** S_1 (mg hydrocarbons/g rock): the quantity of free hydrocarbon present in the rock and that is volatilized below 300°C. **B.** S_2 (mg hydrocarbons/g rock): the amount of hydrocarbon produced by cracking of the kerogen at temperatures up to 550°C. **C.** Hydrogen index (mg HC/g total organic carbon), calculated as $(100 \times S_2)$/TOC.

the "Oxygen Index," which corresponds to the quantity of carbon dioxide relative to the TOC content, could not be determined because of technical problems with the Rock-Eval instrument. Also, the hydrogen index/oxygen index ("van Krevelen-type") diagram, which gives important information about the composition as well as the maturity of the organic matter (e.g., Éspitalié et al. 1977; Peters, 1986), could not be plotted. Thus, conclusions regarding thermal maturity and quality of the organic matter as well as further conclusions about migration and/or in-situ formation of hydrocarbons should be supported by other more precise geochemical methods, such as vitrinite reflectance and gas chromatography studies. According to the TOC contents (1%–2.5%; see below), S_1 and S_2 values of 0.4–0.9 mg HC/g rock and 2–6 mg HC/g rock, respectively, hydrogen index values of 150 to 250 mgHC/gC, and T_{max} values of up to 433°C (Fig. 23; Table 11), the sedimentary rocks recovered near the bottom of Hole 909C appear to be a source rock of good potential for gas and oil, with a still low level of thermal maturity (cf. Peters, 1986).

Carbon, Nitrogen, and Sulfur Concentrations

The results of determinations of inorganic carbon, carbonate, total carbon, total nitrogen, and total sulfur are summarized in Table 12 and presented in Figures 24 and 25.

Carbonate values in the dominant lithologies (i.e., clayey silt, silty clay, and sandy mud) vary between 0.5% and 5%. In the light layers and intervals that commonly occur throughout, carbonate contents reach values as high as 30% to 60% (Fig. 24). According to XRD measurements, this carbonate is mainly composed of dolomite, calcite, and/or siderite, indicating its detrital or authigenic origin.

The total organic carbon (TOC) contents vary between 0.2% and 2.6% (Fig. 24). According to the TOC data, the sedimentary sequence of Site 909 can be divided into four intervals. The upper 140 mbsf (Quaternary in age) are characterized by high-amplitude variations in TOC contents between 0.2% and 1.4%. Between 140 and 645 mbsf (Pliocene to middle(?) Miocene in age), TOC values are significantly higher, ranging from 0.8% and 1.7%. In the interval from 645 to 992 mbsf (early(?) Miocene in age), most of the TOC contents vary between 0.8% and 1.2%, with the higher values of >1% more typical for the lower part. Near the bottom of this interval at 944–955 mbsf, a short distinct minimum in TOC content occurs (0.3% to 0.8%; Fig. 24). Except for one single lower value of 0.6%, the lowermost interval of the sedimentary sequence at Site 909 (992–1061.8 mbsf; early Miocene to late Oligocene in age) is characterized by very high TOC values ranging from 1.4% to 2.6%. The highest values of 1.9% and 2.6% are from the lowermost two cores of late Oligocene age.

The total nitrogen contents range from 0.05% to 0.16% (Table 12). Most of the total sulfur values vary between 0.1% and 1% (Fig. 24). Single peaks of high sulfur values of about 1.5% and 5% occasionally occur (Table 12), probably reflecting sulfide-rich layers (see "Lithostratigraphy" section, this chapter).

Composition of Organic Matter

Total organic carbon/total nitrogen (C/N) ratios and hydrogen index values from Rock-Eval pyrolysis have been used to characterize the type of the organic matter (see "Organic Geochemistry" section, "Site 907" chapter, this volume). Most of the C/N ratios at Site 909

Table 12. Summary of geochemical analyses of sediments in Holes 909A and 909C.

Core, section, interval top (cm)	Depth (mbsf)	TC	IC	TOC	$CaCO_3$	TN	TS	C/N	C/S
151-909A-									
1H-1, 55	0.55	1.37	1.11	0.26	9.2		0.22		1.2
1H-1, 115	1.15	0.81	0.36	0.45	3.0	0.08		5.6	
1H-2, 56	2.06	0.89	0.40	0.49	3.3	0.08		6.1	
1H-3, 55	3.55	0.81	0.39	0.42	3.2	0.10		4.2	
1H-4, 26	4.76	1.23	0.29	0.94	2.4	0.05	0.20	19.0	4.7
1H-5, 54	6.54	1.04	0.56	0.48	4.7	0.07		6.8	
2H-1, 55	8.05	0.73	0.16	0.57	1.3	0.09	0.19	6.3	3.0
2H-2, 114	10.14	0.63	0.42	0.21	3.5	0.06		3.5	
2H-3, 118	11.68	0.93	0.08	0.85	0.7	0.06		14.0	
2H-4, 7	12.07	0.48	0.05	0.43	0.4	0.06	0.09	7.1	4.8
2H-5, 44	13.94	0.52	0.07	0.45	0.6	0.09		5.0	
2H-5, 105	14.55	0.82	0.11	0.71	0.9	0.07		10.0	
2H-6, 45	15.45	0.56	0.13	0.43	1.1				
2H-6, 139	16.39	1.23	0.26	0.97	2.2	0.07		14.0	
3H-1, 65	17.65	0.77	0.02	0.75	0.2	0.12	0.08	6.2	9.4
3H-3, 71	20.71	1.16	0.27	0.89	2.2	0.09	0.11	9.9	8.1
3H-4, 58	22.08	1.41	0.05	1.36	0.4	0.11	0.41	12.3	3.3
3H-6, 64	25.14	0.82	0.07	0.75	0.6	0.09	0.11	8.3	6.8
4H-1, 49	26.99	0.48	0.16	0.32	1.3	0.07	1.97	4.6	0.2
4H-4, 106	32.06	0.55	0.26	0.29	2.2	0.07	0.15	4.1	1.9
4H-6, 107	35.07	0.55	0.33	0.22	2.7				
5H-1, 72	36.72	0.74	0.21	0.53	1.7	0.08	0.04	6.6	13.0
5H-2, 101	38.51	0.44	0.03	0.41	0.2	0.07	0.00	5.8	
5H-4, 37	40.87	0.55	0.04	0.51	0.3	0.09	0.32	5.6	1.6
6H-1, 37	45.87	0.68	0.21	0.47	1.7	0.08	0.23	5.9	2.0
6H-3, 49	48.26	0.86	0.17	0.69	1.4	0.09	0.18	7.6	3.8
6H-5, 114	51.16	1.26	0.09	1.17	0.7	0.12	0.24	9.8	4.9
7H-1, 26	55.76	0.53	0.11	0.42	0.9	0.03	0.08	14.0	5.2
7H-3, 28	58.60	0.30	0.09	0.21	0.7	0.06	0.95	3.5	0.2
7H-5, 27	61.41	1.08	0.27	0.81	2.2	0.11	0.32	7.3	2.5
8H-1, 109	66.09	0.43	0.24	0.19	2.0	0.09	0.10	2.1	1.9
8H-3, 26	68.06	0.67	0.07	0.60	0.6	0.10		6.0	
8H-5, 71	71.33	3.62	2.82	0.80	23.5	0.08		10.0	
9H-1, 102	75.02	0.93	0.21	0.72	1.7	0.10		7.2	
9H-3, 28	77.08	1.03	0.16	0.87	1.3	0.12	1.05	7.2	0.8
9H-5, 28	79.88	0.89	0.09	0.80	0.7	0.11	0.36	7.3	2.2
11H-2, 27	86.07	0.88	0.12	0.76	1.0	0.09	0.34	8.4	2.2
11H-3, 99	88.19	0.82	0.13	0.69	1.1	0.10		6.9	
11H-5, 27	90.27	0.73	0.02	0.71	0.2	0.11		6.4	
151-909C-									
1R-1, 29	85.29	0.81	0.09	0.72	0.7	0.10	0.08	7.2	9.0
3R-1, 33	104.63	0.48	0.03	0.45	0.2	0.07	0.06	6.4	7.5
3R-2, 33	106.13	0.98	0.10	0.88	0.8	0.12	0.18	7.3	4.9
4R-1, 27	114.17	1.53	0.28	1.25	2.3	0.11	0.16	11.3	7.8
4R-3, 27	117.10	1.14	0.15	0.99	1.2	0.12	0.29	8.2	3.4
5R-1, 32	123.92	0.88	0.05	0.83	0.4	0.11	0.06	7.5	14.0
6R-1, 38	133.58	0.46	0.03	0.43	0.2	0.09		4.8	
6R-3, 38	136.58	0.69	0.45	0.24	3.7	0.09	0.09	2.6	2.6
7R-1, 32	143.22	0.87	0.06	0.81	0.5	0.11		7.3	
7R-1, 48	143.38	4.42	3.49	0.93	29.1	0.11		8.4	
7R-3, 23	146.13	0.82	0.16	0.66	1.3	0.10	0.05	6.6	13.0
7R-4, 55	147.95	4.13	3.17	0.96	26.4	0.10		9.6	
8R-1, 39	152.99	1.49	0.03	1.46	0.2	0.15	1.11	9.7	1.3
8R-3, 4	155.64	1.04	0.08	0.96	0.7	0.13	0.10	7.4	9.6
8R-3, 10	155.70	1.79	0.98	0.81	8.2	0.11		7.3	
8R-3, 14	155.74	2.54	1.65	0.89	13.7	0.09		9.9	
8R-3, 18	155.78	1.00	0.12	0.88	1.0	0.11	0.23	8.0	3.8
8R-3, 28	155.88	1.04	0.14	0.90	1.2	0.11	0.16	8.2	5.6
8R-5, 82	159.42	0.82	0.07	0.75	0.6	0.10		7.5	
9R-1, 28	162.58	1.37	0.18	1.19	1.5	0.13		9.2	
9R-1, 91	163.21	3.59	2.96	0.63	24.7				
9R-1, 96	163.26	1.61	0.21	1.40	1.7	0.16	0.05	8.8	28.0
9R-2, 29	164.09	1.08	0.15	0.93	1.2	0.13		7.1	
9R-3, 28	165.58	0.95	0.08	0.87	0.7	0.11		7.9	
9R-3, 134	166.64	4.19	3.37	0.82	28.1	0.09		9.1	
9R-3, 142	166.72	1.50	0.24	1.26	2.0	0.15		8.4	
9R-4, 28	167.08	0.53	0.07	0.46	0.6	0.10		4.6	
10R-1, 23	172.13	1.41	0.37	1.04	3.1	0.09	1.96	11.5	0.5
10R-3, 31	175.21	2.02	0.69	1.33	5.7	0.12	0.23	11.1	5.8
10R-5, 28	178.18	1.30	0.23	1.07	1.9	0.12	0.16	8.9	6.7
10R-6, 0	179.40	1.06	0.08	0.98	0.7	0.12	0.26	8.1	3.7
10R-7, 39	181.29	1.28	0.20	1.08	1.7	0.11	0.18	9.8	6.0
11R-1, 14	181.74	1.07	0.17	0.90	1.4	0.11	0.16	8.2	5.6
11R-3, 80	185.40	1.17	0.12	1.05	1.0	0.12	0.14	8.8	7.5
11R-5, 81	188.41	1.18	0.21	0.97	1.7	0.07	0.22	14.0	4.4
12R-1, 86	192.06	2.17	0.73	1.44	6.1	0.11	0.24	13.1	6.0
12R-3, 91	195.11	1.12	0.12	1.00	1.0	0.12	0.40	8.3	2.5
12R-5, 30	197.50	1.22	0.09	1.13	0.7	0.13	0.40	8.7	2.8
13R-1, 113	201.93	1.01	0.04	0.97	0.3	0.12	0.40	8.1	2.4
13R-2, 24	202.54	1.12	0.11	1.01	0.9	0.12	0.54	8.4	1.9
13R-3, 41	204.21	0.87	0.07	0.80	0.6	0.10	0.51	8.0	1.5
13R-3, 95	204.75	1.13	0.16	0.97	1.3	0.12	3.50	8.1	0.3
13R-4, 40	205.70	0.98	0.06	0.92	0.5	0.11	0.51	8.3	1.8
13R-5, 33	207.13	1.26	0.12	1.14	1.0	0.12	0.34	9.5	3.4
13R-6, 63	208.93	1.02	0.17	0.85	1.4	0.10	0.07	8.5	12.0
13R-6, 106	209.36	4.30	2.79	1.51	23.2	0.11	0.09	13.7	16.8

Table 12 (continued).

Core, section, interval top (cm)	Depth (mbsf)	TC	IC	TOC	$CaCO_3$	TN	TS	C/N	C/S
14R-1, 25	210.75	1.47	0.34	1.13	2.8	0.12	0.15	9.4	7.5
14R-3, 26	213.76	1.38	0.25	1.13	2.1	0.13	0.28	8.7	4.0
14R-5, 44	216.94	1.25	0.24	1.01	2.0	0.12	0.13	8.4	7.8
15R-1, 28	220.38	2.22	0.48	1.74	4.0	0.14	0.11	12.4	15.8
15R-3, 32	223.42	0.80	0.29	0.51	2.4	0.09	0.58	5.6	0.9
16R-1, 51	230.11	1.58	0.24	1.34	2.0	0.13	2.59	10.3	0.5
16R-2, 19	231.29	4.01	2.76	1.25	23.0	0.11	0.41	11.3	3.0
16R-3, 25	232.85	0.87	0.08	0.79	0.7	0.10	0.39	7.9	2.0
16R-5, 25	235.85	1.04	0.09	0.95	0.7	0.12	0.52	7.9	1.8
17R-1, 30	239.50	1.03	0.09	0.94	0.7	0.11	1.02	8.5	0.9
17R-3, 43	242.63	0.81	0.12	0.69	1.0	0.11	0.62	6.3	1.1
17R-5, 33	245.53	0.99	0.08	0.91	0.7	0.11	0.82	8.3	1.1
20R-CC, 7	268.17	1.30	0.19	1.11	1.6	0.12	0.99	9.2	1.1
20R-CC, 14	268.24	6.78	5.80	0.98	48.3	0.08	0.12	12.0	8.1
22R-1, 19	287.69	1.71	0.41	1.30	3.4	0.13	0.80	10.0	1.6
22R-3, 69	291.19	1.24	0.15	1.09	1.2	0.12	1.42	9.1	0.8
22R-5, 79	294.29	1.20	0.10	1.10	0.8	0.12	1.55	9.2	0.7
23R-1, 23	297.33	1.07	0.07	1.00	0.6	0.11	0.57	9.1	1.8
23R-3, 31	300.41	1.53	0.19	1.34	1.6	0.13	0.57	10.3	2.4
23R-3, 85	300.95	6.82	6.17	0.65	51.4	0.08	0.07	8.1	9.3
24R-1, 42	307.22	0.96	0.11	0.85	0.9	0.11	0.61	7.7	1.4
24R-3, 98	310.78	1.46	0.25	1.21	2.1	0.14	0.70	8.6	1.7
24R-5, 99	313.79	1.41	0.16	1.25	1.3	0.14	1.16	8.9	1.1
25R-1, 17	316.57	1.26	0.10	1.16	0.8	0.13	0.74	8.9	1.6
25R-3, 25	319.65	1.75	0.16	1.59	1.3	0.14	0.37	11.3	4.3
26R-1, 31	326.31	1.45	0.23	1.22	1.9	0.12	0.72	10.1	1.7
26R-3, 123	330.23	1.54	0.21	1.33	1.7	0.14	1.40	9.5	0.9
26R-5, 122	333.22	1.51	0.21	1.30	1.7	0.13	1.85	10.0	0.7
27R-1, 25	335.95	1.60	0.23	1.37	1.9	0.14	0.24	9.8	5.7
27R-3, 26	338.96	1.60	0.22	1.38	1.8	0.13	0.22	10.6	6.3
27R-4, 33	340.53		7.02		58.5				
27R-4, 37	340.57	2.05	0.34	1.71	2.8	0.16	0.08	10.7	21.4
28R-1, 54	345.84	1.37	0.24	1.13	2.0	0.12	0.28	9.4	4.0
28R-3, 33	348.63	1.66	0.34	1.32	2.8	0.14	0.07	9.4	18.8
29R-1, 86	355.76	2.05	0.45	1.60	3.7	0.13	0.11	12.3	14.5
29R-3, 80	358.70	4.66	3.29	1.37	27.4	0.12		11.4	
29R-5, 78	361.68	1.17	0.43	0.74	3.6	0.11		6.7	
31R-1, 89	374.99	1.34	0.24	1.10	2.0	0.13	0.96	8.5	1.1
31R-3, 78	377.88	1.88	0.56	1.32	4.7	0.13	0.95	10.1	1.4
31R-5, 72	380.82	1.15	0.23	0.92	1.9	0.13	0.06	7.1	15.0
32R-1, 49	384.09	1.15	0.22	0.93	1.8	0.13	0.77	7.1	1.2
32R-3, 55	387.15	1.06	0.13	0.93	1.1	0.13	0.32	7.1	2.9
32R-5, 51	390.11	1.14	0.23	0.91	1.9	0.12	0.61	7.6	1.5
33R-1, 24	393.34	1.12	0.25	0.87	2.1	0.12	1.31	7.2	0.7
33R-3, 24	396.34	1.22	0.11	1.11	0.9	0.13	0.66	8.5	1.7
33R-5, 24	399.34	1.28	0.31	0.97	2.6	0.12	0.43	8.1	2.2
34R-1, 69	403.49	1.26	0.15	1.11	1.2	0.13	1.20	8.5	0.9
34R-3, 66	406.46	1.15	0.16	0.99	1.3	0.13	0.61	7.6	1.6
34R-4, 87	408.17		0.23		1.9				
34R-5, 87	409.67	1.18	0.21	0.97	1.7	0.13	0.78	7.4	1.2
35R-1, 89	413.29	0.90	0.12	0.78	1.0	0.10	0.41	7.8	1.9
35R-3, 91	416.31	1.06	0.10	0.96	0.8	0.13	0.64	7.4	1.5
35R-5, 90	419.30	1.02	0.09	0.92	0.7	0.11	0.81	8.3	1.1
35R-7, 52	421.92	1.00	0.13	0.87	1.1	0.13	1.08	6.7	0.8
36R-1, 20	422.30	1.25	0.17	1.08	1.4	0.14	0.75	7.7	1.4
36R-3, 20	425.30	1.00	0.12	0.88	1.0	0.12	0.78	7.3	1.1
36R-5, 20	428.30	1.12	0.19	0.93	1.6	0.13	0.62	7.1	1.5
37R-1, 28	431.98	1.20	0.17	1.03	1.4	0.13	0.71	7.9	1.4
37R-3, 108	435.78	1.23	0.13	1.10	1.1	0.13	0.69	8.5	1.6
37R-5, 94	438.64	1.42	0.26	1.16	2.2	0.13	0.39	8.9	3.0
37R-7, 42	441.12	1.67	0.34	1.33	2.8	0.12	0.36	11.1	3.7
38R-1, 34	441.64	1.88	0.50	1.38	4.2	0.13	0.08	10.6	17.2
38R-2, 118	443.98		5.64		47.0				
38R-3, 64	444.94		0.37		3.1				
39R-1, 24	451.24	3.87	2.57	1.30	21.4	0.12	0.00	10.8	
39R-1, 89	451.89	1.32	0.34	0.98	2.8	0.12	0.12	8.1	8.1
40R-1, 33	460.93	1.17	0.16	1.01	1.3	0.12	0.44	8.4	2.3
40R-2, 93	463.03	0.99	0.10	0.89	0.8	0.12		7.4	
40R-3, 42	464.02	1.13	0.19	0.94	1.6	0.13	1.72	7.2	0.6
40R-4, 65	465.75	1.16	0.13	1.03	1.1	0.12		8.6	
40R-5, 10	466.70	1.12	0.11	1.01	0.9	0.12		8.4	
41R-1, 68	470.98	1.30	0.11	1.19	0.9	0.14	0.97	8.5	1.2
41R-3, 78	474.08	1.31	0.21	1.10	1.7	0.13	0.30	8.5	3.7
41R-5, 64	476.94	1.24	0.21	1.03	1.7	0.12		8.6	
41R-7, 21	479.51	1.46	0.24	1.22	2.0	0.13		9.4	
42R-1, 58	480.58	1.34	0.24	1.10	2.0	0.13	0.37	8.5	3.0
42R-3, 82	483.82	1.04	0.20	0.84	1.7	0.11		7.6	
42R-5, 72	486.72	1.35	0.30	1.05	2.5	0.14	0.27	7.5	3.9
43R-1, 61	490.11	1.21	0.18	1.03	1.5	0.14	0.26	7.4	4.0
43R-3, 43	492.93	1.21	0.17	1.04	1.4	0.11		9.4	
43R-5, 86	496.36	1.38	0.27	1.11	2.2	0.12		9.2	
44R-1, 27	499.27		0.38		3.2				
44R-3, 52	502.52	1.00	0.08	0.92	0.7	0.10		9.2	
44R-5, 64	505.64	1.34	0.22	1.12	1.8	0.12	0.21	9.3	5.3
45R-1, 81	509.41	1.43	0.26	1.17	2.2	0.13	0.27	9.0	4.3
45R-3, 70	512.30	1.52	0.39	1.13	3.2	0.09		12.5	
45R-5, 69	515.29	2.45	1.16	1.29	9.7	0.13	0.07	9.9	18.4
46R-1, 35	518.65	1.74	0.36	1.38	3.0	0.12	0.08	11.5	17.2

Table 12 (continued).

Core, section, interval top (cm)	Depth (mbsf)	TC	IC	TOC	$CaCO_3$	TN	TS	C/N	C/S
46R-3, 78	522.08	1.61	0.27	1.34	2.2	0.13	0.06	10.3	22.3
47R-1, 74	528.74	1.02	0.23	0.79	1.9	0.13		6.1	
47R-3, 84	531.84	1.36	0.37	0.99	3.1	0.08		12.0	
47R-5, 75	534.75	1.36	0.26	1.10	2.2	0.13	0.33	8.5	3.3
48R-1, 46	538.16	1.33	0.24	1.09	2.0	0.13	0.85	8.4	1.3
48R-3, 106	541.76	1.83	0.70	1.13	5.8	0.12	0.23	9.4	4.9
48R-5, 74	544.44	1.14	0.09	1.05	0.7	0.12	0.45	8.8	2.3
49R-1, 27	547.57	1.31				0.08			
49R-3, 49	550.09	1.36	0.20	1.16	1.7	0.13	0.32	8.9	3.6
49R-5, 57	553.17	1.64	0.36	1.28	3.0	0.13	0.19	9.8	6.7
49R-7, 85	556.39	1.66	0.21	1.45	1.7	0.14	0.20	10.3	7.2
49R-7, 123	556.77	1.79	0.23	1.56	1.9	0.14	0.19	11.1	8.2
50R-1, 34	557.24	1.95	0.41	1.54	3.4	0.14	0.17	11.0	9.1
50R-3, 76	560.66	1.55	0.17	1.38	1.4	0.15	0.17	9.2	8.1
51R-1, 32	566.92	1.33	0.35	0.98	2.9	0.11	0.72	8.9	1.3
51R-1, 63	567.23	5.15	3.82	1.33	31.8	0.10	0.17	13.3	7.8
51R-3, 59	570.19	1.03	0.10	0.93	0.8	0.13	0.41	7.1	2.2
51R-4, 110	572.20	1.48	0.48	1.00	4.0	0.13	0.38	7.7	2.6
51R-4, 135	572.45	1.48	0.33	1.15	2.7	0.13	0.22	8.8	5.2
52R-1, 7	576.27	1.26	0.19	1.07	1.6	0.13	0.16	8.2	6.7
52R-2, 38	578.08	1.45	0.14	1.31	1.2	0.12	0.36	10.9	3.6
52R-3, 94	580.14	1.42	0.26	1.16	2.2	0.12	0.23	9.7	5.0
52R-4, 61	581.31	6.93	5.66	1.27	47.1	0.09	0.09	14.1	14.1
53R-1, 33	586.13	1.08	0.11	0.97	0.9	0.12	0.17	8.1	5.7
53R-3, 57	589.37	1.20	0.18	1.02	1.5	0.12	0.17	8.5	6.0
53R-5, 77	592.57	1.07	0.10	0.97	0.8	0.11	0.56	8.8	1.7
54R-1, 19	595.69	1.32	0.17	1.15	1.4	0.12	0.19	9.6	6.0
54R-2, 63	597.63	1.16	0.12	1.04	1.0	0.12	0.15	8.7	6.9
55R-1, 14	605.24	5.52	4.48	1.04	37.3	0.09	0.10	11.5	10.4
55R-1, 18	605.28	2.05	0.38	1.67	3.2	0.15	0.52	11.1	3.2
55R-1, 26	605.36	2.32	0.89	1.43	7.4	0.14	0.19	10.2	7.5
55R-3, 33	608.43	1.06	0.18	0.88	1.5	0.12	2.92	7.3	0.3
55R-5, 32	611.42	1.05	0.06	0.99	0.5	0.12	0.32	8.2	3.1
55R-6, 0	612.60	1.20	0.09	1.11	0.7	0.13	0.22	8.5	5.0
56R-1, 40	615.20	1.33	0.22	1.11	1.8	0.14	4.90	7.9	0.2
57R-1, 48	624.88	1.16	0.13	1.03	1.1	0.13	0.50	7.9	2.1
57R-3, 44	627.84	1.21	0.16	1.05	1.3	0.12	1.09	8.8	1.0
57R-5, 55	630.95	1.62	0.36	1.26	3.0	0.13	0.21	9.7	6.0
58R-1, 69	634.79	2.05	0.50	1.55	4.2	0.16	0.24	9.7	6.5
58R-2, 14	635.74	1.65	0.31	1.34	2.6	0.13	0.17	10.3	7.9
59R-1, 56	644.26	1.82	0.35	1.47	2.9	0.14	0.15	10.5	9.8
59R-3, 52	647.22	1.45	0.35	1.10	2.9	0.13	0.53	8.5	2.1
59R-5, 42	650.12	0.99	0.11	0.88	0.9	0.11	0.25	8.0	3.5
59R-6, 20	651.40	0.97	0.04	0.93	0.3	0.12	0.30	7.7	3.1
60R-1, 53	653.93	1.21	0.16	1.05	1.3	0.13	0.78	8.1	1.3
60R-3, 32	656.72	1.71	0.65	1.06	5.4	0.12	0.21	8.8	5.0
60R-5, 48	659.88	0.89	0.06	0.83	0.5	0.11	0.28	7.5	2.9
61R-1, 101	664.01	1.25	0.19	1.06	1.6	0.13	0.78	8.2	1.4
61R-3, 118	667.18	1.03	0.17	0.86	1.4	0.12	0.19	7.1	4.5
61R-5, 75	669.75	1.15	0.23	0.92	1.9	0.12	0.21	7.6	4.4
62R-1, 20	672.90	0.99	0.09	0.90	0.7	0.12	0.80	7.5	1.1
62R-3, 54	676.24	1.05	0.21	0.84	1.7	0.12	0.36	7.0	2.3
62R-5, 75	679.45	1.27	0.17	1.10	1.4	0.12	0.29	9.2	3.8
63R-1, 37	682.67	1.09	0.10	0.99	0.8	0.12	0.69	8.2	1.4
63R-3, 57	685.87	1.02	0.10	0.92	0.8	0.12	0.17	7.6	5.4
64R-1, 33	692.33	1.05	0.13	0.92	1.1	0.13	0.14	7.1	6.6
64R-3, 124	696.24	1.09	0.18	0.91	1.5	0.12	0.15	7.6	6.0
64R-5, 128	699.28	1.03	0.09	0.94	0.7	0.14	0.24	6.7	3.9
65R-1, 22	701.82	1.22	0.13	1.09	1.1	0.13	1.44	8.4	0.8
65R-3, 28	704.88	1.12	0.11	1.01	0.9	0.13	1.01	7.8	1.0
65R-5, 26	707.86	0.99	0.13	0.86	1.1	0.12	0.37	7.1	2.3
65R-7, 10	710.70	1.13	0.24	0.89	2.0	0.12	0.10	7.4	8.9
66R-1, 22	711.32	0.93	0.05	0.88	0.4	0.12	0.41	7.3	2.1
67R-1, 59	721.39	1.01	0.16	0.85	1.3	0.13	0.13	6.5	6.5
67R-3, 74	724.54	1.24	0.26	0.98	2.2	0.13	0.65	7.5	1.5
67R-5, 53	727.33	1.09	0.16	0.93	1.3	0.12	0.55	7.7	1.7
68R-1, 44	730.84	1.51	0.42	1.09	3.5	0.13	0.90	8.4	1.2
68R-3, 55	733.95	1.97	1.09	0.88	9.1	0.11	0.22	8.0	4.0
69R-1, 78	740.78	1.79	0.86	0.93	7.2	0.12	0.21	7.7	4.4
69R-3, 96	743.96	1.08	0.12	0.96	1.0	0.11	0.22	8.7	4.3
69R-5, 76	746.76	1.02	0.14	0.88	1.2	0.11	0.62	8.0	1.4
70R-1, 73	750.33	2.49	1.77	0.72	14.7	0.10	0.49	7.2	1.4
70R-3, 0	752.60	1.22	0.39	0.83	3.2	0.10	0.35	8.3	2.4
70R-3, 87	753.47	0.73	0.08	0.65	0.7	0.10	0.96	6.5	0.7
70R-5, 33	755.93	1.00	0.12	0.88	1.0	0.12	1.54	7.3	0.6
71R-1, 12	759.42	0.98	0.17	0.81	1.4	0.11	0.69	7.3	1.2
71R-3, 70	763.00	1.12	0.21	0.91	1.7	0.12	0.34	7.6	2.7
71R-5, 70	766.00	0.97	0.12	0.85	1.0	0.11	0.38	7.7	2.2
72R-1, 22	769.22	0.87	0.07	0.80	0.6	0.11	2.08	7.3	0.4
72R-2, 45	770.95	1.09	0.10	0.99	0.8	0.12	1.08	8.2	0.9
72R-3, 45	772.45	0.97	0.12	0.85	1.0	0.11	1.12	7.7	0.8
72R-4, 45	773.95	0.91	0.12	0.79	1.0	0.11	0.42	7.2	1.9
72R-5, 45	775.45	1.14	0.20	0.94	1.7	0.13	1.21	7.2	0.8
72R-6, 34	776.84	1.13	0.11	1.02	0.9	0.13	1.87	7.8	0.6
73R-2, 22	780.42	1.01	0.05	0.96	0.4	0.11	0.55	8.7	1.7
73R-3, 58	782.28	0.94	0.06	0.88	0.5	0.11	0.66	8.0	1.3
73R-5, 54	785.24	0.90	0.11	0.79	0.9	0.11	0.64	7.2	1.2
73R-6, 15	786.35	4.12	3.15	0.97	26.2	0.11	0.13	8.8	7.4

Table 12 (continued).

Core, section, interval top (cm)	Depth (mbsf)	TC	IC	TOC	$CaCO_3$	TN	TS	C/N	C/S
74R-1, 37	788.67	1.23	0.12	1.11	1.0	0.13	0.16	8.5	6.9
74R-2, 28	790.08	1.12	0.19	0.93	1.6	0.11	0.45	8.4	2.0
74R-3, 52	791.82	1.09	0.25	0.84	2.1	0.11	0.27	7.6	3.1
74R-4, 115	793.95	0.98	0.10	0.88	0.8	0.12	0.82	7.3	1.1
74R-5, 129	795.59	1.13	0.13	1.00	1.1	0.12	0.50	8.3	2.0
75R-1, 79	798.79	1.05	0.16	0.89	1.3	0.12	1.07	7.4	0.8
75R-3, 79	801.79	3.07	2.26	0.81	18.8	0.12	0.10	6.7	8.1
75R-5, 0	804.00	0.90	0.09	0.81	0.7	0.77	0.35	1.0	2.3
75R-5, 118	805.18	0.91	0.15	0.76	1.2	0.13	0.23	5.8	3.3
76R-1, 47	808.07	1.24	0.22	1.02	1.8	0.13	0.09	7.8	11.3
76R-3, 74	811.34	1.03	0.16	0.87	1.3	0.15	2.95	5.8	0.3
76R-5, 77	814.37	1.29	0.29	1.00	2.4	0.11	0.30	9.1	3.3
76R-5, 135	814.95	1.36	0.31	1.05	2.6	0.14		7.5	
77R-1, 105	818.35		0.06		0.5				
77R-3, 88	821.18		0.17		1.4				
78R-1, 113	828.13		0.15		1.2				
78R-3, 42	830.42	1.33	0.23	1.10	1.9	0.13		8.5	
80R-1, 22	846.42	1.44	0.31	1.13	2.6	0.67		1.7	
80R-3, 38	849.58	1.23	0.25	0.98	2.1	0.16		6.1	
80R-5, 43	852.63	1.54	0.19	1.35	1.6	0.14		9.6	
80R-7, 21	855.41	1.23	0.22	1.01	1.8	0.14		7.2	
81R-1, 39	856.29	1.15	0.19	0.96	1.6	0.14		6.8	
81R-3, 51	859.41	1.15	0.15	1.00	1.2	0.10		10.0	
82R-1, 19	865.69	1.51	0.59	0.92	4.9	0.13		7.1	
82R-1, 89	866.39	3.94	2.67	1.27	22.2	0.12		10.6	
84R-1, 66	885.46	1.24	0.10	1.14	0.8	0.12	0.26	9.5	4.4
84R-3, 64	888.44		0.06		0.5				
84R-5, 13	890.93	1.25	0.15	1.10	1.2	0.13	0.59	8.5	1.9
85R-1, 90	895.30	1.15	0.24	0.91	2.0	0.11	0.78	8.3	1.1
86R-1, 81	904.91	1.17	0.10	1.07	0.8	0.12	1.45	8.9	0.7
86R-3, 33	907.43	1.27	0.06	1.21	0.5	0.12	2.44	10.1	0.5
87R-1, 63	914.43	1.13	0.16	0.97	1.3	0.12	0.20	8.1	4.8
88R-1, 90	924.30	1.15	0.05	1.10	0.4	0.13	0.64	8.5	1.7
88R-2, 90	925.80	1.04	0.14	0.90	1.2	0.12	1.21	7.5	0.7
89R-1, 67	933.77	1.37	0.29	1.08	2.4	0.11	0.28	9.8	3.9
90R-1, 26	943.06	2.86	1.89	0.97	15.7	0.10	0.09	9.7	11.0
90R-1, 112	943.92		0.18		1.5				
90R-2, 70	945.00	0.60	0.26	0.34	2.2	0.06	0.76	5.6	0.5
90R-2, 145	945.75		0.20		1.7				
91R-1, 26	952.66	1.09	0.28	0.81	2.3	0.12	0.10	6.7	8.1
91R-1, 49	952.89	2.30	1.67	0.63	13.9	0.11	0.54	5.7	1.1
91R-2, 79	954.69		0.30		2.5				
91R-2, 110	955.00	1.24	0.34	0.90	2.8	0.12	0.40	7.5	2.2
91R-2, 145	955.35		0.20		1.7				
92R-1, 89	962.99	1.20	0.16	1.04	1.3	0.12	0.73	8.7	1.4
92R-2, 0	963.60		0.88		7.3				
93R-1, 27	971.97	1.48	0.30	1.18	2.5	0.12	1.74	9.8	0.7
93R-2, 103	974.23	5.58	4.48	1.10	37.3	0.09	0.10	12.2	11.0
94R-1, 88	982.18	1.24	0.16	1.08	1.3	0.13	0.44	8.3	2.5
94R-3, 16	984.46	5.46	4.47	0.99	37.2	0.10	0.86	9.9	1.1
95R-1, 65	991.35	1.50	0.35	1.15	2.9	0.13	1.18	8.8	1.0
95R-2, 0	992.20		0.23		1.9				
95R-2, 11	992.31	1.70	0.29	1.41	2.4	0.15	1.34	9.4	1.1
96R-1, 39	1000.79	1.59	0.12	1.47	1.0	0.14	1.30	10.5	1.1
97R-1, 40	1010.40	1.62	0.11	1.51	0.9	0.13	0.15	11.6	10.0
98R-1, 46	1020.16	0.85	0.22	0.63	1.8	0.11	0.05	5.7	12.0
99R-1, 59	1029.79	1.97	0.54	1.43	4.5	0.14	0.21	10.2	6.8
100R-2, 41	1040.71	1.72	0.29	1.43	2.4	0.14	0.95	10.2	1.5
101R-1, 44	1048.84	1.68	0.16	1.52	1.3	0.13	1.57	11.7	1.0
101R-2, 74	1050.64	1.83	0.30	1.53	2.5	0.13	0.28	11.7	5.5
102R-1, 25	1052.95	1.81	0.34	1.47	2.8	0.13	0.14	11.3	10.5
102R-2, 123	1055.43	1.93	0.40	1.53	3.3	0.13	0.08	11.7	19.1
102R-3, 76	1056.46	1.95	0.11	1.84	0.9	0.15	0.25	12.2	7.4
102R-4, 52	1057.72	3.04	0.45	2.59	3.7	0.15	0.09	17.2	28.8
102R-4, 75	1057.95	1.81	0.21	1.60	1.7	0.13	1.40	12.3	1.1
103R-1, 32	1058.32	3.04	1.18	1.86	9.8	0.14	0.11	13.3	16.9
103R-2, 145	1060.95	1.83	0.28	1.55	2.3	0.16	0.14	9.7	11.1
103R-3, 57	1061.57	2.12	0.50	1.62	4.2	0.14	0.06	11.6	27.0

Notes: IC = inorganic carbon; $CaCO_3$ = carbonate; TC = total carbon; TOC = total organic carbon; TN = total nitrogen; TS = total sulfur; C/N = total organic carbon/total nitrogen ratios; C/S = total organic carbon/total sulfur ratios.

vary between 6 and 10 (Figs. 24 and 25), suggesting that major amounts of marine organic matter are preserved in the 909 sediments. Higher C/N ratios of >10 occur in the upper Quaternary, Pliocene, and middle Miocene as well as near the Miocene/Oligocene boundary, and probably reflect the presence of major amounts of terrigenous material.

The limited amount of Rock-Eval data does not support the C/N results in general. The hydrogen index (HI) values are generally low (35 to 110 mgHC/gC), suggesting a high proportion of terrigenous material present in the sediments of Site 909. In the lowermost 60 m only, hydrogen index values are significantly higher (150 to 380 mgHC/gC) and indicate that increased amounts of marine organic matter are preserved. Based on a correlation between hydrogen index values and kerogen microscopy data derived from DSDP data (Stein et al., 1986), 30% to 70% of the organic matter might be of marine origin. These first rough estimates of the composition of the organic matter, however, have to be checked by further shore-based, more detailed organic geochemical investigations.

Based on these first shipboard results, which suggest distinct long-term and short-term variations in marine and terrigenous organ-

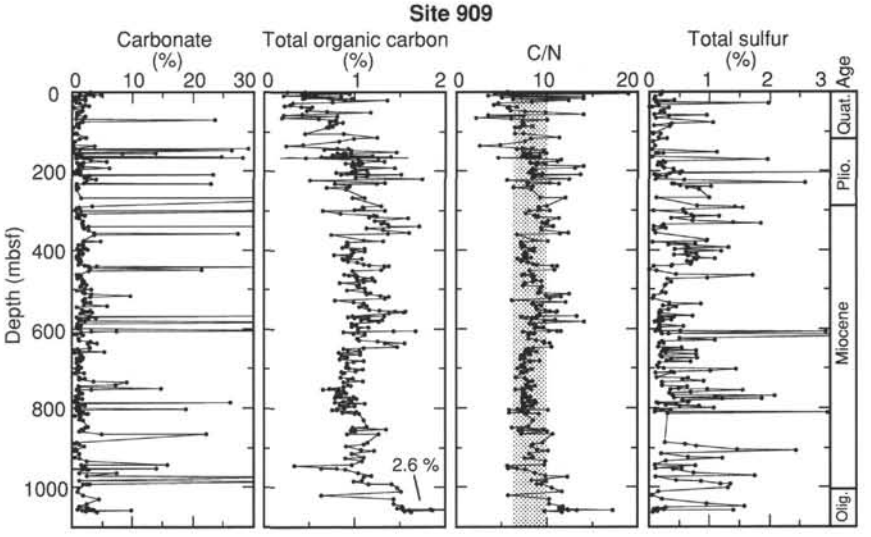

Figure 24. Carbonate contents, total organic carbon contents, organic carbon/total nitrogen (C/N) ratios, and total sulfur contents in sediments at Site 909. Shaded area in the C/N record marks range of dominantly marine organic matter; C/N ratios >10 may suggest significant amounts of terrigenous organic matter.

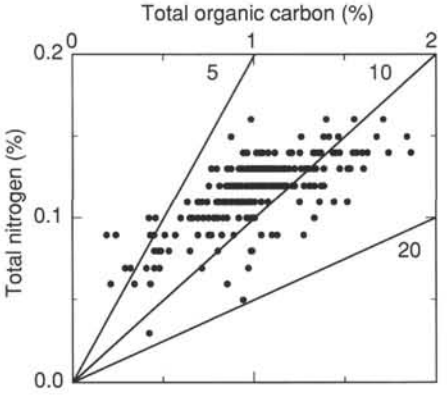

Figure 25. Diagram of total organic carbon vs. total nitrogen. Lines of C/N ratios of 5, 10, and 20 are indicated.

ic carbon fluxes, the sedimentary record of Site 909 gives an excellent opportunity for a detailed organic-geochemical study of the history of surface-water productivity and climatic change during the last ~25 m.y. It seems to be possible to correlate the long-term organic carbon record of Site 909 to similar records at Site 907 (see "Organic Geochemistry" section, "Site 907" chapter, this volume) and Site 645 (Leg 105, Baffin Bay; Stein, 1991b). The middle Miocene organic carbon maximum and the middle Pliocene decrease in organic carbon contents, for example, also occur at Sites 645 and 907 and might reflect regional (or, if they correlate with similar records from other parts of the world oceans, global) paleoceanographic and/or paleoclimatic events (e.g., a middle Pliocene event of extended Northern Hemisphere glaciation and sea-ice cover). For more precise interpretations of the data in terms of paleoenvironment and its change through time, of course, more detailed information about the composition of the organic material (i.e., marine vs. terrigenous) as well as the calculation of flux rates of organic carbon is necessary.

PHYSICAL PROPERTIES

Introduction

The shipboard physical properties program at Site 909 included nondestructive measurements of bulk density, bulk magnetic susceptibility, compressional-wave velocity, and total natural gamma activity on whole sections of core using the multi-sensor track (MST), as well as discrete measurements of thermal conductivity, compressional-wave velocity, shear strength, and index properties. The downhole temperature measurements are also reported here. Methodology is discussed in the "Explanatory Notes" chapter (this volume).

At Site 909 problems associated with biogenic gas (see "Organic Geochemistry" section, this chapter) were experienced for the first time during Leg 151. This gas expands and is released during transit to the sea surface (creating expansion voids) and during core cutting. If present in appreciable quantities (>~10^3 ppm) it can destroy the structural integrity and increase the proportion of gas-filled spaces within the sediment framework. Consequently, volumetric measurements can be distorted, and those measurements requiring a continuous solid framework or 100% saturation for their success (e.g., thermal conductivity, velocity) are of poor quality.

Three holes were drilled using both rotary and hydraulic piston coring techniques. Holes 909A and 909B produced shallow APC cores. Sediment was retrieved in Hole 909A to 92.5 mbsf (11 cores), and in Hole 909B to 135.1 mbsf (16 cores). Core recovery was usually complete (>100%). Gas appeared as a confounding factor in measurements of physical properties at this site beyond Core 151-909A-3H and -4H. Sediment was retrieved in Hole 909C from 85.00 to 1061.8 mbsf (103 cores), using entirely rotary drilling techniques. The sediment recovered was generally badly disturbed. In many cases the liner was incompletely filled, and large cracks and gaps were evident throughout many sections. Hole 909C was finally abandoned because of high concentrations of both gas and traces of oil.

Whole-core Measurements

Figures 26, 27, and 28 show the results of GRAPE density, magnetic susceptibility, natural gamma activity, and compressional-wave velocity for Holes 909A, 909B, and 909C, respectively. Velocities became erratic below about 25 mbsf in Holes 909A and 909B, probably because of the disruptive effect of gas expansion (see "Compressional-wave Velocity" section, this chapter) and measurements of this parameter were terminated at this depth. Velocity measurements were not made in Hole 909C because of the relatively high degree of core disturbance associated with rotary coring. The records from Hole 909C have been filtered using a fast Fourier transform routine to accentuate the major downhole trends. Variations in GRAPE density, magnetic susceptibility, and natural gamma activity occur on a wide range of depth scales, from high-frequency variations on the sub-meter scale to trends spanning several hundred meters. The high-

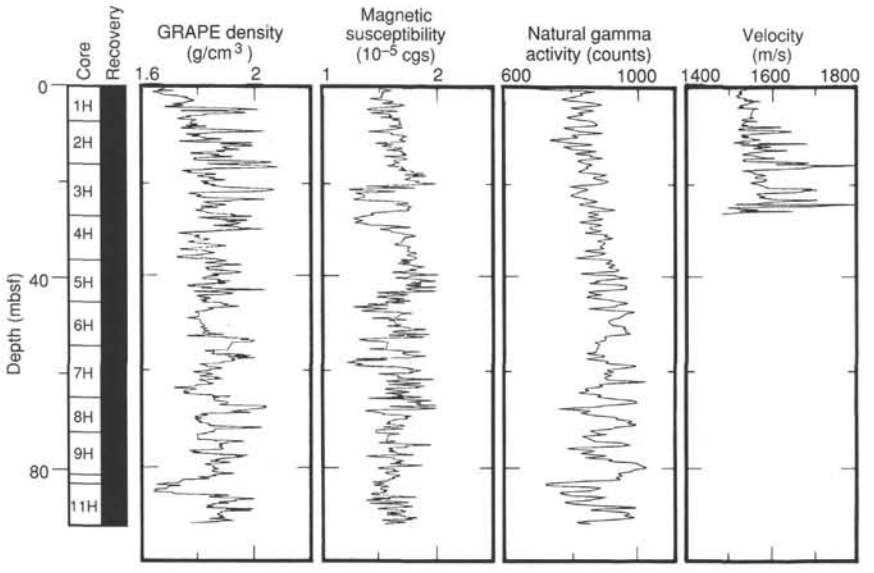

Figure 26. GRAPE density, magnetic susceptibility (logarithmic scale), natural gamma activity, and compressional-wave velocity for Hole 909A. Data were filtered using a fast Fourier transform routine.

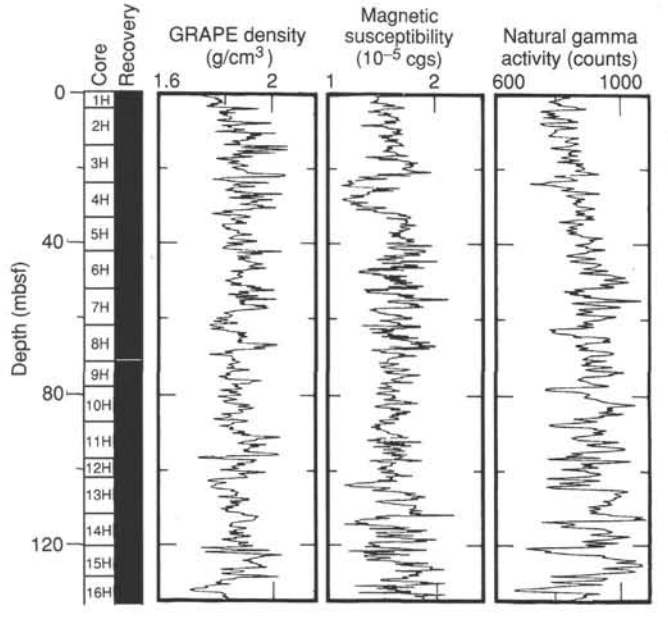

Figure 27. GRAPE density, magnetic susceptibility (logarithmic scale), and natural gamma activity for Hole 909B. Data were filtered using a fast Fourier transform routine.

er frequency variations are best seen in Figures 26 and 27, which are plotted on an expanded scale. These variations permit high-resolution (with several correlatable GRAPE density and magnetic susceptibility features per core) between-hole correlations in the upper ~70 mbsf of the APC-cored interval at this site. Below this depth, detailed between-hole correlations are extremely difficult, probably because of disruption of the stratigraphy by gas expansion. Figure 28 illustrates that on a gross scale GRAPE density and natural gamma activity covary down the section, and that these parameters vary inversely with magnetic susceptibility. A notable feature of the record is the interval of high but fluctuating magnetic susceptibility values and generally low natural gamma activity in the middle part of the section, from ~450 to 750 mbsf. However, this interval does not correspond to any lithologic subdivision of the site (see "Lithostratigraphy" section, this chapter).

Thermal Conductivity

Thermal conductivity was measured in Holes 909A and 909C only. In Hole 909A, 35 discrete measurements were performed to a depth of 84 mbsf; 202 measurements were performed in Hole 909C to 756 mbsf. Throughout each core, sediment disturbance was high because of drilling disturbance or gas; therefore, measurements displaying high drift or large error have been edited. Care was taken to avoid visually cracked portions of the sediment section, although internal voids could not always be anticipated.

Thermal conductivity measurements are characterized by weak gradients and a high degree of scatter throughout the sediment column. The average conductivity is 1.36 ± 0.24 W/m·K, and the range of conductivities measured was 0.71–2.33 W/m·K. A very weak correlation of thermal conductivity with water content occurs downhole (Fig. 29), and the strong inverse and nonlinear relationship commonly reported for deep-sea clays (e.g., Lovell, 1985) cannot be seen. However, a more detailed examination of the data reveals a number of gradients and subtle covariability. Over vertical distances of ~70–100 m, regions of higher conductivity are broadly associated with more compact, lower porosity sediments (e.g., 310–434 mbsf). A gradient in thermal conductivity, although irregular, is perceptible over the interval 0–24 mbsf, corresponding to where the steepest gradients in bulk density and porosity exist. Evidence also suggests a weak increase in thermal conductivity below ~600 mbsf. A mean conductivity for this interval is 1.45 W/m·K. All thermal conductivity data are summarized in Table 13.

Bottom-hole Temperature Measurements and Geothermal Gradient

Hole temperatures were determined at the seafloor and at three depths in Hole 909A by the Adara Temperature Tool. The equilibrium temperature was calculated (see "Explanatory Notes" chapter, this volume) and the results are as follows: mud line, 0.878°C; 33.9 mbsf, 2.319°C; 62.4 mbsf, 5.133°C; and 84.4 mbsf, 7.363°C. The geothermal gradient determined by a least squares fit of these data was estimated at 97.6°C/km (Fig. 30). The thermal gradient and the average geothermal conductivity of 1.36 W/m·K were used to estimate the heat flow for Site 909 at 134 mW/m^2.

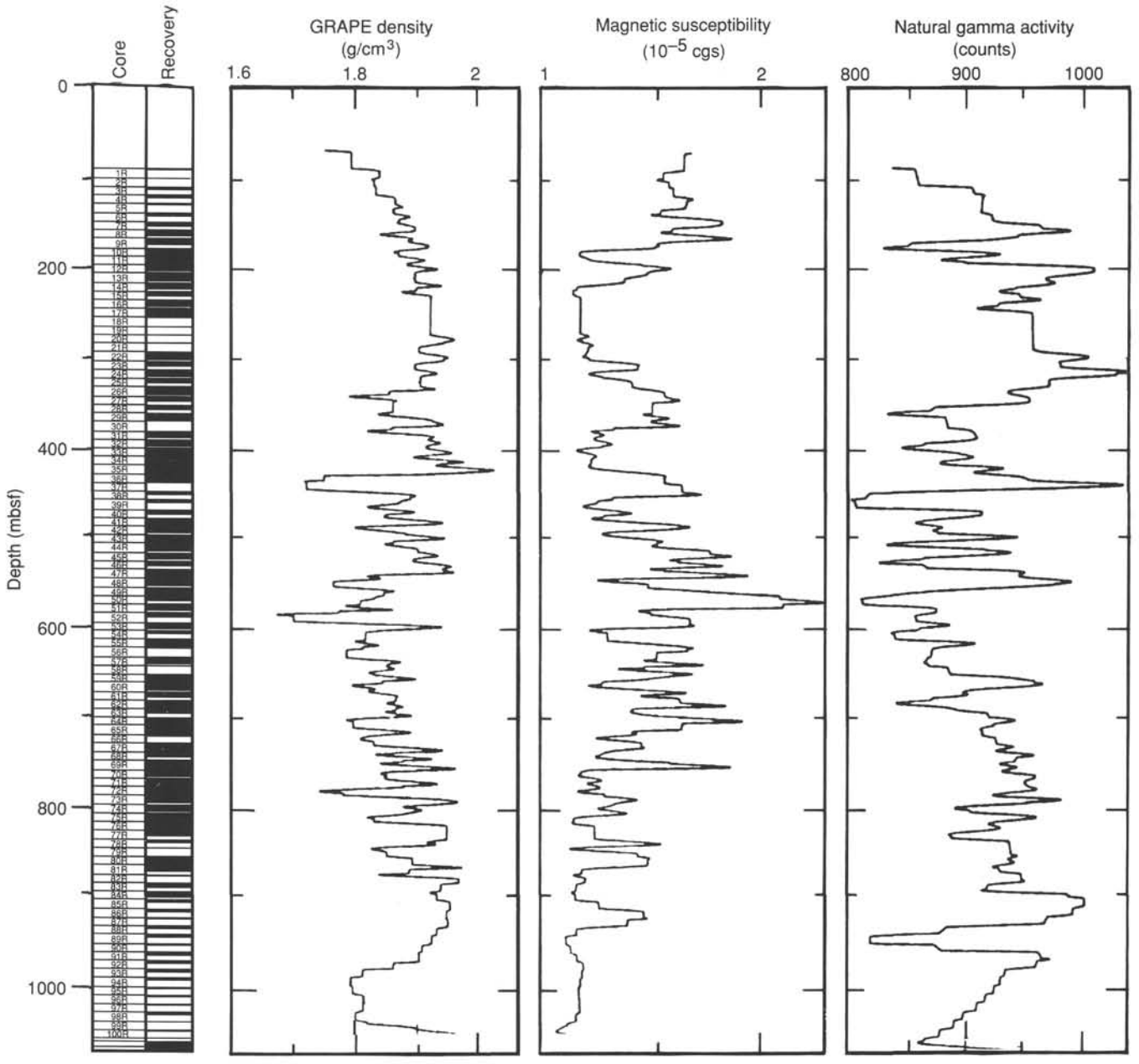

Figure 28. GRAPE density, magnetic susceptibility (logarithmic scale), and natural gamma activity for Hole 909C. Data were filtered using a fast Fourier transform routine.

Split-core Measurements

Compressional-wave Velocity

The Digital Sound Velocimeter and the Hamilton Frame were used to measure the speed of passage of a compressional wave through the sediment. These waves require a continuous medium through which to transmit their energy, and, therefore, undisturbed sediments with no cracks or air-filled pores in the section (which attenuate the acoustic signal) are a prerequisite for good quality data. The presence of both micropores and macroscopic cracks in the cores precluded measurement of velocity below a depth of 24 mbsf in both Holes 909A and 909B. Severe drilling disturbance limited measurements in Hole 909C to between 610 and 1058 mbsf, at which depth the sediments consisted of intact lithified shale and siltstones. Velocity data is presented in Table 14.

Reasonable results were obtained to 24 mbsf in Holes 909A and 909B with recorded values in the range 1490–1700 m/s (Fig. 31). The fluctuations in the data likely reflect interbedded stiff and softer mud layers observed in the laboratory. Peaks in wave velocity at 4.9 and 15 mbsf correspond well to excursions in the bulk density to above 2.0 g/cm^3, probably in response to an increase in the coarse (silt) fraction. A third peak is evident in both holes at about 20–23 mbsf where velocities exceed 1600 m/s. This is coincident with marked changes in the index properties and strength data suggesting the presence of an indurated, slightly more compact layer at this depth.

Measurements on sediments retrieved from below 610 m in Hole 909C comprised lithified shale, siltstone, and sandstone. These sedi-

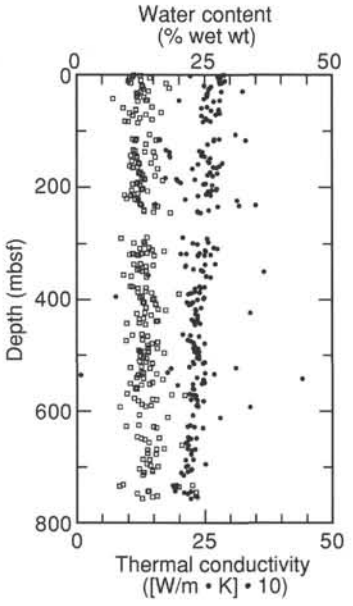

Figure 29. Water content (closed circles) and thermal conductivity (open squares) for Hole 909C.

ments were stiff, although not completely incompressible, and therefore exhibited significantly higher mean velocities (Fig. 31). A mean compressional-wave velocity for all data from Hole 909C was 1830 ± 143 m/s, within a range of 1547–2045 m/s. The lack of any velocity data at intermediate depths precludes assessment of the depth variation of acoustic velocity. However, the increase from 1521 m/s at 22.10 mbsf (Hole 909A) to 1751 m/s at 610 mbsf (Hole 909C) indicates a weak downhole gradient. Data from the wireline log (see "Downhole Measurements" section, this chapter) suggest this trend may be linear.

Replicate measurements using the Hamilton Frame were performed on hard, cemented sandstone blocks cut from the least disturbed parts of Cores 151-909C-88R and -90R. These consistently gave extremely high velocities of 4371 ± 191 m/s and 4374 ± 464 m/s, respectively. Although not typical of velocities at this site, these data demonstrate the influence cementation can have on the acoustic properties of deep marine sediments.

Shear Strength

Data from the rotary vane shear device and the hand-held penetrometer from Holes 909A, 909B, and 909C are plotted together in Figure 32. The vane shear device was used reliably down to 175 mbsf, and the penetrometer was used from 37–209 mbsf. Both devices show a general linear dependence of strength on depth from approximately 6 kPa at the mud-line (determined using the vane) to 100–200 kPa at 160–170 mbsf. Below this depth, the penetrometer data for Hole 909C indicate an increase in strength to 204 kPa at 101 mbsf. Between-hole correlation for each device is good, and slight increases in sediment strength caused by increases in bulk density (e.g., at 43 and 135–144 mbsf; Fig. 33) are picked up by both instruments. Both the vane and penetrometer data show greater heterogeneity (scatter) in sediment strength below ~100 mbsf, so this is more likely a sedimentological effect and not simply an instrument-related or operator-related bias. The distinct increase in the rate of change of strength with depth below ~160 mbsf is unclear. This occurs in the absence of any significant increase in bulk density, although this is roughly a zone where sediment index properties become significantly less variable (Fig. 33). This zone is generally coincident with the horizon where dropstone abundance falls steeply (to below four per

Table 13. Thermal conductivity measurements from Holes 909A and 909C.

Core, section, interval top (cm)	Depth (mbsf)	M	P #	TC_{corr} (W/m·K)	Std dev (W/m·K)	Drift (°C/min)
151-909A-						
1H-1, 75	0.75	F	332	1.120	0.00255	0.024
1H-2, 75	2.25	F	325	1.253	0.00364	0.008
1H-3, 75	3.75	F	338	1.091	0.00240	0.008
1H-4, 75	5.25	F	17	1.439	0.00352	0.013
2H-2, 75	9.75	F	332	1.267	0.00183	0.008
2H-3, 75	11.25	F	325	1.016	0.00180	–0.032
2H-5, 75	14.25	F	338	1.061	0.00322	–0.015
2H-6, 75	15.75	F	17	1.760	0.00366	0.010
3H-2, 75	19.25	F	332	1.283	0.00219	0.001
3H-3, 75	20.75	F	325	1.290	0.00206	0.022
3H-5, 75	23.75	F	338	1.821	0.00253	0.006
3H-6, 75	25.25	F	17	1.312	0.00264	0.009
4H-2, 75	28.75	F	332	1.409	0.00282	0.017
4H-3, 75	30.25	F	325	1.264	0.00181	0.019
4H-5, 75	33.25	F	338	1.181	0.00227	–0.003
4H-6, 75	34.75	F	17	1.198	0.00275	0.004
5H-2, 75	38.25	F	332	1.181	0.00240	0.007
5H-3, 75	39.75	F	325	1.320	0.00178	0.013
6H-1, 40	45.90	F	332	1.365	0.00256	0.022
6H-1, 40	45.90	F	332	1.389	0.00213	0.026
6H-2, 40	47.40	F	325	1.203	0.00232	–0.007
7H-2, 75	57.66	F	332	1.483	0.00320	0.017
7H-3, 75	59.07	F	325	0.916	0.00329	–0.036
7H-5, 75	61.89	F	339	1.159	0.00227	–0.021
7H-6, 75	63.30	F	17	1.161	0.00296	0.010
8H-2, 75	67.15	F	332	1.654	0.00164	0.016
8H-3, 75	68.55	F	325	1.042	0.00287	–0.001
8H-5, 75	71.37	F	339	1.364	0.00288	0.019
8H-7, 75	73.05	F	17	1.100	0.00396	0.037
9H-3, 75	77.55	F	325	1.241	0.00240	–0.006
9H-5, 75	80.35	F	339	1.475	0.00284	0.024
10H-1, 50	83.10	F	332	0.957	0.00395	0.002
10H-1, 100	83.60	F	325	1.016	0.00199	0.005
151-909C-						
1R-1, 75	85.75	F	332	1.200	0.00181	0.012
4R-1, 50	114.40	F	332	1.168	0.00321	0.030
4R-1, 100	114.90	F	338	1.105	0.00178	0.019
4R-2, 50	115.90	F	39	1.621	0.00380	0.035
4R-2, 100	116.40	F	350	1.563	0.00260	0.035
4R-3, 25	117.08	F	17	1.153	0.00411	0.002
5R-1, 25	123.85	F	332	1.357	0.00238	0.033
6R-1, 75	133.95	F	332	1.115	0.00396	0.020
6R-2, 75	135.45	F	338	1.152	0.00305	0.016
6R-3, 75	136.95	F	339	1.339	0.00363	0.006
6R-4, 25	137.95	F	350	1.507	0.00299	0.034
7R-1, 75	143.65	F	332	1.061	0.00234	0.001
7R-1, 75	143.65	F	332	1.060	0.00232	0.030
7R-2, 75	145.15	F	338	1.183	0.00243	0.026
7R-3, 75	146.65	F	339	1.542	0.00264	0.039
7R-4, 75	148.15	F	350	1.178	0.00270	0.029
8R-1, 75	153.35	F	332	1.080	0.00301	0.007
8R-3, 75	156.35	F	338	1.213	0.00337	0.038
8R-4, 75	157.85	F	339	1.457	0.00262	0.027
8R-4, 75	157.85	F	339	1.457	0.00262	0.027
8R-5, 75	159.35	F	350	1.236	0.00217	0.035
9R-1, 75	163.05	F	332	1.040	0.00173	0.024
9R-2, 75	164.55	F	338	1.196	0.00232	0.014
9R-3, 75	166.05	F	339	1.104	0.00273	0.009
9R-4, 75	167.55	F	350	1.593	0.00347	0.033
10R-3, 75	175.65	F	338	1.219	0.00188	0.025
10R-6, 75	180.15	F	350	1.538	0.00222	0.026
11R-3, 70	185.30	F	338	1.338	0.00170	0.034
11R-4, 75	186.85	F	339	1.324	0.00287	0.018
11R-5, 75	188.35	F	350	1.690	0.00159	0.013
12R-1, 75	191.95	F	332	1.203	0.00255	0.016
12R-2, 75	193.45	F	338	1.171	0.00749	–0.003
12R-3, 75	194.95	F	339	1.106	0.00501	0.035
12R-4, 75	196.45	F	350	1.245	0.00228	0.010
13R-2, 75	203.05	F	332	1.302	0.00187	0.037
13R-3, 75	204.55	F	338	1.269	0.00242	0.036
13R-4, 75	206.05	F	339	1.085	0.00293	0.022
13R-5, 75	207.55	F	350	1.391	0.00200	0.021
14R-2, 100	213.00	F	338	1.126	0.00273	0.015
14R-3, 100	214.50	F	339	0.942	0.00990	0.013
14R-4, 100	216.00	F	350	1.072	0.00121	0.001
15R-2, 75	222.35	F	338	1.154	0.00193	0.000
15R-3, 75	223.85	F	339	1.201	0.00311	0.033
15R-4, 75	225.35	F	350	1.609	0.00410	0.051
16R-1, 75	230.35	F	332	1.242	0.00275	0.024
16R-2, 75	231.85	F	338	1.276	0.00261	0.005
16R-3, 75	233.35	F	339	1.530	0.00175	0.022
16R-4, 75	234.85	F	350	1.592	0.00157	0.024
17R-3, 75	242.95	F	338	1.320	0.00284	0.029
17R-4, 75	244.45	F	339	1.505	0.00326	0.034
17R-5, 75	245.95	F	350	1.836	0.00376	0.039

Table 13 (continued).

Core, section, interval top (cm)	Depth (mbsf)	M	P #	TC_{corr} (W/m·K)	Std dev (W/m·K)	Drift (°C/min)
22R-2, 75	289.75	F	332	1.383	0.00261	0.032
22R-3, 75	291.25	F	338	0.873	0.00859	–0.006
23R-1, 75	297.85	F	332	1.326	0.00195	0.031
23R-2, 75	299.35	F	338	1.127	0.00430	0.017
23R-3, 70	300.80	F	339	1.343	0.00328	0.024
24R-2, 75	309.05	F	338	1.238	0.00244	0.024
24R-4, 75	312.05	F	339	1.474	0.00231	0.019
24R-5, 75	313.55	F	350	1.721	0.00416	0.038
27R-1, 75	336.45	F	332	1.250	0.00392	0.029
27R-2, 75	337.95	F	338	1.121	0.00301	0.017
27R-3, 75	339.45	F	339	1.503	0.00400	0.027
27R-4, 75	340.95	F	350	1.360	0.00268	0.034
28R-1, 75	346.05	F	332	1.235	0.00362	0.022
28R-2, 75	347.55	F	338	1.189	0.00314	0.017
28R-3, 75	349.05	F	339	1.363	0.00345	0.022
28R-4, 75	350.55	F	350	1.293	0.00397	0.022
29R-2, 75	357.15	F	332	0.923	0.00260	0.017
29R-3, 75	358.65	F	338	1.075	0.00210	0.017
29R-4, 75	360.15	F	339	1.367	0.00341	0.021
32R-2, 75	385.85	F	332	1.351	0.00105	0.027
32R-3, 75	387.35	F	338	1.202	0.00243	0.038
32R-4, 75	388.85	F	339	1.466	0.00254	0.037
32R-5, 75	390.35	F	350	2.006	0.00155	0.037
33R-2, 75	395.35	F	332	1.284	0.00189	0.037
33R-3, 75	396.85	F	338	1.242	0.00442	0.030
33R-4, 75	398.35	F	339	1.521	0.00142	0.035
33R-5, 75	399.85	F	350	1.487	0.00243	0.034
34R-2, 80	405.10	F	332	1.323	0.00252	0.024
34R-2, 80	405.10	F	332	1.305	0.00205	0.018
34R-3, 75	406.55	F	338	1.308	0.00279	0.023
34R-4, 75	408.05	F	339	1.548	0.00261	0.020
34R-5, 75	409.55	F	350	1.552	0.00333	0.035
35R-2, 75	414.65	F	332	1.364	0.00272	0.013
35R-4, 75	417.65	F	339	1.595	0.00205	0.030
35R-5, 75	419.15	F	350	1.750	0.00185	0.020
36R-2, 75	424.35	F	332	1.339	0.00241	0.040
36R-3, 75	425.85	F	338	1.184	0.00342	0.020
36R-5, 75	428.85	F	339	1.460	0.00248	0.027
37R-2, 75	433.95	F	332	1.315	0.00231	0.009
37R-3, 75	435.45	F	338	1.233	0.00209	0.023
37R-5, 75	438.45	F	339	1.586	0.00334	0.014
37R-6, 75	439.95	F	350	1.557	0.00288	0.020
38R-1, 75	442.05	F	332	1.234	0.00258	0.017
38R-2, 75	443.55	F	338	0.982	0.00458	0.014
38R-3, 70	445.00	F	339	1.352	0.00474	0.026
40R-2, 40	462.50	F	332	1.277	0.00334	0.031
40R-4, 75	465.85	F	339	1.388	0.00291	0.027
41R-2, 75	472.55	F	332	1.288	0.00245	0.016
41R-3, 75	474.05	F	338	0.976	0.00707	0.021
41R-5, 75	477.05	F	339	1.589	0.00272	0.028
41R-6, 75	478.55	F	350	1.475	0.00348	0.017
42R-2, 75	482.25	F	332	1.389	0.00251	0.027
42R-5, 70	486.70	F	339	1.410	0.00967	0.038
42R-6, 19	487.69	F	350	1.578	0.00911	–0.006
43R-2, 75	491.75	F	332	1.222	0.00267	0.006
43R-3, 75	493.25	F	338	1.327	0.00244	0.019
43R-3, 75	493.25	F	338	1.408	0.00114	0.028
43R-4, 75	494.75	F	339	1.398	0.00330	0.013
43R-5, 75	496.25	F	350	1.717	0.00884	0.030
44R-2, 75	501.25	F	332	1.248	0.00130	0.032
44R-4, 75	504.25	F	339	1.307	0.00371	0.028
44R-5, 75	505.75	F	350	1.373	0.00503	–0.007
45R-2, 75	510.85	F	332	1.237	0.00213	0.012
45R-3, 75	512.35	F	338	1.346	0.00138	0.007
45R-4, 75	513.85	F	339	1.480	0.00273	0.015
45R-5, 75	515.35	F	350	1.481	0.00208	0.024
46R-2, 50	520.30	F	338	1.264	0.00269	0.009
46R-3, 75	522.05	F	339	1.047	0.00396	0.009
46R-4, 75	523.55	F	350	1.431	0.00929	0.031
47R-2, 75	530.25	F	332	1.258	0.00212	0.027
47R-3, 75	531.75	F	338	1.305	0.00293	0.013
47R-4, 75	533.25	F	339	1.556	0.00276	0.005
47R-5, 75	534.75	F	350	1.198	0.00739	0.023
48R-3, 75	541.45	F	338	1.306	0.00285	0.022
48R-4, 75	542.95	F	339	1.682	0.00244	0.033
49R-2, 75	548.85	F	332	1.481	0.00210	0.037
49R-3, 75	550.35	F	338	1.038	0.00503	0.009
49R-4, 75	551.85	F	339	1.416	0.00251	0.039
49R-5, 75	553.35	F	350	1.257	0.00752	–0.008
50R-1, 75	557.65	F	332	1.166	0.00299	0.038
50R-2, 75	559.15	F	338	1.138	0.00278	0.007
50R-3, 75	560.65	F	339	1.174	0.00379	0.024
51R-2, 75	568.85	F	338	0.982	0.00540	0.020
52R-1, 75	576.95	F	332	1.123	0.00349	0.015
52R-2, 75	578.45	F	338	1.482	0.00518	0.028
52R-3, 75	579.95	F	339	1.561	0.00392	0.030
52R-4, 75	581.45	F	350	1.201	0.00582	–0.006
55R-2, 50	607.10	F	332	1.217	0.00259	0.021
55R-5, 35	611.45	F	339	1.773	0.00217	0.039
57R-1, 75	625.15	F	332	1.216	0.00287	0.035
57R-2, 60	626.50	F	338	0.961	0.00245	0.024
59R-5, 75	650.45	F	350	1.328	0.00557	0.034
60R-2, 75	655.65	F	332	1.413	0.00237	0.034
60R-5, 75	660.15	F	350	2.054	0.00731	–0.015
61R-3, 80	666.80	F	338	1.710	0.00243	0.035
61R-5, 80	669.80	F	350	1.383	0.00228	–0.001
62R-2, 80	675.00	F	332	1.384	0.00253	0.008
62R-3, 80	676.50	F	338	1.545	0.00496	0.012
63R-3, 70	686.00	F	339	1.293	0.00324	–0.004
63R-4, 25	687.05	F	350	1.423	0.00441	–0.016
70R-2, 75	751.85	F	332	1.564	0.00262	0.031
70R-3, 75	753.35	F	338	1.474	0.00488	0.006
70R-5, 75	756.35	F	350	1.277	0.00291	0.012

Notes: M = method used, either F = full-space or H = half-space; P # = probe number used for test; TC_{corr} = thermal conductivity corrected for drift; Std dev = standard deviation of the measurement.

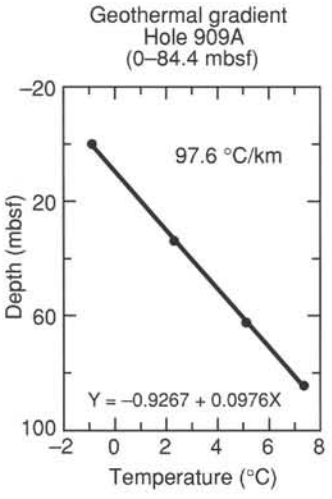

Figure 30. Geothermal temperature gradient in Hole 909A (0–84.4 mbsf) measured by the Adara tool.

core, normalized to recovery), but this should not be a factor because, in all cases, measurements were performed in undisturbed sediment. Therefore, this strength increase may reflect some fundamental change in sedimentation pattern or mode. Shear strength data for each of the holes are summarized in Table 15.

Index Properties

Selected data from the index properties measurements at Site 909C are shown in Figure 33, and summarized in Table 16. Data from all three holes give complete depth coverage down to 1061.6 mbsf. The mean trend of index properties reflects a consolidation profile for virtually homogeneous terrigenous marine muds. Bulk density increases from a mud-line value of ~1.60–1.70 g/cm^3 to 2.30–2.40 g/cm^3 at 1000 mbsf. Commensurate decreases in porosity range from surface values of 68% to ~25%. The void ratio changes systematically as well, decreasing from ~2.1 at the mud line to ~0.33 at 1000 mbsf. Unlike other sites on this leg, however, bulk density (and hence dry density and porosity) does not approach a constant value, even at 1000 mbsf. This differs from other sites, where compaction gradients at this depth are considerably smaller. Grain density exhibits a slight linear decrease with depth to the base of the section at 1061.6 mbsf,

Table 14. Compressional-wave velocity measurements, Site 909.

Core, section, interval (cm)	Depth (mbsf)	Tool	Velocity Perp (m/s)
151-909A-			
1H-1, 25–32	0.25	dsv	1501
1H-2, 50–57	2.00	dsv	1503
1H-3, 50–57	3.50	dsv	1506
1H-4, 25–32	4.75	dsv	1641
1H-4, 50–57	5.00	dsv	1643
1H-4, 50–57	5.00	dsv	1531
1H-5, 50–57	6.50	dsv	1500
2H-1, 53–60	8.03	dsv	1506
2H-2, 58–65	9.58	dsv	1590
2H-3, 48–55	10.98	dsv	1501
2H-4, 54–62	12.54	dsv	1550
2H-5, 44–51	13.94	dsv	1525
2H-6, 38–45	15.38	dsv	1582
2H-7, 27–34	16.77	dsv	1477
3H-1, 60–67	17.60	dsv	1514
3H-2, 28–35	18.78	dsv	1533
3H-3, 43–50	20.43	dsv	1629
3H-3, 67–74	20.67	dsv	1575
3H-4, 55–62	22.05	dsv	1521
151-909B-			
1H-1, 50–57	0.50	dsv	1506
1H-2, 50–57	2.00	dsv	1506
1H-3, 50–57	3.50	dsv	1513
2H-1, 50–57	4.90	dsv	1649
2H-1, 50–57	4.90	dsv	1601
2H-1, 120–127	5.60	dsv	1492
2H-2, 50–57	6.40	dsv	1554
2H-3, 50–57	7.90	dsv	1510
2H-4, 50–57	9.40	dsv	1525
2H-6, 50–57	12.40	dsv	1561
3H-1, 25–32	14.15	dsv	1493
3H-1, 50–57	14.40	dsv	1668
3H-1, 120–127	15.10	dsv	1681
3H-2, 25–32	15.65	dsv	1699
3H-2, 55–62	15.95	dsv	1542
3H-2, 93–100	16.33	dsv	1689
3H-2, 117–124	16.57	dsv	1508
3H-3, 50–57	17.40	dsv	1503
3H-4, 50–57	18.90	dsv	1492
3H-5, 45–52	20.35	dsv	1526
3H-6, 55–62	21.95	dsv	1629
4H-1, 56–63	23.96	dsv	1533
151-909C-			
55R-4, 27–29	609.87	ham	1751
55R-4, 27–29	609.87	ham	2036
62R-4, 100–102	678.20	ham	1952
62R-4, 145–147	678.65	ham	1824
63R-2, 100–102	684.80	ham	1548
63R-4, 40–42	687.20	ham	1926
64R-3, 140–142	696.40	ham	1729
64R-3, 140–142	696.40	ham	1802
66R-1, 89–91	711.99	ham	1794
69R-3, 52–54	743.52	ham	1816
71R-1, 120–122	760.50	ham	1744
71R-1, 129–131	760.59	ham	1865
72R-1, 90–92	769.90	ham	1661
73R-4, 115–117	784.35	ham	1960
74R-1, 115–117	789.45	ham	1741
75R-3, 95–97	801.95	ham	1928
75R-6, 120–122	806.70	ham	1983
75R-6, 120–122	806.70	ham	1895
76R-2, 100–102	810.10	ham	1671
76R-3, 30–32	810.90	ham	1681
76R-4, 80–82	812.90	ham	1655
76R-4, 80–82	812.90	ham	1558
80R-1, 145–147	847.65	ham	1825
80R-5, 145–147	853.65	ham	1729
81R-2, 145–147	858.85	ham	1987
81R-3, 79–81	859.69	ham	1978
82R-2, 40–42	867.40	ham	1987
83R-4, 46–48	880.06	ham	2006
84R-3, 90–92	888.70	ham	2045
88R-2, 56–58	925.46	ham	4394
88R-2, 56–58	925.46	ham	4180
88R-2, 56–58	925.46	ham	4238
88R-2, 56–58	925.46	ham	4672
90R-1, 50–52	943.30	ham	1841
90R-2, 68–70	944.98	ham	1571
90R-2, 80–82	945.10	ham	3726
90R-2, 80–82	945.10	ham	4831
90R-2, 80–82	945.10	ham	4479
90R-2, 80–82	945.10	ham	4461
91R-2, 64–66	954.54	ham	1933
91R-2, 110–112	955.00	ham	1890
92R-1, 79–81	962.89	ham	1817
92R-2, 129–131	964.89	ham	1950
94R-3, 21–23	984.51	ham	2272
98R-1, 139–141	1021.09	ham	1705
99R-1, 107–109	1030.27	ham	1972
100R-2, 10–12	1040.40	ham	2084
101R-1, 42–44	1048.82	ham	2084
101R-2, 45–47	1050.35	ham	2094
102R-1, 25–27	1052.95	ham	2074
102R-2, 124–126	1055.44	ham	2105
102R-4, 50–52	1057.70	ham	2136
103R-1, 113–115	1059.13	ham	2273

Note: Tool = device used for measurement, either dsv = digital sound velocimeter or ham = Hamilton Frame. Perp = perpendicular.

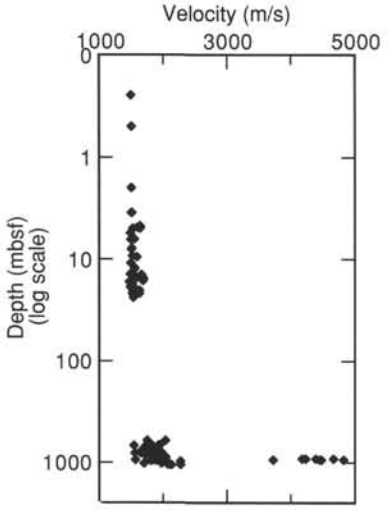

Figure 31. Velocity data from Holes 909A and 909B (0.25–23.96 mbsf) and Hole 909C (609.87–1059.13 mbsf).

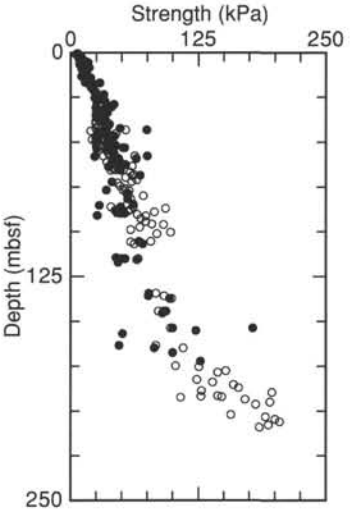

Figure 32. Strength measurements from Holes 909A, 909B, and 909C. Closed circles = vane shear data; open circles = penetrometer data.

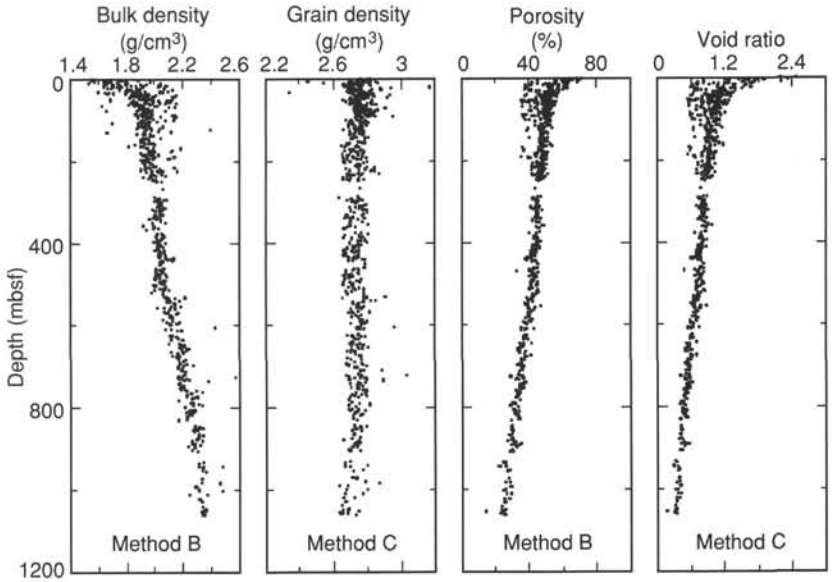

Figure 33. Selected index property measurements from Hole 909C.

probably in response to a general, weak coarsening in grain size and a decrease in the clay fraction with depth (particularly below 550 mbsf; see "Lithostratigraphy" section, this chapter).

The upper layer sediments (0–160 mbsf) record a much higher variability in sediment properties compared with deeply buried sediments. Closely spaced (on the order of 0.5–1.0 m) sediment layers display significant differences with respect to bulk density, water content, and void ratio. The wide scatter evident in the porosity data (and the general poor correlation with the GRAPE density, see Fig. 26) strongly suggests that disturbance caused by gas has influenced the quality of the data. However, this may also be quantitative evidence of alternating firm (higher sand content) and soft (clay-rich) sections. These heterogeneous upper layers grade into a more uniform sediment below a depth of about 150 mbsf, roughly the depth of the Quaternary/Pliocene boundary (see "Biostratigraphy" section, this chapter). To 540 mbsf, consolidation increases, but at a slower rate, tending to a bulk density of ~2.05 g/cm^3. A large proportion of this section (287–513 mbsf) coincides with lithologic Unit II, which comprises massively bedded, homogeneous silty clays.

The bulk-density profile reveals a significant discontinuity at 540 mbsf, almost exactly at the boundary between lithologic Unit II and the laminated silts and clays of lithologic Subunit IIIA. Bulk density increases from ~2.05 g/cm^3 to 2.15 g/cm^3 within several tens of meters. Beneath this, bulk density increases roughly linearly to 2.36 g/cm^3 at the base of the hole (1061 mbsf), where lithified siltstones are found. This entire lower section of the hole, therefore, documents a considerably higher rate of compaction with respect to overlying sediments, with much steeper density and water content gradients. Undoubtedly this is because of the laminated structure of the sediments in lithologic Unit III, in which coarser layers permit the egress of water, allowing sediments to compact further. The increase in density, where sediment structure changes, demonstrates clearly how sediment structure and composition exert a significant influence on physical properties. Although the very fine structure of lithologic Subunit IIIA cannot be related to the variability in index properties, local peaks in the bulk density (e.g., ~800, 900, and 950 mbsf) correlate reasonably well with wide intervals of higher sand content (>5%; see "Lithostratigraphy" section, this chapter).

Geotechnical Units

Four geotechnical units are proposed on the basis of the physical properties data. Statistics abstracted from the index properties data summarizing these units may be found in Table 17. Geotechnical Unit G-I extends from the mud line to approximately 25 mbsf. These muds exhibit the steepest gradients in sediment properties. Geotechnical Unit G-II represents the downhole decrease in the rate of change of sediment properties to 150 mbsf. Both units are characterized by a generally wider variability in sediment properties in relation to deeper units. Geotechnical Unit G-III is a comparatively uniform layer, exhibiting only limited increases in compaction, to 530 mbsf. Geotechnical Unit G-IV represents the high-density, steeper gradient section containing sedimentary structures, and extends to the base of the hole at 1061 mbsf.

DOWNHOLE MEASUREMENTS

Logging Operations

Two Schlumberger tool strings were run in Hole 909C: the quad combination and the Formation MicroScanner. The wireline heave compensator (WHC) was used to counter mild ship heave (0.1–0.3 m of motion). Due to anticipated poor hole conditions and the deviated nature of the borehole indicated from the multishot tool (see "Operations" section, this chapter) the conical sidewall entry sub (CSES) was rigged up. Hole 909C was logged in two sections because of operational limitations when using the CSES. A summary description of the logging tool strings used during Leg 151 is found in the "Explanatory Notes" chapter of this volume. A summary of the logging operations at Hole 909C is given in Table 18.

The base of pipe was initially set at 590.6 mbsf in preparation for logging the lower half of the hole. The quad combination tool string comprising sonic (SDT), induction (DIT), lithodensity (HLDT) and natural gamma-ray (NGT) tools along with the Lamont-Doherty temperature logging tool (TLT) was run first. An attempt was made to run the tool string down in open hole, but progress was stopped by a bridge at 701 mbsf. The tool was pulled back into pipe, and the drill string was then run to the base of the hole, where 38 m of fill was found. The tool string was deployed for a second time and reached a depth of 1013 mbsf (drilled TD = 1061.8 mbsf). Data were recorded at a logging speed of 900 ft/hr from 1013 mbsf to the end of pipe (pulled up to 561 mbsf). A repeat upgoing log was then recorded at 900 ft/hr from 705 to 591 mbsf. The HLDT was run in high-resolution mode recording data at 1.2-in. increments during the main run, but the tool failed during the repeat pass and recorded no data.

Table 15. Shear strength measurements, Site 909.

Core, section, interval (cm)	Depth (mbsf)	SN	Vane (kPa)	Res (kPa)	Pen (kPa)
151-909A-					
1H-1, 55–56	0.55	1	7	5	
1H-2, 55–56	2.05	1	9	4	
1H-3, 55–56	3.55	1	8	3	
1H-4, 55–56	5.05	1	15	10	
1H-5, 55–56	6.55	1	9	7	
2H-1, 56–57	8.06	1	12	12	
2H-2, 61–62	9.61	1	11	5	
2H-3, 53–54	11.03	1	15	7	
2H-4, 57–58	12.57	1	13	9	
2H-5, 46–47	13.96	1	20	11	
2H-6, 41–42	15.41	1	17	8	
2H-7, 30–31	16.80	1	28	19	
3H-1, 64–65	17.64	1	22	12	
3H-2, 30–31	18.80	1	22	12	
3H-3, 70–71	20.70	1	22	12	
3H-4, 58–59	22.08	1	24	14	
3H-5, 56–57	23.56	1	32	18	
3H-6, 82–83	25.32	1	23	13	
3H-7, 28–29	26.28	1	31	17	
4H-1, 102–103	27.52	1	26	14	
4H-2, 87–88	28.87	1	35	17	
4H-3, 98–99	30.48	1	24	133	
4H-4, 93–94	31.93	1	31	15	
4H-5, 87–88	33.37	1	36	20	
4H-6, 106–107	35.06	1	25	14	
4H-7, 41–42	35.91	1	25	14	
5H-1, 108–109	37.08	1	34	17	
5H-2, 101–102	38.51	1	35	16	
5H-3, 89–90	39.89	1	37	18	
5H-4, 108–109	41.58	1	35	16	
5H-5, 105–106	43.05	1	75	55	
5H-6, 106–107	44.56	1	27	15	
5H-7, 35–36	45.35	1	31	17	
5H-1, 105–106	37.05				27
5H-2, 105–106	38.55				32
5H-3, 105–106	40.05				38
5H-4, 105–106	41.55				35
5H-5, 105–106	43.05				54
5H-6, 105–106	44.55				33
5H-7, 45–46	45.45				33
6H-1, 66–67	46.16	1	28		
6H-2, 53–54	47.53	1	24	18	
6H-3, 50–51	48.27	1	26	14	
6H-4, 96–97	49.56	1	25	11	
6H-5, 114–115	51.16	1	25		
6H-6, 96–97	52.40	1	25	20	
6H-7, 78–79	53.64	3	25	15	
6H-1, 70–71	46.20				41
6H-2, 70–71	47.70				25
6H-3, 70–71	48.47				21
6H-4, 70–71	49.30				27
6H-5, 70–71	50.72				35
6H-6, 70–71	52.14				43
6H-7, 70–71	53.56				42
7H-1, 92–93	56.42	3	41	20	
7H-2, 99–100	57.90	3	24		
7H-3, 100–101	59.32	3	47	20	
7H-4, 100–101	60.73	3	42	20	
7H-5, 95–96	62.09	3	48	30	
7H-6, 100–101	63.55	3	37	20	
7H-7, 100–101	65.05	3	47		
7H-1, 67–68	56.17				37
7H-2, 67–68	57.58				32
7H-3, 67–68	58.99				42
7H-4, 60–61	60.33				46
7H-5, 60–61	61.74				46
7H-6, 60–61	63.15				60
7H-7, 60–61	64.65				42
8H-1, 25–26	65.25				44
8H-2, 25–26	66.65				58
8H-3, 25–26	68.05				62
8H-4, 25–26	69.46				54
8H-5, 25–26	70.87				65
8H-6, 25–26	71.89				60
8H-7, 25–26	72.55				46
9H-1, 25–26	74.25				48
9H-2, 25–26	75.65				53
9H-3, 25–26	77.05				57
9H-4, 25–26	78.45				55
9H-5, 25–26	79.85				71
11H-4, 50–51	89.10	3	52	15	
11H-4, 100–101	89.60	3	49	16	
11H-2, 30–31	86.10				16
11H-2, 105–106	86.85				93
11H-3, 30–31	87.50				59
11H-4, 30–31	88.90				82
11H-5, 30–31	90.30				65
151-909B-					
1H-1, 109–110	1.09	3	5	4	
1H-2, 109–110	2.59	1	11	10	
1H-3, 120–121	4.20	1	11	7	
2H-1, 110–111	5.50	1	17	8	
2H-2, 107–108	6.97	1	9	5	
2H-3, 107–108	8.47	1	18	6	
2H-4, 125–126	10.15	1	12	6	
2H-6, 125–126	13.15	1	11	11	
3H-1, 109–110	14.99	1	19	10	
3H-2, 122–123	16.62	1	14	8	
3H-2, 48–49	15.88	1	18	8	
3H-3, 119–120	18.09	1	19	12	
3H-4, 119–120	19.59	1	20	10	
3H-5, 114–115	21.04	1	22	12	
3H-6, 121–122	22.61	1	24	12	
4H-1, 60–61	24.00	1	27	15	
4H-1, 98–99	24.38	1	30	12	
4H-2, 74–75	25.64	1	29	12	
4H-3, 88–89	27.28	1	34	15	
4H-4, 102–103	28.92	1	42	18	
4H-5, 99–100	30.39	3	40	20	
4H-6, 75–76	31.65	3	33	16	
4H-7, 32–33	32.72	3	25	14	
5H-1, 60–61	33.50	3	27	10	
5H-2, 60–61	35.00	3	29	15	
5H-3, 60–61	36.50	3	27	14	
5H-4, 50–51	37.90	3	29	14	
5H-5, 70–71	39.60	3	37	20	
5H-6, 93–94	41.33	3	33	16	
5H-7, 47–48	42.37	3	48	24	
5H-1, 75–76	33.65				27
5H-2, 75–76	35.15				25
5H-3, 75–76	36.65				29
5H-4, 75–76	38.15				25
5H-5, 75–76	39.65				25
5H-6, 75–76	41.15				27
5H-7, 30–31	42.20				25
6H-1, 115–116	43.55	3	31	12	20
6H-2, 115–116	45.05	3	36	18	44
6H-3, 110–111	46.50	3	43	23	38
6H-4, 115–116	48.05	3	37	15	30
6H-5, 117–118	49.57	3	36	17	33
6H-6, 115–116	51.05	3	42	25	28
6H-7, 50–51	51.90	3	42	21	44
7H-1, 105–106	52.95	3	51	30	52
7H-2, 117–118	54.57	3	35	19	27
7H-3, 115–116	56.05	3	42	25	42
7H-4, 116–117	57.56	3	75	31	62
7H-5, 115–116	59.05	3	64	26	47
7H-6, 115–116	60.55	3	48	21	41
7H-7, 13–14	61.03	3	40	15	35
8H-1, 103–104	62.43	3	53	19	
8H-3, 103–104	65.43	3	49	24	
8H-5, 110–111	68.50	3	68	15	
8H-1, 115–116	62.55				54
8H-3, 115–116	65.55				39
8H-5, 120–121	68.60				60
9H-1, 110–111	72.00	3	41	23	
9H-4, 110–111	76.50	3	35	21	
9H-1, 120–121	72.10				41
9H-4, 120–121	76.60				51
10H-1, 110–111	78.50	3	56	15	55
10H-3, 115–116	81.55	3	56	20	59
10H-5, 120–121	84.60	3	61	30	55
11H-1, 110–111	88.00	3	43	14	
11H-2, 110–111	89.50	3	45	15	
11H-3, 105–106	90.95	3	26	30	
11H-1, 125–126	88.15				56
11H-2, 120–121	89.60				52
11H-3, 120–121	91.10				74
11H-4, 120–121	92.60				69
11H-5, 125–126	94.15				74
11H-6, 135–136	95.75				79
11H-7, 15–16	96.05				91
12H-1, 90–91	97.30				67
12H-2, 90–91	98.80				59
12H-3, 90–91	100.30				98
12H-4, 20–21	101.10				84
151-909C-					
1R-1, 25–26	85.25	1	28		
1R-1, 100–101	86.00	1	49	17	39
3R-1, 111–112	105.41	1	66		78
3R-1, 125–126	105.55	3	67	25	59
3R-2, 108–109	106.88	3	70	25	62
4R-1, 46–47	114.36	3	44		
4R-1, 108–109	114.98	3	50	14	
4R-1, 125–126	115.15	3	53	20	66
4R-2, 25–26	115.65	3	65	30	
4R-3, 25–26	117.08	3	46	25	
6R-1, 110–111	134.30	3	77	22	83
6R-2, 110–111	135.80	3	76	29	92

Table 15 (continued).

Core, section, interval (cm)	Depth (mbsf)	SN	Vane (kPa)	Res (kPa)	Pen (kPa)
6R-3, 110–111	137.30	3	97	25	99
7R-1, 132–133	144.22	3	91	30	
7R-1, 138–139	144.28	3	94	25	86
7R-2, 110–111	145.50	3	90	25	
8R-1, 110–111	153.70	3	100	36	98
8R-1, 117–118	153.77	3	178		
8R-2, 110–111	155.20	3	122	37	123
8R-3, 117–118	156.77	4	51	13	
9R-1, 100–101	163.30	4	47		83
9R-2, 100–101	164.80	4	82	20	110
9R-4, 53–54	167.33	4	100	16	100
10R-1, 40–41	172.30	4	127	30	
10R-2, 120–121	174.60				103
10R-3, 40–41	175.30				126
10R-4, 110–111	177.50				152
10R-5, 40–41	178.30				144
11R-1, 75–76	182.35				124
11R-2, 75–76	183.85				139
11R-3, 75–76	185.35				159
11R-4, 75–76	186.85				164
11R-5, 110–111	188.70				128
11R-6, 40–41	189.50				197
12R-1, 40–41	191.60				144
12R-1, 65–66	191.85				127
12R-1, 85–86	192.05				148
12R-1, 120–121	192.40				108
12R-2, 79–80	193.49				171
12R-3, 75–76	194.95				195
12R-4, 75–76	196.45				181
13R-1, 120–121	202.00				157
13R-2, 75–76	203.05				190
13R-3, 75–76	204.55				200
13R-4, 75–76	206.05				204
13R-5, 75–76	207.55				194
13R-6, 75–76	209.05				185

Notes: SN = numbered spring used to make the measurement. Vane = undrained shear strength; Res = residual shear strength; Pen = unconfined shear strength as measured by the penetrometer.

The second tool string run into the hole was the Formation MicroScanner (FMS), in combination with an NGT tool. The tool string was deployed from the drill pipe just above the fill at the bottom of the hole, and an upgoing log was recorded at 1400 ft/hr from 1010–941 mbsf. The tool was then lowered back down the hole in an attempt to repeat a section over the bottom interval, but was stopped by a bridge at 965 mbsf. The main upgoing log was then recorded at 1400 ft/hr over the interval 965–597 mbsf.

No time was available to run the geochemical tool string in the lower half of the hole, as the priority was to run the quad-combination tool string in the upper part of the hole. In preparation to log the upper half of Hole 909C, the CSES was removed from the drill string, the pipe was pulled up to 80 mbsf, and the CSES was re-attached. The quad combination tool string was rigged up for the second time and deployed with the pipe set at 99 mbsf, but bridges blocked the tool string's downward progress in the open hole. The drill pipe eventually was run in to 551 mbsf, where the tool string was pumped out of pipe and reached a depth of 735 mbsf. The main upgoing log was recorded at a logging speed of 900 ft/hr from this depth to the mud line, providing a good overlap with the previous run in the bottom portion of the hole. The caliper measurement of the HLDT was functional during this run, but no density data were recorded because of a tool failure. No time was available for further logging runs.

Log Quality

The main logs from Hole 909C are shown in Figures 34 and 35. The logs are generally of good quality, although within the pipe the sonic, induction, and density data are invalid and the natural gamma-ray data are highly attenuated. As Hole 909C is quite wide and rugose, especially in the upper portion (see the hole caliper in Fig. 35), some logs have suffered in quality. The white area in the center of Figure 35 shows the diameter of a gauge hole drilled with the RCB coring bit, and the shaded areas show how much wider the hole is than originally drilled. Flat sections in the log mark where the caliper on the HLDT reached its maximum extension and where the eccentered tool could drift away from the borehole wall. These sections also represent areas where the density data and to a lesser degree the resistivity data may be degraded by the large borehole diameter.

For the most part, the velocity data from the logs are of very good quality. Some cycle skipping and other noise is present in the raw log data, but shipboard processing of the traveltimes eliminated most of these excursions. The sonic velocity presented in Fig. 35 is the processed data. Hole width also affected the natural gamma-ray activity log by artificially raising the count rate where the hole is narrow and lowering it where it is wide. This type of artifact is most obvious between 440 and 100 mbsf (Fig. 34) where the high "spikes" are caused by narrow borehole diameter at these intervals (see Fig. 35). Shore-based processing has corrected the logs for these environmental factors.

As can be seen from Figure 36, Hole 909C has a severe deviation from the vertical, ranging from 14° at 600 mbsf to a maximum of 25.6° at 1010 mbsf. The deviation strongly eccentralizes logging tool strings in the borehole. This in itself should not adversely affect most of the measurements, as the tool strings tend normally to be eccentralized. The most serious potential problem is with the FMS tool. The caliper arms of the tool are not especially powerful, and with a deviation over ~15°, the lateral component of the tool weight may partially force the pads to close. This may both affect the magnitude of the caliper reading and result in poor contact with the borehole wall for two of the four orthogonal pads of the FMS. Despite the 25° deviation in the lower section of the hole, the preliminary FMS data look of fairly good quality, and the FMS caliper data correlate well with the HLDT caliper. The HLDT caliper can be similarly affected but to a less severe degree, because it is more powerful.

Results

Temperature

The TLT was deployed on both runs of the quad combination tool string in Hole 909C (Fig. 37). The base of the hole was reached only on the first logging run, giving a bottom-hole (1013 mbsf) temperature of 44.5°C and a mud-line temperature of –1.45°C. An accurate thermal gradient cannot be obtained from this single measurement because cold seawater was circulated in the hole during drilling and during logging operations, which cools the adjacent formation; a minimum of three bottom-hole-temperature measurements over a period of time is required to extrapolate the true bottom-hole temperature and, hence, calculate the true thermal gradient. Nevertheless, the temperature gradient must have been greater than 45.4°C/km.

Lithology

The interval logged in Hole 909C (~1010–90 mbsf) covers lithostratigraphic Units I through III, (see "Lithostratigraphy" section, this chapter). This Quaternary to Miocene lithologic sequence is primarily a homogeneous, dark gray silty clay. Within Subunit IIIB sandy intervals with tight folds appear, probably representing slumps.

The expression of these units in the logs is for the most part subtle. The wet-bulk density profile, a combination of estimates from the resistivity log and from discrete shipboard measurements, best shows features correlatable to the lithostratigraphic units (Fig. 38). Unit I is marked by rapidly increasing bulk density downhole, and high-frequency, high-amplitude variations about the mean. Unit II, in contrast, has almost constant bulk density although it is also characterized by high-frequency variations in density with depth. The lithostratigraphic Unit I/II boundary (248 mbsf) is, however, distinctly deeper than the transition expressed by the bulk-density curve

Table 16. Index property measurements from Site 909.

Core, section, interval (cm)	Depth (mbsf)	WC-d (%)	WC-w (%)	WBD[a] (g/cm³)	WBD[b] (g/cm³)	GD[a] (g/cm³)	GD[b] (g/cm³)	DBD[a] (g/cm³)	DBD[b] (g/cm³)	Por[a] (%)	Por[b] (%)	VR[a]	VR[b]
151 -909A-													
1H-1, 113–115	1.13	71.65	41.74	1.65	1.70	3.24	2.93	0.96	0.99	67.23	69.40	2.05	2.27
1H-2, 54–56	2.04	69.75	41.09	1.64	1.63	2.76	2.82	0.97	0.96	65.74	65.22	1.92	1.88
1H-2, 128–130	2.78	59.40	37.26	1.74	1.70	2.81	2.98	1.09	1.07	63.34	61.93	1.73	1.63
1H-3, 53–55	3.53	67.42	40.27	1.67	1.63	2.71	2.91	1.00	0.97	65.70	64.06	1.92	1.78
1H-3, 112–114	4.12	86.97	46.52	1.58	1.54	2.75	2.96	0.84	0.82	71.54	69.97	2.51	2.33
1H-4, 29–31	4.79	31.37	23.88	1.97	1.94	2.70	2.78	1.50	1.48	46.00	45.23	0.85	0.83
1H-4, 54–56	5.04	47.93	32.40	1.80	1.79	2.78	2.81	1.21	1.21	56.76	56.49	1.31	1.30
1H-5, 52–54	6.52	65.75	39.67	1.69	1.58	2.45	2.94	1.02	0.95	65.37	61.09	1.89	1.57
2H-1, 56–58	8.06	81.74	44.98	1.53	1.57	2.77	2.56	0.84	0.86	67.16	68.83	2.05	2.21
2H-2, 21–23	9.21	27.17	21.36	2.05	2.02	2.73	2.81	1.61	1.59	42.65	42.02	0.74	0.72
2H-2, 61–63	9.61	47.27	32.10	1.81	1.78	2.71	2.85	1.23	1.21	56.76	55.59	1.31	1.25
2H-2, 111–113	10.11	57.83	36.64	1.73	1.70	2.74	2.89	1.10	1.08	61.95	60.73	1.63	1.55
2H-3, 52–54	11.02	62.40	38.42	1.66	1.68	2.78	2.70	1.02	1.03	62.15	62.86	1.64	1.69
2H-3, 119–121	11.69	33.43	25.06	1.94	1.85	2.54	2.78	1.46	1.39	47.54	45.31	0.91	0.83
2H-4, 5–7	12.05	37.84	27.45	1.90	1.88	2.74	2.82	1.38	1.36	50.99	50.25	1.04	1.01
2H-4, 57–59	12.57	47.39	32.15	1.75	1.78	2.73	2.63	1.19	1.21	54.91	55.76	1.22	1.26
2H-5, 46–48	13.96	61.98	38.26	1.71	1.67	2.76	2.91	1.05	1.03	63.74	62.49	1.76	1.67
2H-5, 108–110	14.58	41.25	29.21	1.87	1.84	2.73	2.83	1.32	1.30	53.24	52.36	1.14	1.10
2H-6, 37–39	15.37	27.51	21.58	2.03	1.99	2.69	2.78	1.59	1.56	42.70	41.92	0.75	0.72
2H-6, 42–44	15.42	44.55	30.82	1.83	1.81	2.75	2.82	1.27	1.25	55.11	54.41	1.23	1.19
2H-7, 31–33	16.81	27.08	21.31	2.03	1.99	2.67	2.76	1.60	1.57	42.14	41.35	0.73	0.71
3H-1, 63–65	17.63	59.95	37.48	1.71	1.68	2.71	2.87	1.07	1.05	62.63	61.35	1.68	1.59
3H-2, 30–32	18.80	52.12	34.26	1.77	1.73	2.71	2.83	1.16	1.14	59.00	57.94	1.44	1.38
3H-3, 70–72	20.70	40.77	28.96	1.67	1.82	2.67	2.24	1.19	1.29	47.15	51.50	0.89	1.06
3H-3, 139–141	21.39	58.77	37.01	2.04	1.53	2.17	4.92	1.29	0.97	73.81	55.42	2.82	1.24
3H-4, 58–60	22.08	63.07	38.67	1.69	1.65	2.69	2.87	1.04	1.01	63.85	62.31	1.77	1.65
3H-5, 26–28	23.26	40.37	28.76	1.87	1.84	2.72	2.81	1.33	1.31	52.57	51.76	1.11	1.07
3H-5, 46–48	23.46	24.54	19.70	2.07	2.04	2.69	2.77	1.66	1.64	39.86	39.16	0.66	0.64
3H-5, 141–143	24.41	50.27	33.45	1.82	1.76	2.75	2.97	1.21	1.17	59.32	57.44	1.46	1.35
3H-6, 63–65	25.13	41.65	29.40	1.90	1.85	2.77	2.93	1.34	1.30	54.39	52.94	1.19	1.13
3H-7, 16–18	26.16	43.07	30.11	1.88	1.83	2.76	2.94	1.32	1.28	55.29	53.70	1.24	1.16
4H-1, 47–49	26.97	40.93	29.04	1.88	1.85	2.76	2.86	1.34	1.31	53.33	52.45	1.14	1.10
4H-1, 141–143	27.91	27.02	21.27	2.05	2.02	2.73	2.81	1.61	1.59	42.52	41.86	0.74	0.72
4H-2, 31–33	28.31	45.79	31.41	1.81	1.78	2.68	2.80	1.24	1.22	55.59	54.50	1.25	1.20
4H-2, 89–91	28.89	33.22	24.93	1.93	1.92	2.70	2.74	1.45	1.44	47.04	46.67	0.89	0.88
4H-3, 38–40	29.88	25.59	20.37	2.07	2.02	2.69	2.79	1.64	1.61	41.06	40.19	0.70	0.67
4H-3, 96–98	30.46	44.65	30.87	1.85	1.82	2.77	2.89	1.28	1.26	55.70	54.68	1.26	1.21
4H-4, 47–49	31.47	44.44	30.77	1.65	1.82	2.76	2.27	1.14	1.26	49.64	54.49	0.99	1.20
4H-4, 108–110	32.08	43.32	30.23	1.84	1.80	2.69	2.82	1.29	1.26	54.35	53.21	1.19	1.14
4H-5, 42–44	32.92	37.57	27.31	1.90	1.86	2.69	2.80	1.38	1.35	50.67	49.61	1.03	0.98
4H-5, 109–111	33.59	40.29	28.72	1.71	1.84	2.70	2.35	1.22	1.31	48.00	51.46	0.92	1.06
4H-6, 25–27	34.25	43.16	30.15	1.87	1.83	2.78	2.89	1.30	1.28	54.87	53.91	1.22	1.17
4H-6, 108–110	35.08	40.78	28.97	1.87	1.84	2.71	2.83	1.33	1.30	52.93	51.91	1.12	1.08
4H-7, 41–43	35.91	50.20	33.42	1.80	1.76	2.75	2.89	1.20	1.17	58.56	57.35	1.41	1.34
5H-1, 71–73	36.71	36.43	26.70	1.94	1.91	2.78	2.86	1.42	1.40	50.41	49.70	1.02	0.99
5H-1, 126–128	37.26	42.65	29.90	1.88	1.85	2.81	2.93	1.32	1.29	54.93	53.87	1.22	1.17
5H-2, 14–16	37.64	23.44	18.99	2.16	2.10	2.79	2.91	1.75	1.70	39.94	38.97	0.67	0.64
5H-2, 101–103	38.51	16.65	14.27	1.91	2.53	3.34	2.22	1.63	2.17	26.53	35.18	0.36	0.54
5H-3, 17–19	39.17	32.60	24.58	2.01	1.95	2.76	2.94	1.52	1.47	48.30	46.77	0.93	0.88
5H-3, 98–100	39.98	47.92	32.40	1.83	1.79	2.80	2.95	1.24	1.21	57.99	56.66	1.38	1.31
5H-4, 36–38	40.86	36.33	26.65	1.95	1.92	2.80	2.90	1.43	1.41	50.72	49.84	1.03	0.99
5H-4, 109–111	41.59	35.08	25.97	1.96	1.91	2.75	2.87	1.45	1.42	49.58	48.45	0.98	0.94
5H-5, 45–47	42.45	34.10	25.43	1.99	1.94	2.78	2.92	1.48	1.45	49.30	48.08	0.97	0.93
5H-5, 105–107	43.05	22.41	18.31	2.15	2.09	2.73	2.85	1.75	1.71	38.37	37.41	0.62	0.60
5H-6, 49–51	43.99	33.06	24.84	1.99	1.95	2.78	2.90	1.50	1.46	48.34	47.23	0.94	0.90
5H-6, 105–107	44.55	37.48	27.26	1.95	1.90	2.79	2.94	1.42	1.38	51.81	50.46	1.08	1.02
5H-7, 34–36	45.34	37.52	27.28	1.93	1.88	2.73	2.87	1.40	1.37	51.26	49.99	1.05	1.00
6H-1, 38–40	45.88	34.96	25.90	1.93	1.90	2.70	2.81	1.43	1.41	48.90	47.98	0.96	0.92
6H-1, 77–79	46.27	41.17	29.17	1.89	1.85	2.77	2.90	1.34	1.31	53.85	52.65	1.17	1.11
6H-2, 54–56	47.54	36.05	26.50	1.95	1.91	2.77	2.88	1.43	1.40	50.32	49.33	1.01	0.97
6H-3, 50–52	48.27	35.68	26.30	1.93	1.89	2.70	2.81	1.42	1.39	49.48	48.42	0.98	0.94
6H-4, 97–99	49.57	37.43	27.23	1.91	1.88	2.72	2.83	1.39	1.36	50.85	49.83	1.03	0.99
6H-5, 112–114	51.14	42.39	29.77	1.85	1.82	2.70	2.81	1.30	1.28	53.78	52.78	1.16	1.12
6H-6, 33–35	51.77	34.94	25.89	1.95	1.90	2.70	2.84	1.44	1.41	49.22	47.93	0.97	0.92
6H-6, 95–97	52.39	21.11	17.43	2.12	2.08	2.66	2.74	1.75	1.72	36.11	35.37	0.57	0.55
6H-7, 19–21	53.05	30.18	23.19	1.99	1.96	2.70	2.79	1.53	1.50	45.08	44.29	0.82	0.80
6H-7, 76–78	53.62	27.60	21.63	2.04	1.99	2.70	2.81	1.60	1.56	43.09	42.10	0.76	0.73
7H-1, 25–27	55.75	40.51	28.83	1.88	1.84	2.72	2.83	1.34	1.31	52.80	51.84	1.12	1.08
7H-1, 99–101	56.49	35.82	26.37	1.93	1.89	2.71	2.83	1.42	1.39	49.76	48.61	0.99	0.95
7H-2, 25–27	57.16	25.88	20.56	2.08	2.01	2.68	2.83	1.65	1.60	41.66	40.33	0.71	0.68
7H-2, 99–101	57.90	31.45	23.92	1.99	1.95	2.71	2.82	1.51	1.48	46.36	45.41	0.86	0.83
7H-3, 25–27	58.57	36.45	26.71	1.93	1.89	2.73	2.85	1.42	1.39	50.34	49.29	1.01	0.97
7H-3, 99–101	59.31	42.83	29.99	1.84	1.82	2.72	2.81	1.29	1.27	53.97	53.24	1.17	1.14
7H-4, 25–27	59.98	40.56	28.86	1.88	1.84	2.71	2.84	1.34	1.31	52.96	51.71	1.13	1.07
7H-4, 99–101	60.72	39.40	28.26	1.90	1.85	2.70	2.88	1.37	1.32	52.52	50.92	1.11	1.04
7H-5, 25–27	61.39	40.42	28.78	1.89	1.86	2.77	2.88	1.35	1.32	53.17	52.18	1.14	1.09
7H-5, 99–101	62.13	35.29	26.09	1.77	1.94	2.83	2.38	1.31	1.43	45.00	49.34	0.82	0.97
7H-6, 25–27	62.80	46.90	31.93	1.82	1.79	2.74	2.86	1.24	1.22	56.66	55.63	1.31	1.25
7H-6, 99–101	63.54	45.16	31.11	1.86	1.81	2.76	2.94	1.28	1.25	56.45	54.90	1.30	1.22

Notes: WC-d = water content (% dry sample weight); WC-w = water content (% wet sample weight); WBD = wet-bulk density; GD = grain density; DBD = dry-bulk density; Por = porosity; VR = void ratio.

[a]Value calculated using Method B.

[b]Value calculated using Method C.

As a guide to the reader, the first page of this table is reproduced here. The entire table is given in the CD-ROM (back pocket).

Table 17. Statistical properties of geotechnical units defined for Site 909.

Geotechnical unit		Bulk density (g/cm^3)	Dry density (g/cm^3)	Water content (% wet wt)	Water content (% dry wt)	Grain density (g/cm^3)	Porosity (%)	Void ratio
I	Mean	1.76	1.21	51.04	32.96	2.71	55.90	1.35
(0-25 mbsf)	Max	2.04	1.66	86.97	46.51	2.80	69.97	2.33
	Min	1.54	0.84	24.54	19.70	2.45	39.16	0.64
	n = 29							
II	Mean	1.93	1.40	26.77	37.07	2.77	49.36	1.01
(25-150 mbsf)	Max	2.40	1.75	47.43	90.21	3.17	71.20	2.47
	Min	1.55	0.81	17.43	12.13	2.33	35.37	0.54
	n = 228							
III	Mean	2.02	1.54	23.36	30.60	2.73	44.70	0.81
(150-530 mbsf)	Max	2.19	1.81	31.08	45.09	2.87	53.82	1.16
	Min	1.82	1.25	15.03	18.06	2.30	32.63	0.49
	n = 234							
IV	Mean	2.23	1.87	16.42	19.86	2.73	34.12	0.53
(530-1061 mbsf)	Max	2.58	2.26	39.59	65.54	3.16	56.08	1.28
	Min	2.03	1.33	5.98	6.36	1.99	14.55	0.17
	n = 198							

Table 18. Summary of logging operations at Hole 909C.

9 Sept. 1993	
08:30	Last core on deck. Prepare hole for logging. Rig up CSES with pipe set at 590.6 mbsf.
10 Sept. 1993	
00:44	Rig up NGT-SDT-HLDT-DIT (+TLT)
01:50	RIH with NGT-SDT-HLDT-DIT (+TLT).
03:10	Unable to pass bridge at 701 mbsf; pull tool back into pipe and RIH with pipe to TD.
05:42	TD with tool reached at 1013 mbsf. Main upgoing log at 900 ft/hr from 1013 to 562 mbsf. HLDT run in high-resolution mode.
07:30	RIH for repeat section. Upgoing log from 705 mbsf to EOP (591 mbsf). HLDT tool failed on repeat run. POOH.
10:15	Rig up NGT-FMS.
11:00	RIH with NGT-FMS. RIH with drill pipe to TD.
13:28	TD with tool reached at 1010 mbsf; upgoing log at 1100 ft/hr from here to 941 mbsf.
13:47	RIH for main log, stopped by bridge at 965 mbsf. Upgoing log at 1400 ft/hr from 965 to 597 mbsf. POOH.
16:30	Prepare to log upper portion of hole, remove CSES from drill string, pull pipe to 80 mbsf and re-attach CSES.
19:00	Rig up NGT-SDT-HLDT-DIT (+TLT).
20:20	RIH with NGT-SDT-HLDT-DIT (+TLT). EOP at 99 mbsf. Stopped by bridge at 206 mbsf. Pull tool back into pipe and RIH with drill pipe to 331 mbsf.
22:13	Pump tool out of pipe and RIH. Unable to pass a second bridge at 368 mbsf. Pull tool back into pipe and RIH with drill string to 551 mbsf.
23:28	Main upgoing log at 900 ft/hr from 735 mbsf to mud line.
11 Sept. 1993	
02:35	End of upgoing log. POOH.
03:15	Rig down (2 hr). End of logging operations.

Notes: Times given in Universal Time Coordinated (UTC). Drillers TD (total depth) = 1061.8 mbsf. WD (water depth) = 2529.0 mbrf. POOH = pull out of hole. RIH = run in hole. EOP = end of pipe. For explanation of logging tools, see "Downhole Measurements" section, this chapter.

(~200 mbsf). The Unit II/III boundary marks the top of an interval characterized by increasing bulk density downhole and with low-frequency bulk-density variations.

Formation MicroScanner

The logging pass with the Formation MicroScanner not only provided images of the borehole between 1010 and 590 mbsf, but also provided important data about the deviation of the borehole from vertical. Unlike the other Leg 151 drill sites, Hole 909C was not vertical but instead deviated consistently to the Northeast. The deviation from vertical increased almost linearly from about 13° at 590 mbsf to 25.6° at the base of the hole (Fig. 36). The FMS-measured vertical hole deviation roughly coincides with the measurements of apparent dip of bedding in the recovered cores; the in-situ beds are probably flat-lying. Figure 39A illustrates the apparent dip of the beds caused by the deviated borehole.

The direction of the deviation was roughly constant, along a true azimuth of 048°N (Fig. 40). As the direction is constant, one can use the apparent dip of bedding within the cores to orient samples for detailed anisotropy studies of sediment fabric or magnetic properties. The cause of the hole deviation is not immediately apparent, although we suspect that the hole is following a direction of minimum stress within the sediments. Whether this direction fits with regional tectonic patterns has yet to be determined.

Subunit IIIB is characterized by folded bedding, interpreted as slump structures. These disturbed beds are primarily apparent in the FMS images in the intervals 1005–998 mbsf and 966–959 mbsf, corresponding well to the lithological descriptions of core material. An example of these structures is shown in Figure 39B. Post-cruise processing of the FMS data should considerably increase the quality of the images and provide computed dips of the beds downhole (the processed images and dipmeter data can be found on CD-ROM inside the back cover of this volume).

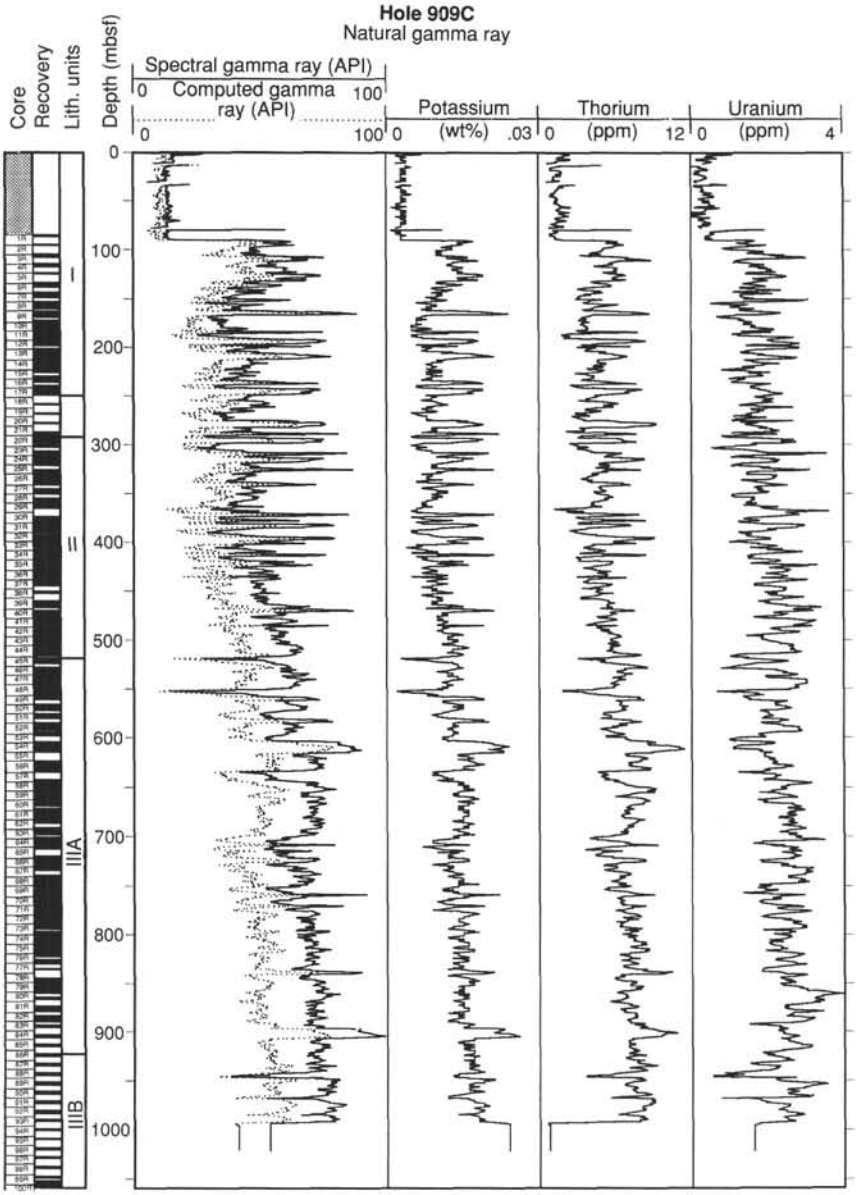

Figure 34. Data from the natural gamma-ray spectrometry tool (NGT) recorded on the quad combination tool string. The logs have undergone a linear 5-point (0.76 m) moving average filter for presentation clarity.

Porosity and Density Estimates from Resistivity

We calculated porosity (see "Explanatory Notes" chapter, this volume) using the deep phasor induction resistivity log (IDPH) from the dual induction tool with set values for the Archie (1942) equation of $a = 1$ and $m = 1.8$, based upon a calibration with the porosities measured on discrete samples (see "Physical Properties" section, this chapter). The fluid resistivity R_w is calculated based on its known relationships to temperature and salinity (Keller, 1982). Temperature was taken from the internal temperature measurement of the logging tool and interstitial salinities from core measurements (see "Inorganic Geochemistry" section, this chapter). In the temperature range encountered at this hole, R_w varies significantly downhole, and therefore a log of R_w was calculated as a function of depth.

The calculated porosities have a good correlation with those determined from discrete core samples (Fig. 41). The overall trends of the borehole profiles are similar, as are individual deviations from it. However, the logging estimates of porosity are slightly lower in the upper part of the borehole than are the discrete shipboard measurements.

Assuming a constant grain density for the aluminosilicate fraction of the sediment, the resistivity log also can be used to calculate a wet-bulk density profile for Hole 909C. Such a calculated density, combined with discrete physical property measurements (Fig. 38), was used to generate a synthetic seismogram for Site 909 (see "Seismic Stratigraphy" section, this chapter). The discrete measurements and the estimated density from logs actually match each other more closely than the porosity data set, because the grain density was not constant but trended from relatively high values near the surface (~2.8 g/cm^3) to lower values at depth (~2.7 g/cm^3). This trend in grain density offsets some of the difference between estimated and measured porosity in the shallow sediments of the borehole.

SEISMIC STRATIGRAPHY

Introduction

A synthetic seismogram was generated from the velocity and density profiles at Site 909 to correlate reflectors in the seismic section

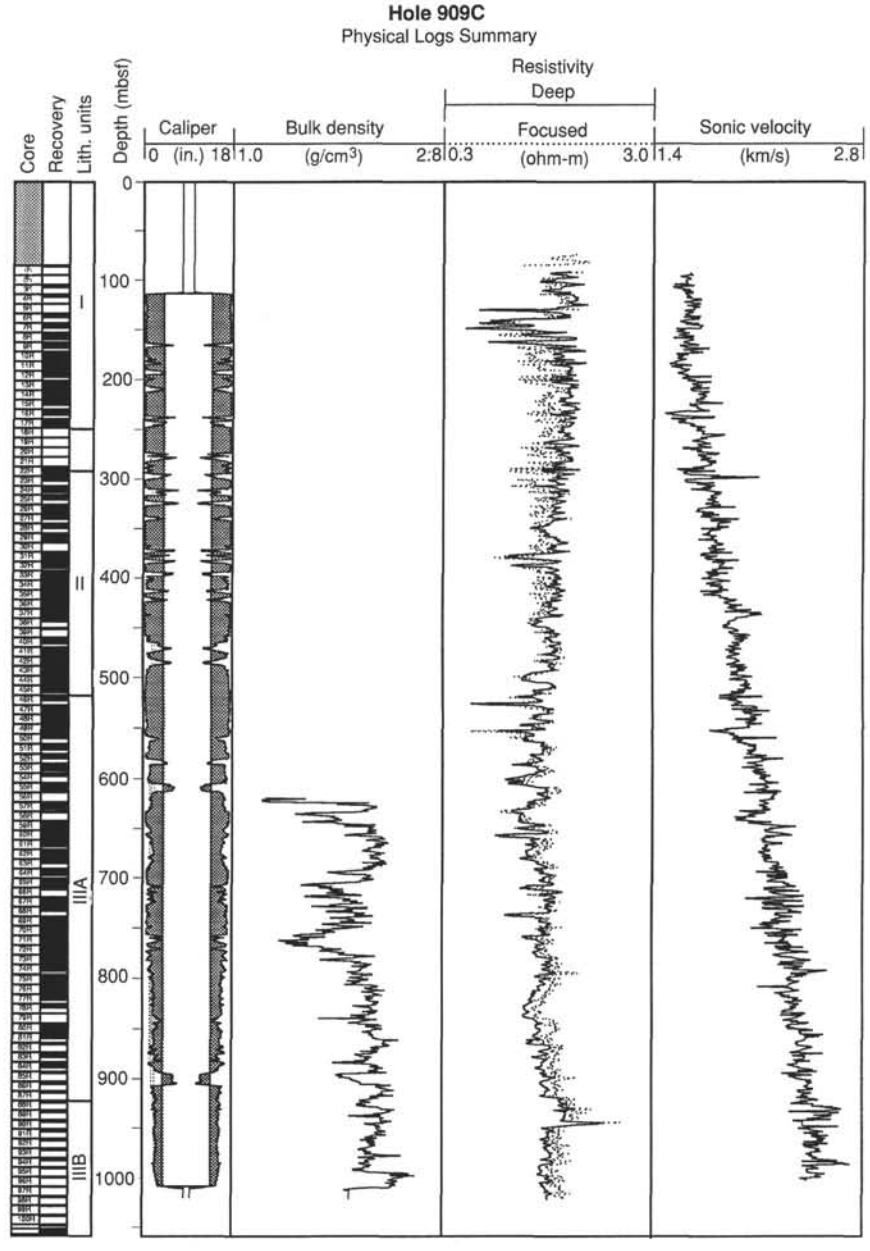

Figure 35. Caliper data from the high-temperature lithodensity tool (HLDT) shown with bulk-density data from the HLDT, deep phasor induction and spherically focused resistivity from the phasor dual induction tool (DIT), and sonic velocity data from the long-spaced digital sonic tool (SDT). The central white area in the caliper log represents the RCB bit size (9-7/8 in.), and the shading represents the "washed-out" portion of the hole from the bit size to actual measured diameter. All three curves have undergone a linear 5-point (0.76 m) moving average filter for presentation clarity.

to stratigraphic changes. The acoustic impedance profile (the product of density and velocity) and the profile of reflection coefficients (the rate of change of acoustic impedance) were determined both as a function of depth and of two-way acoustic traveltime. Convolution of the reflection coefficient profile with an assumed source acoustic wavelet resulted in a synthetic seismogram to compare with the measured seismic section.

The seismic section used for correlation is the line BU-20-81, collected by University of Bergen, Norway. Site 909 is located at shotpoint 465.

Acoustic Wavelet

Line BU-20-81 is a processed multichannel line. The acoustic signal of the original source has been, for the most part, removed. An approximation of a zero-phase single wavelet was constructed with a peak at 20 ms to match the signal returned from the seafloor in the seismic record.

Reflection Coefficients

Discrete measurements of density and compressional velocity on the recovered cores (see "Physical Properties" section, this chapter) were combined with logging data (see "Downhole Measurements" section, this chapter) to form a profile of reflection coefficients for Site 909. The logs provided detailed velocity data on the interval between 92 and 1003 mbsf. The raw logs were reprocessed at sea by comparing traveltimes for the different acoustic paths recorded by the SDT sonic tool and eliminating obvious cycle skips and occasional intervals of poor data. Velocity measurements on recovered core were invalid below 24 mbsf. To make a complete velocity profile, a linear interpolation of velocities was made through the gap between the two data sets. Because Hole 909C deviated from vertical, true vertical depth in the hole was calculated from the deviations measured by the FMS tool string between 590 and 1010 mbsf. The change in dip was approximately constant and was extrapolated up to a level of 0° deviation (128 mbsf) and down to the base of the hole.

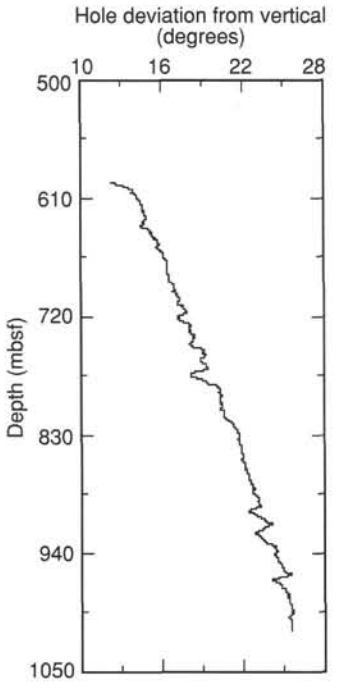

Figure 36. Hole deviation from vertical as a function of depth from the general purpose inclinometry tool (GPIT) of the FMS tool string.

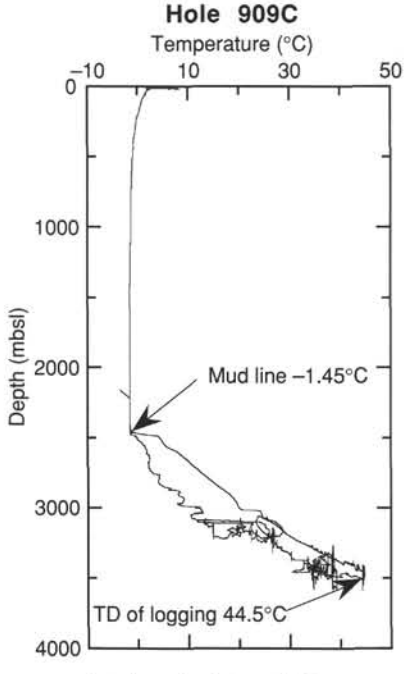

Figure 37. Temperature data from the Lamont-Doherty temperature logging tool (TLT) run on the first run of the quad-combination tool string. The depths are calculated from pressure readings and are approximate only. The complex nature of the curve is caused by the tool going up and down the hole when operational difficulties were encountered.

Based upon this extrapolation, significant differences (>5 m) between the cored depth and true vertical depth only occurred below 605 mbsf (cored depth). True vertical depth of the base of the hole is 1023 mbsf, as compared with 1061 m cored depth.

The composite velocity profile can be used to convert between mbsf and two-way traveltime (TWT) in the seismic section. A quicker but still accurate conversion can be made by the following second-order equation:

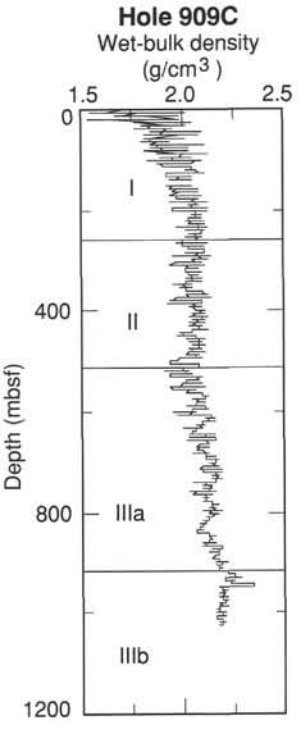

Figure 38. Combined density data from downhole log and discrete shipboard measurements on core. Log density estimated from the deep phasor induction resistivity (IDPH) log. Shipboard data <93 mbsf; log data 93–1010 mbsf. I–III = lithostratigraphic units.

$$Z = 7.6 + 0.664(TWT) + 0.000319(TWT)^2, \quad (1)$$

where Z is mbsf (cored depth), and TWT is two-way traveltime in milliseconds. The conversion between true vertical depth (TVD) and TWT is the following expression:

$$TVD = 4.8 + 0.700(TWT) + 0.000260(TWT)^2. \quad (2)$$

HLDT density measurements were nonexistent above 590 mbsf because of a tool failure (see "Downhole Measurements" section, this chapter) and were not used to create the density profile at Site 909. Instead, the deep resistivity log was inverted to create a pseudo-density log for the interval between 91 and 1022 mbsf using a grain density of 2.73 g/cm^3 (see "Explanatory Notes" chapter, this volume). The estimated densities from the logs were combined with measured bulk density on cores from the upper 91 m of Hole 909A.

The resulting velocity and density data were interpolated to a 1-m sample spacing, and were used to generate an acoustic impedance profile for Site 909 (Fig. 42). Also shown on the figure are the lithostratigraphic subunits (see "Lithostratigraphy" section, this chapter) and the synthetic seismogram.

Synthetic Seismogram

Figure 43 compares the synthetic seismogram shown in Figure 42 to seismic reflection line BU-20-81 through Site 909. The synthetic seismogram matches the recorded profile reasonably well, but is not as good as that achieved at other Leg 151 sites. The lack of a tight correlation is probably due to the lack of any strongly reflecting horizons

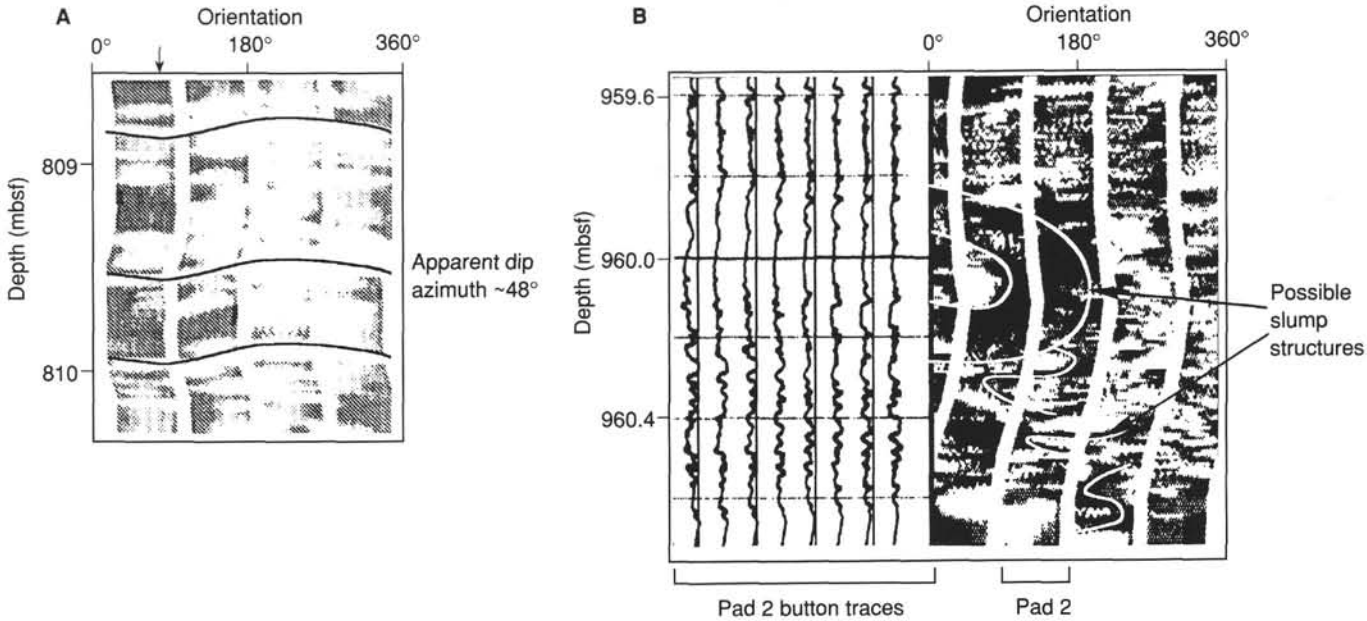

Figure 39. Oriented microresistivity images from the four orthogonal pads of the FMS: the lighter the color the more resistive the beds. **A.** Image showing the apparent dip of the beds caused by the hole deviation. **B.** Image showing the interpretation of slump structures. On the left side, the microresistance traces from eight of the individual "buttons" on pad number 2 are shown, with resistance decreasing to the left.

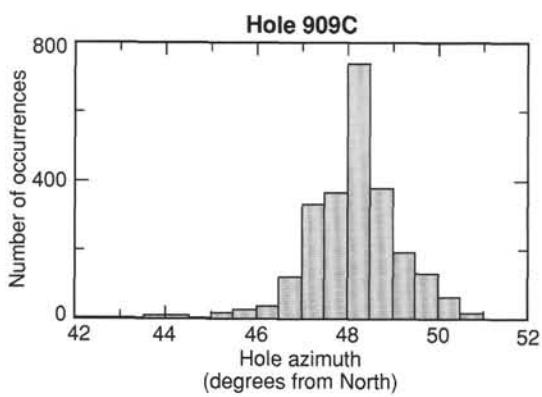

Figure 40. Histogram of hole azimuth values (degrees from true North) measured by the general purpose inclinometry tool (GPIT) of the FMS tool string.

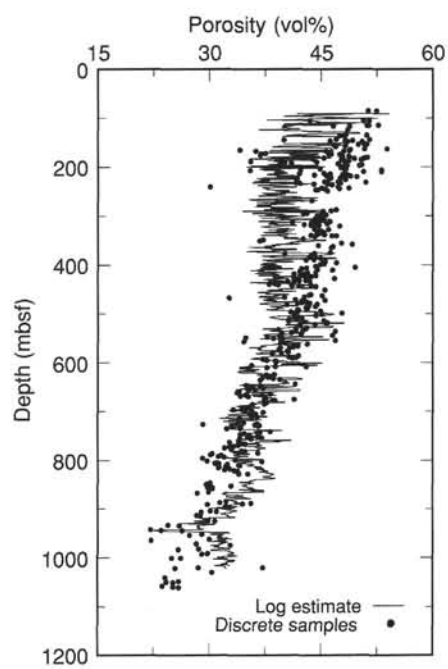

Figure 41. Porosity derived from the IDPH resistivity log compared with porosity measurements on discrete core samples. The input resistivity data and the final porosity log are unsmoothed.

in most of the sediment and to the accumulated small errors in velocity measured by the logs. The sediments at Site 909 are mostly silty clays, and the velocity and density variations downhole are subtle. Small errors in velocity or density thus can significantly strengthen or weaken the observed reflectors. In addition, Hole 909C was the deepest one drilled during Leg 151, and the accumulation of errors in the TWT estimate downhole is more significant here than at other sites.

Lithostratigraphic Unit I is distinguished by a large number of reflectors, which correlate well between the synthetic seismogram and the seismic profile (Fig. 43). The Unit I/II transition occurs at a distinct triplet of reflectors (I_j–I_l) that are poorly resolved in the synthetic seismogram. Below this boundary, the reflectors become more widely spaced. The Unit II/III boundary occurs just above another prominent triplet of reflectors (III_a–III_c) at 0.63 s TWT. In the synthetic seismogram these reflectors are about 20 ms shallower than are the equivalent reflectors in the seismic profile. A transition to weak and laterally variable reflectors occurs below reflector III_h. The match between the synthetic seismogram and the seismic profile below this reflector is only fair, but this is in part because of the variability in the sediment column itself.

Ms 151IR-107

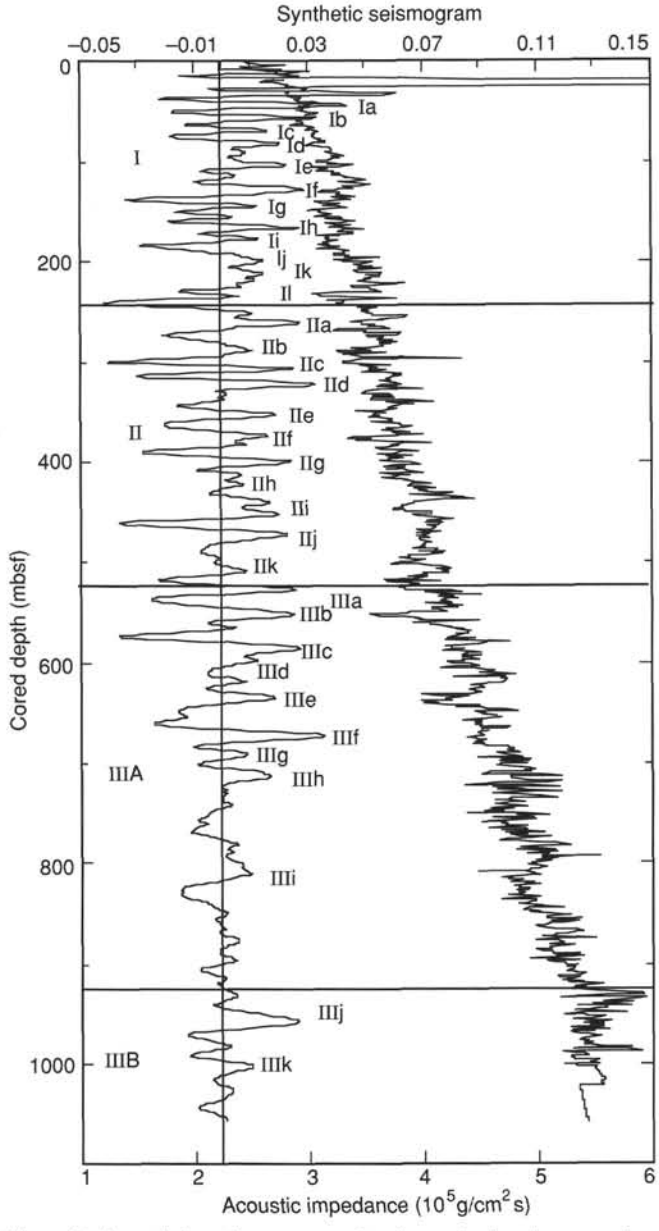

Figure 42. Acoustic impedance compared to the synthetic seismogram from Hole 909C. Also shown are the lithostratigraphic unit boundaries from the "Lithostratigraphy" section (this chapter).

NOTE: For all sites drilled, core-description forms ("barrel sheets") and core photographs can be found in Section 6, beginning on page 465. Forms containing smear-slide data can be found in Section 7, beginning on page 849. Thin-section descriptions are given in Section 8, beginning on page 885, and sediment thin sections in Section 9, beginning on page 895. Dropstone descriptions are included in Section 10, beginning on page 903.

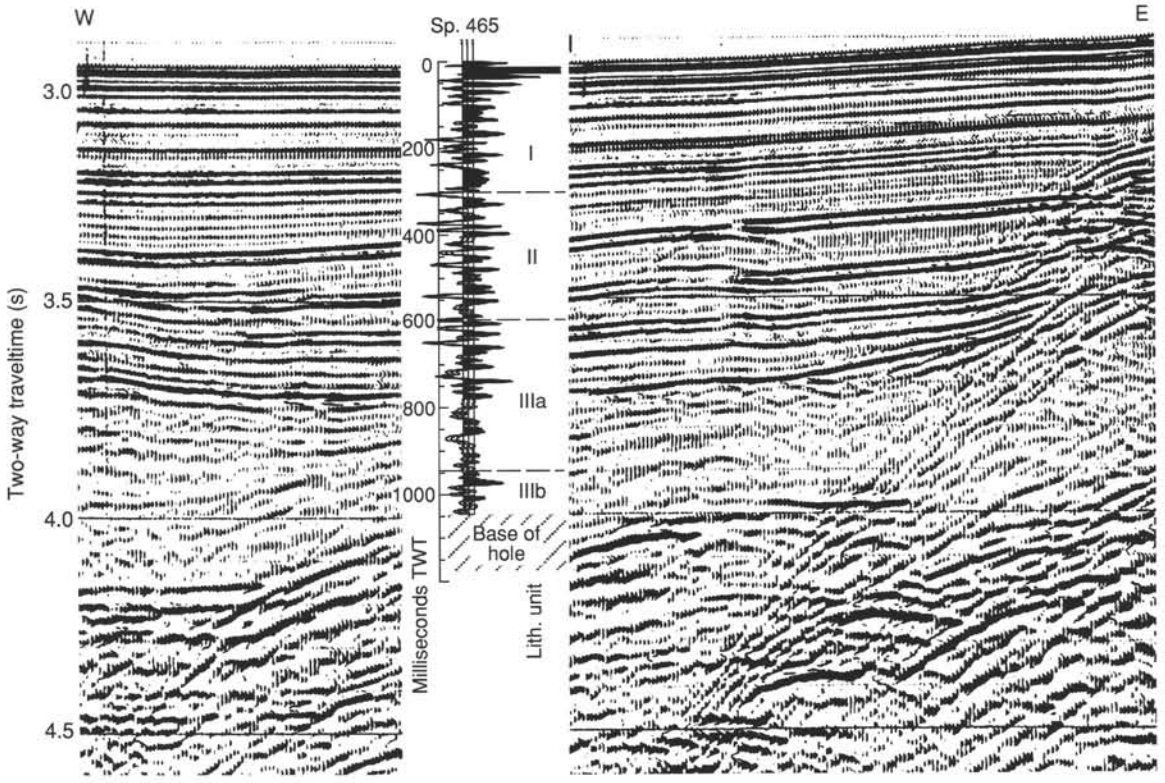

Figure 43. Comparison between synthetic seismogram from Site 909 and equivalent seismic section on line BU-20-81. The base of reflector Il marks the litho-stratigraphic Unit I/II transition, whereas the top of IIIa marks the Unit II/III boundary.

SHORE-BASED LOG PROCESSING

Hole 909C

Bottom felt: 2529 mbrf
Total penetration: 1061.8 mbsf
Total core recovered: 604.77 m (61%)

Logging Runs

Logging string 1:: DIT/SDT/HLDT/NGT (lower section)
Logging string 2: FMS/GPIT/NGT (lower section, main and repeat). No FMS/GPIT/NGT run in the upper section due to time limitations.
Logging string 3: DIT/SDT/HLDT/NGT (upper section; HLDT failed to operate in this section).

Wireline heave compensator was used to counter ship heave resulting from the mild sea state conditions.

Drill Pipe/Bottom-hole Assembly/Casing

The following drill pipe depths are as they appear on the logs after differential depth shift (see **Depth shift** section) and depth shift to the seafloor. As such, there might be a discrepancy with the original depths given by the drillers on board. Possible reasons for depth discrepancies are ship heave, use of wireline heave compensator, and drill-string and/or wireline stretch.

DIT/HLDT/SDT/NGT (lower section): Bottom of drill pipe at 589 mbsf.
FMS/GPIT/NGT (lower section): Bottom of drill pipe at 590 mbsf.
DIT/HLDT/SDT/NGT (upper section): Bottom of drill pipe at 89 mbsf.

Processing

Depth shift: Lower DIT/HLDT/SDT/NGT has been depth shifted with reference to upper FMS/GPIT/NGT and then both lower DIT/HLDT/SDT/NGT and upper FMS/GPIT/NGT have been depth shifted with reference to upper DIT/SDT/HLT/NGT. Lower FMS/GPIT/NGT has been applied a constant depth shift of 0.53 m. All logs have then been shifted to the seafloor (–2526 m). This amount differs from the bottom-felt depth because the mud line on the logs is 3 m higher than the drillers' depth.

A list of the amount of differential depth shifts applied at this hole is available upon request.

Gamma-ray processing: NGT data were processed to correct for borehole size and type of drilling fluid.

Acoustic data processing: The sonic logs have been processed to eliminate some of the noise and cycle skipping experienced during recording.

Quality Control

Hole diameter was recorded by the hydraulic caliper on the HLDT tool (CALI) and by the caliper on the FMS string (C1 and C2).

Invalid gamma-ray data were detected at 11.5, 31, and 77.5 mbsf (DIT/HLDT/SDT/NGT string, upper section).

The HLDT tool did not work in the upper part of the hole. Invalid density data were detected at 685, 716, and 994 mbsf.

Note: Details of standard shore-based processing procedures are found in the "Explanatory Notes" chapter, this volume. For further information about the logs, please contact:

Cristina Broglia
Phone: 914-365-8343
Fax: 914-365-3182
E-mail: chris@ldeo.columbia.edu

Elizabeth Pratson
Phone: 914-365-8313
Fax: 914-365-3182
E-mail: beth@ldeo.columbia.edu

Hole 909C: Resistivity-Velocity-Natural Gamma Ray Log Summary

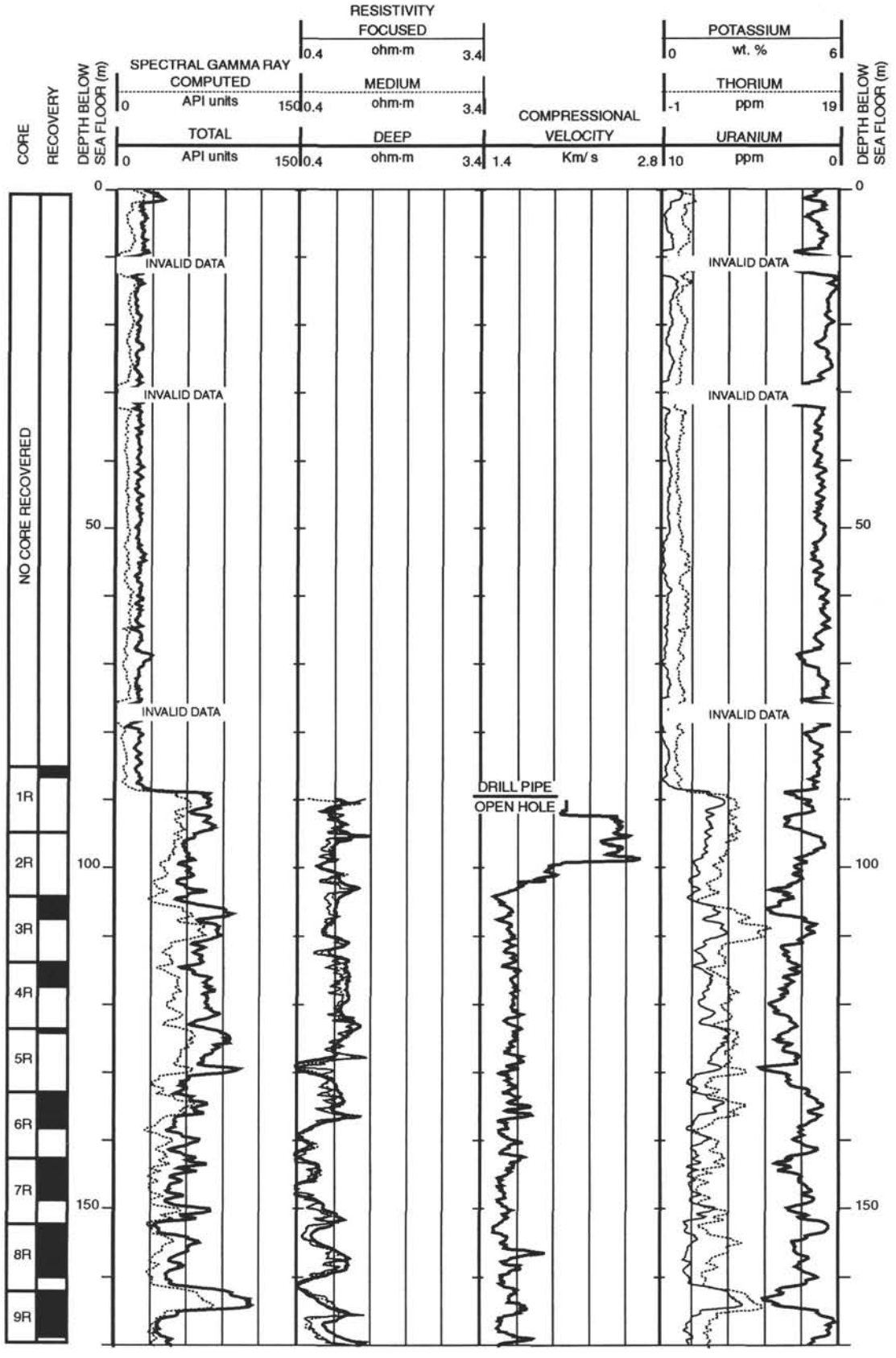

Hole 909C: Resistivity-Velocity-Natural Gamma Ray Log Summary

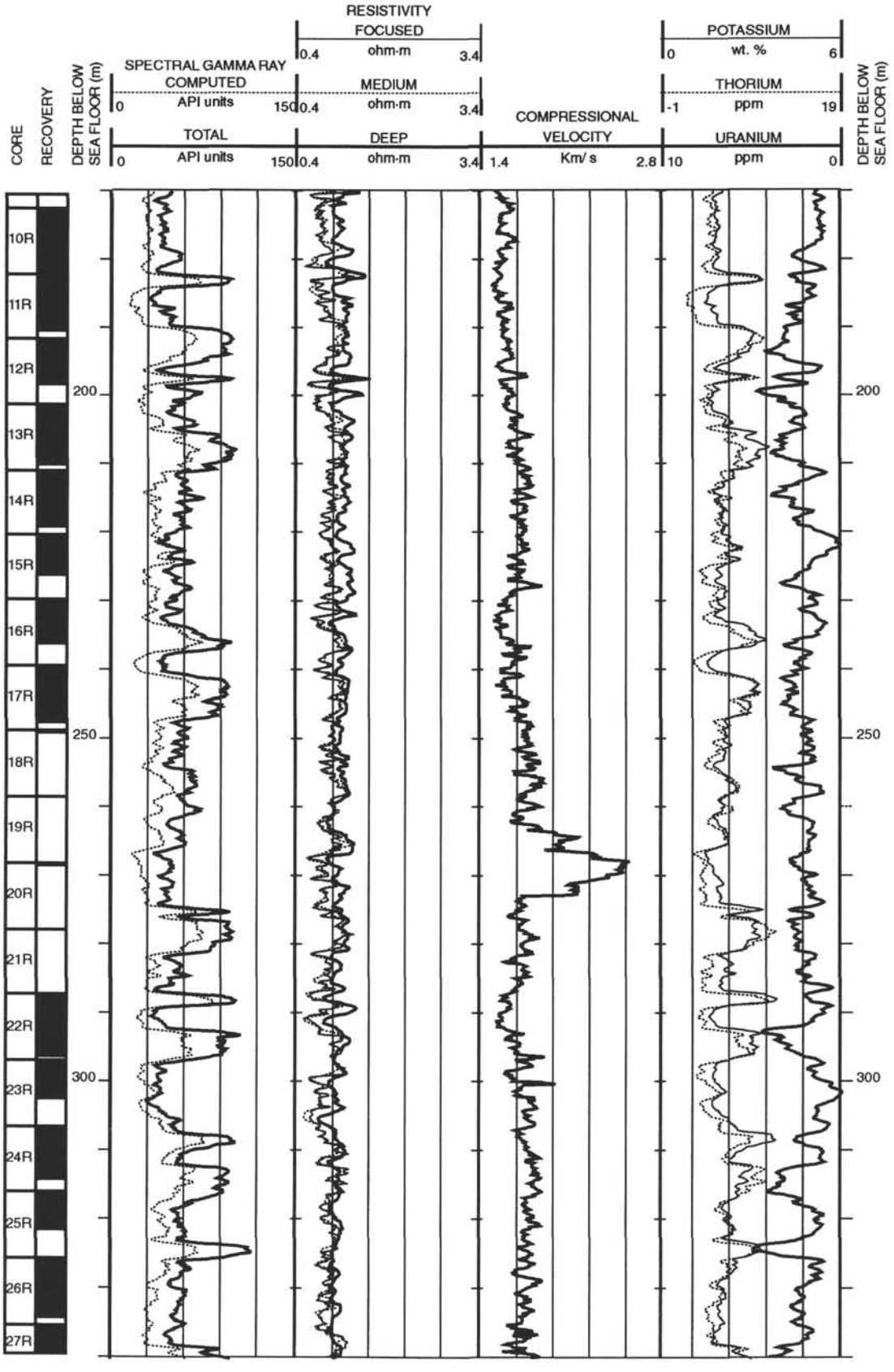

Hole 909C: Resistivity-Velocity-Natural Gamma Ray Log Summary

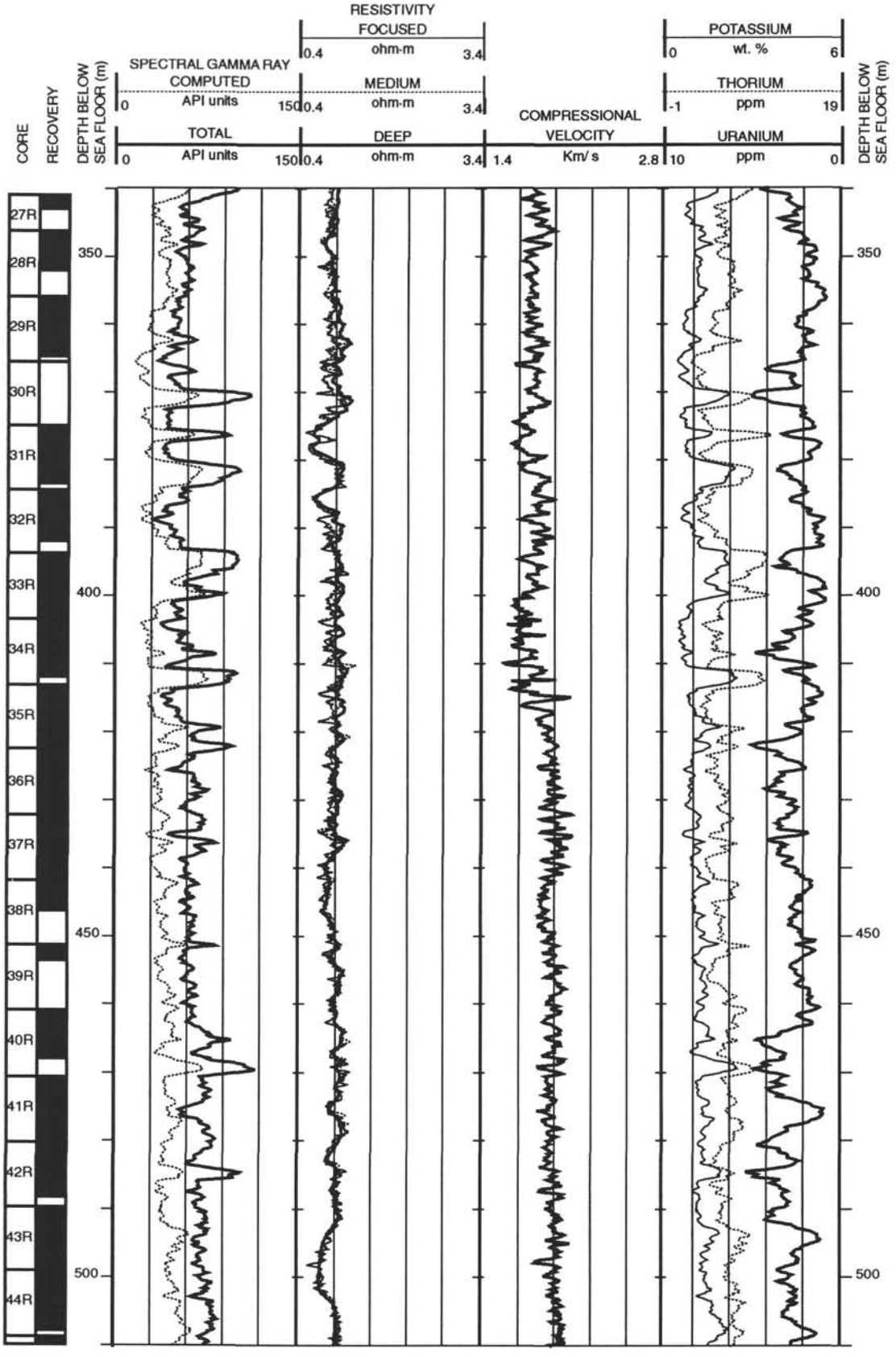

Hole 909C: Resistivity-Velocity-Natural Gamma Ray Log Summary

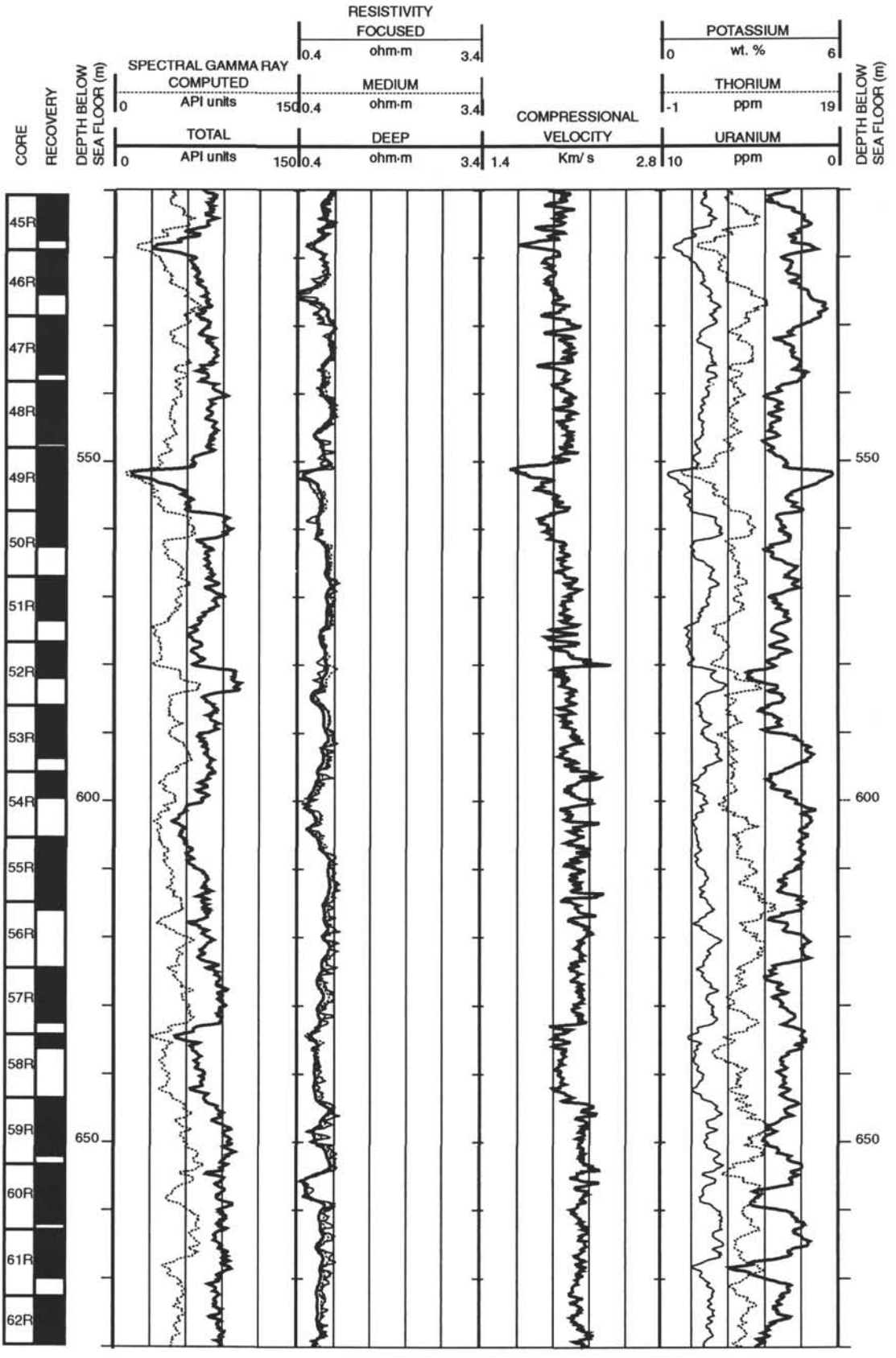

Hole 909C: Resistivity-Velocity-Natural Gamma Ray Log Summary

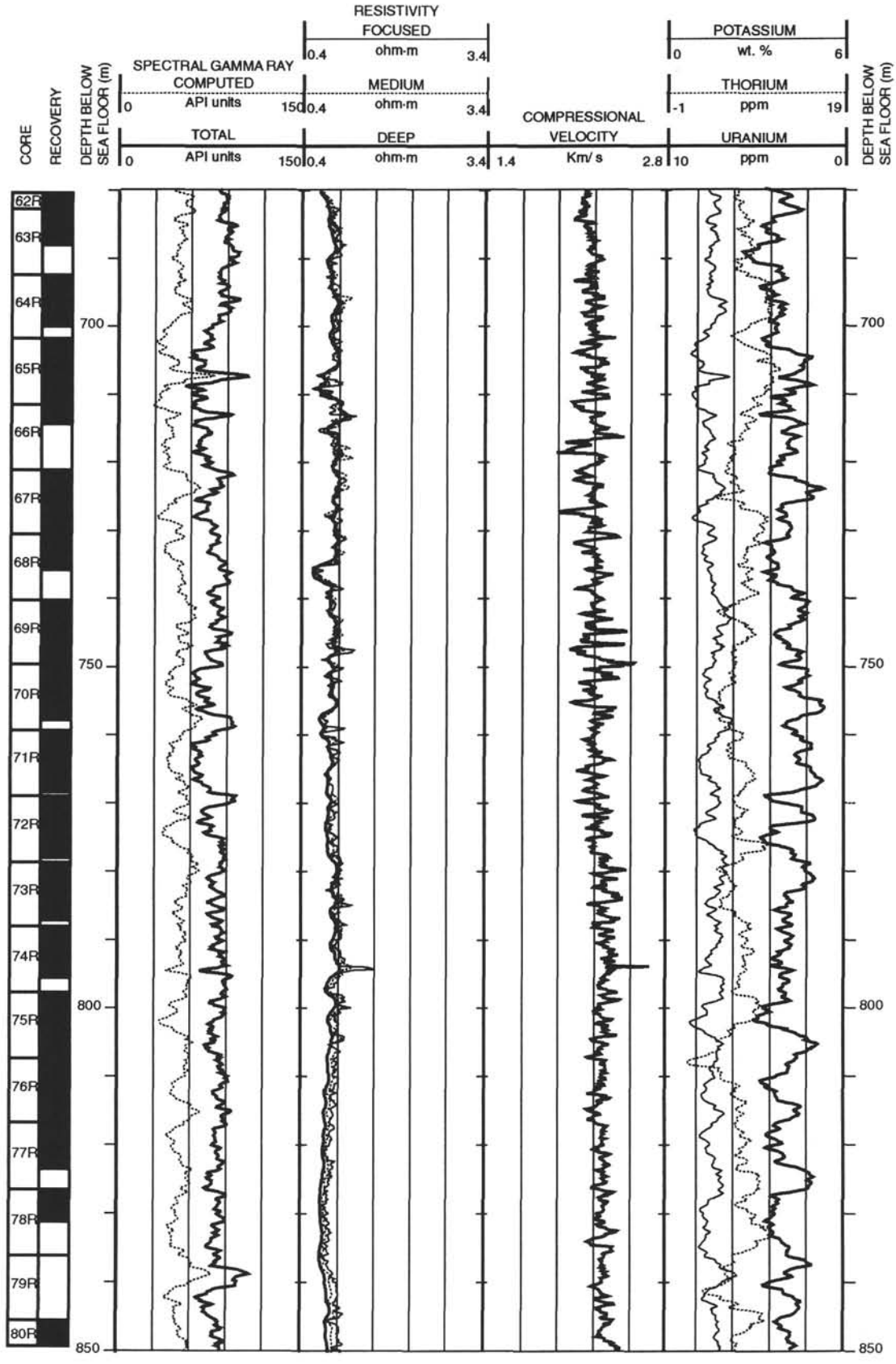

Hole 909C: Resistivity-Velocity-Natural Gamma Ray Log Summary

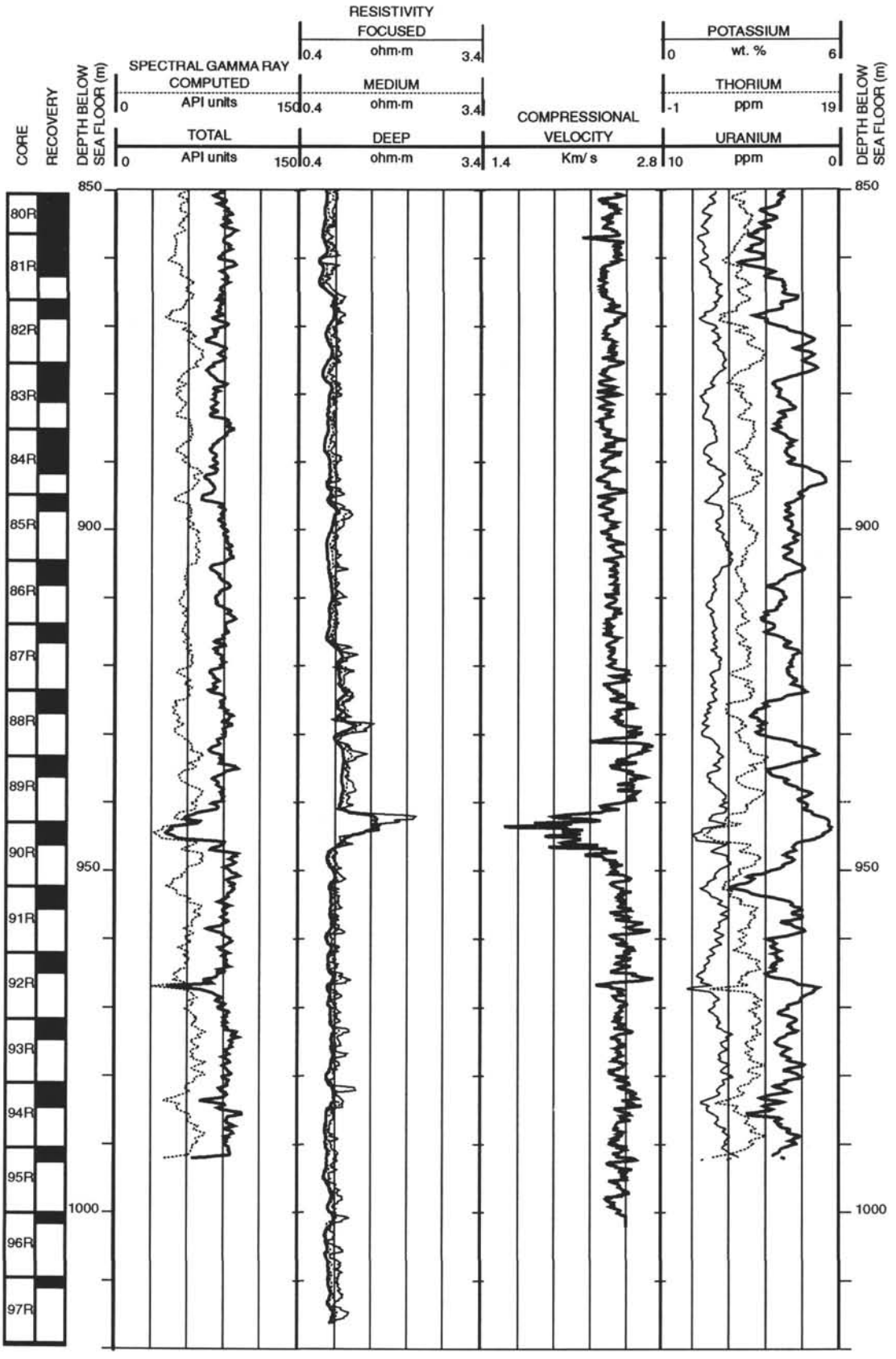

Hole 909C: Density-Natural Gamma Ray Log Summary

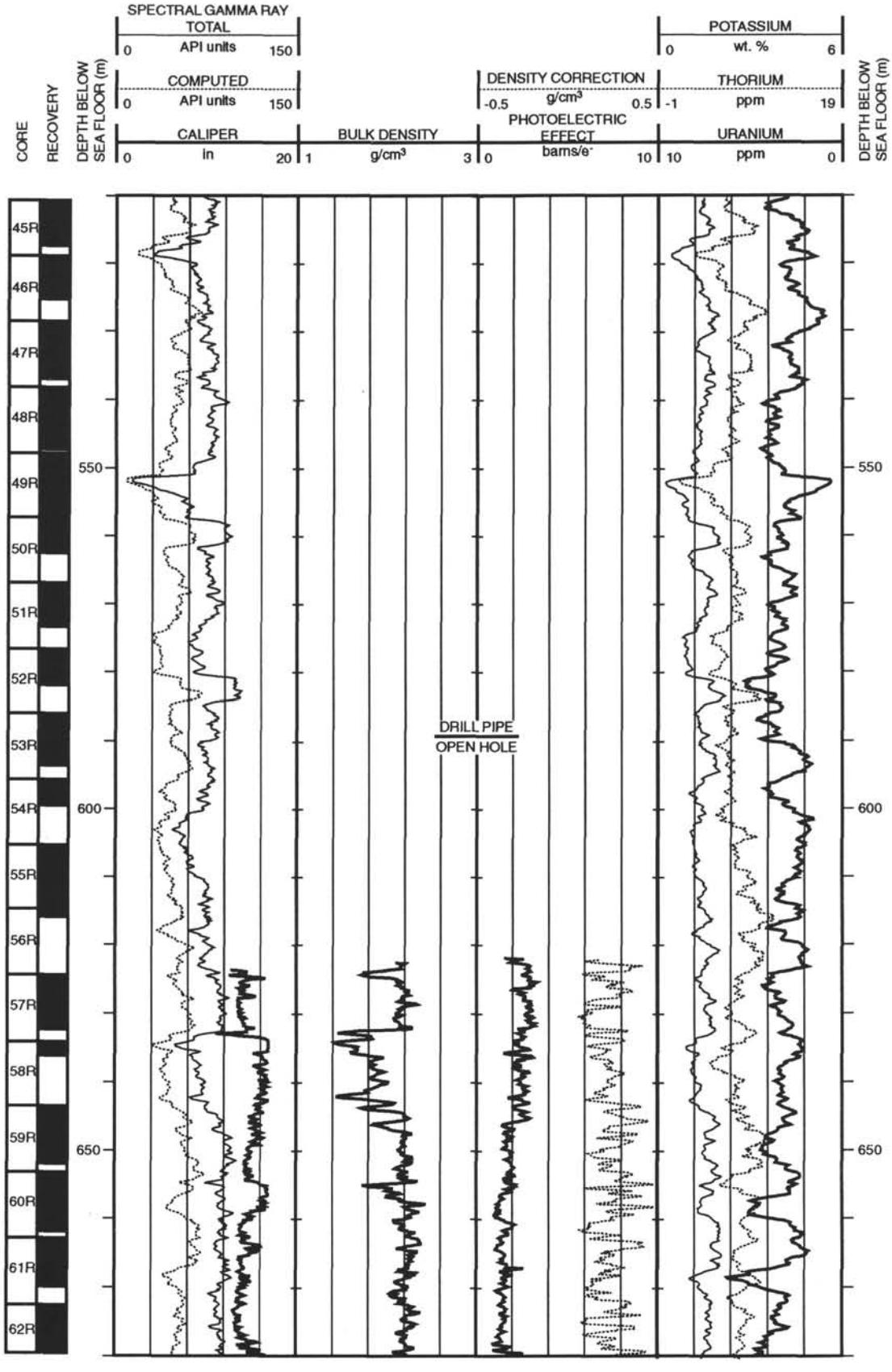

Hole 909C: Density-Natural Gamma Ray Log Summary

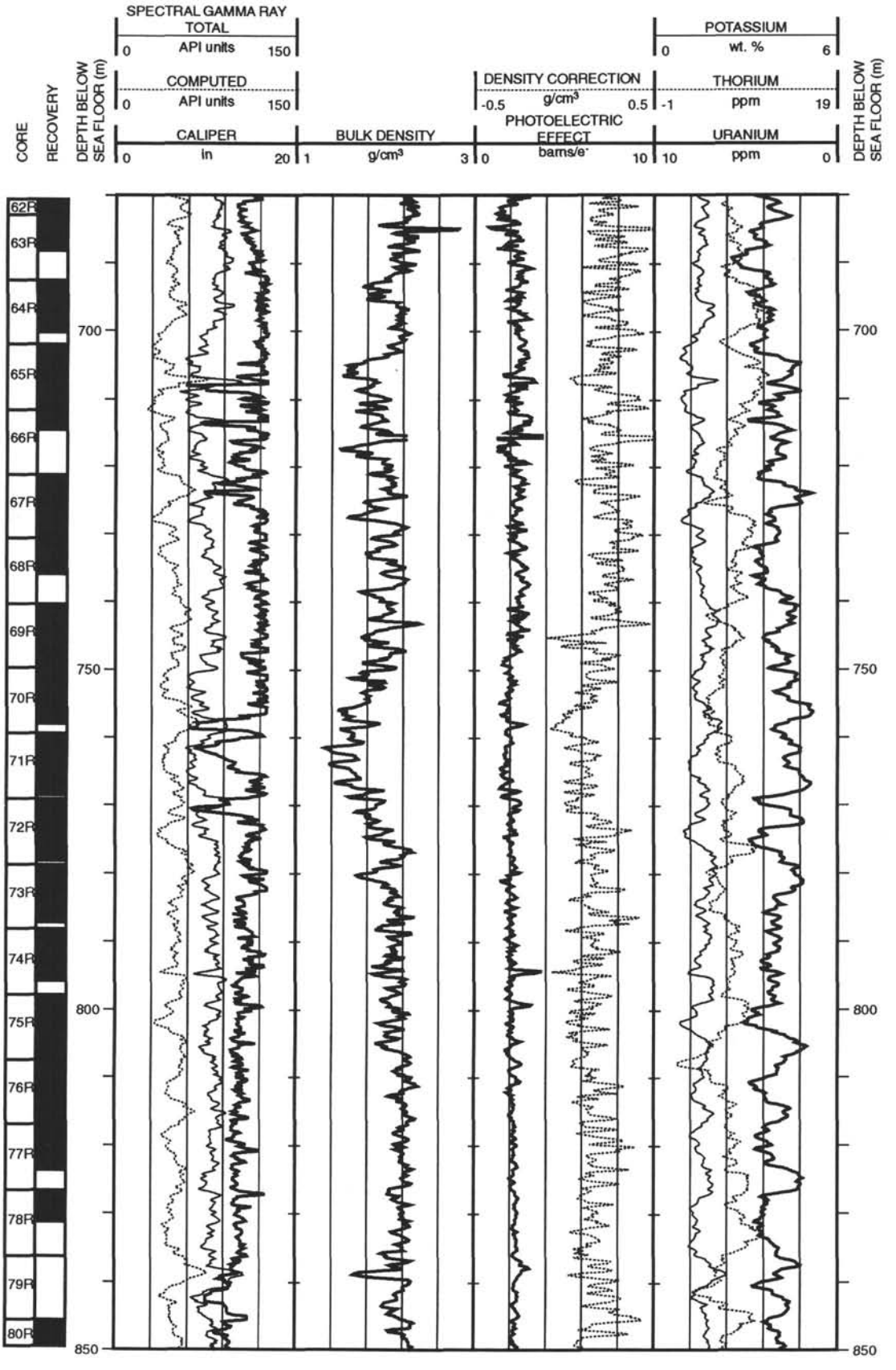

Hole 909C: Density-Natural Gamma Ray Log Summary